NUREG/CR-2609
ORNL/NUREG-75

ornl

OAK RIDGE NATIONAL LABORATORY

UNION CARBIDE

Thermal-Hydraulic Test Facility Bundle 3 In-Core Instrumentation and Operating History

L. J. Ott

Prepared for the U.S. Nuclear Regulatory Commission
Office of Nuclear Regulatory Research
Under Interagency Agreements DOE 40-551-75 and 40-552-75

OPERATED BY
UNION CARBIDE CORPORATION
FOR THE UNITED STATES
DEPARTMENT OF ENERGY

Printed in the United States of America. Available from
National Technical Information Service
U.S. Department of Commerce
5285 Port Royal Road, Springfield, Virginia 22161

Available from

GPO Sales Program
Division of Technical Information and Document Control
U.S. Nuclear Regulatory Commission
Washington, D.C. 20555

NUREG/CR-2609
ORNL/NUREG-75
Dist. Category AN

Contract No. W-7405-eng-26

Engineering Technology Division

THERMAL-HYDRAULIC TEST FACILITY BUNDLE 3 IN-CORE INSTRUMENTATION AND OPERATING HISTORY

L. J. Ott

Manuscript Completed - August 3, 1982
Date Published - August 1982

Prepared for the U.S. Nuclear Regulatory Commission
Office of Nuclear Regulatory Research
Under Interagency Agreements DOE 40-551-75 and 40-552-75

NRC FIN No. B0125

Prepared by the
OAK RIDGE NATIONAL LABORATORY
Oak Ridge, Tennessee 37830
operated by
UNION CARBIDE CORPORATION
for the
DEPARTMENT OF ENERGY

CONTENTS

LIST OF FIGURES

LIST OF TABLES

THERMAL-HYDRAULIC TEST FACILITY BUNDLE 3 IN-CORE INSTRUMENTATION AND OPERATING HISTORY

L. J. Ott

ABSTRACT

This report presents the chronological history of the Thermal-Hydraulic Test Facility (THTF) Bundle 3. This bundle is one of the most extensively instrumented bundles ever used in light-water reactor safety research. This compilation documents the in-core instrument measurement sites and operating history for the original Bundle 3 and two major refurbishments to the bundle. Additional information (such as radial dimensions and surface emissivity) that will be needed for thermal analysis of the fuel rod simulator responses during THTF testing is also provided.

---

1. INTRODUCTION

The Oak Ridge National Laboratory (ORNL) Pressurized-Water Reactor (PWR) Blowdown Heat Transfer (BDHT) Separate Effects Program[1] is an experimental separate effects study of heat transfer phenomena in rod bundles under conditions typical of various reactor accident scenarios. Primary test results are obtained from the Thermal-Hydraulic Test Facility (THTF), a large nonnuclear experimental loop with a test section that contains an array of indirectly electrically heated fuel rod simulators (FRSs) with a 3.66-m (12-ft) heated length.

The FRSs used in the first rod bundle in the THTF had a dual-sheath design (see idealized rod cross section in Fig. 1.1) with thermocouples being located in the center of the FRS and in axial grooves machined in the inner sheath. The sheath thermocouples allow the determination of the transient surface temperature and surface heat flux of the FRS during experiments in the THTF (Refs. 2 and 3). Bundle 1 was a 7 x 7 matrix containing 49 active FRSs 10.7 mm (0.422 in.) in diameter. These Bundle 1 FRSs were reduced to their final outside diameter by swaging; this operation crushed the embedded thermocouples to a somewhat elliptical shape and pulled the edges of the milled groove away from the outer sheath, thus forming air pockets around the thermocouples. Two-dimensional modeling of these BDHT FRSs using HEATING5 (Ref. 4), a generalized heat conduction code developed at ORNL, revealed severe perturbations in the surface heat flux and temperature driving potential caused by the presence of the sheath thermocouple and the air pockets surrounding the thermocouple.[5] The local surface flux was perturbed by as much as 30% of the mean flux with an additional 1% perturbation per mil (0.025 mm) of eccentricity of the heating element with respect to the outer sheaths.

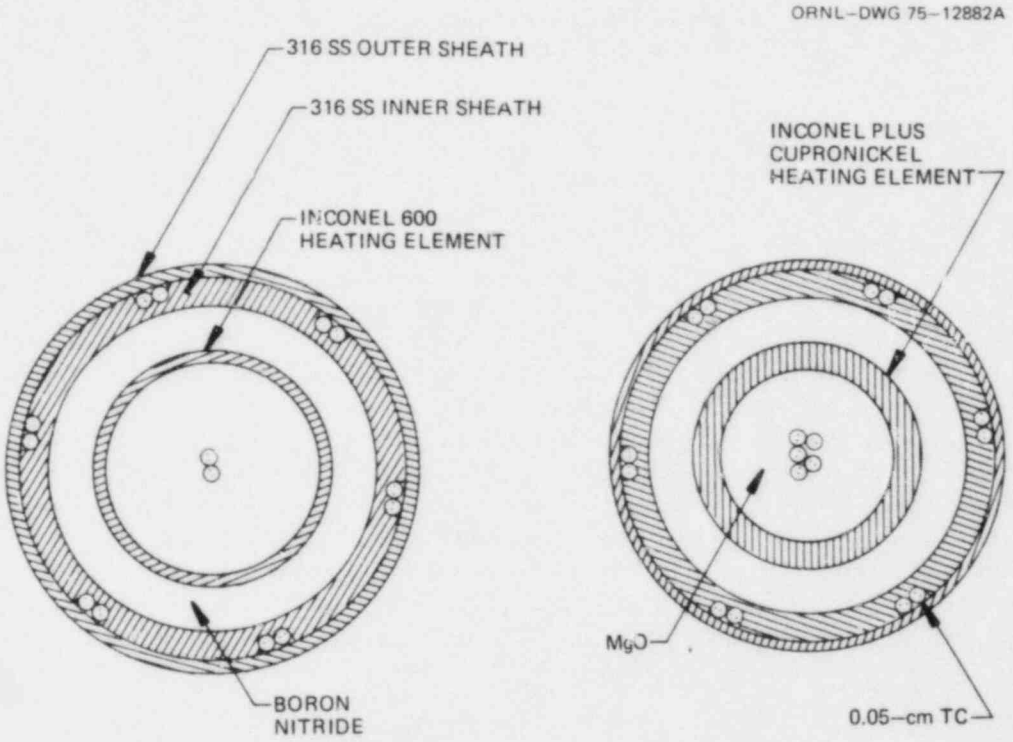

Fig. 1.1. Heater rod cross section.

On May 3, 1979, Bundle 1 was removed from the THTF test section after surviving 38 blowdowns and 223 h at power (10.5 h at a full power of 122 kW per rod) with only two FRS failures.[6] Rods 39 and 47 failed because of low electrical resistance between the heating element and ground.

Assembly of THTF Bundle 2 was completed on February 6, 1978. Bundle 2 was a 7 x 7 matrix containing 45 active rods 10.7 mm (0.422 in.) in diameter and 4 inactive rods nominally 13.9 mm (0.547 in.) in diameter.[7] These FRSs differed in design from Bundle 1 FRSs only in a slightly thicker (~0.127-mm) outer stainless steel sheath. During construction many of these FRSs developed extensive cracks in the inner stainless steel sheath in the bottom of the grooves machined for the sheath thermocouples. Because moisture could easily enter the boron nitride (BN) insulation through these cracks, the integrity of the cracked FRSs was questionable. The assembled Bundle 2 has never been installed in the THTF.

Problem areas encountered in the Bundle 1 and 2 FRSs were essentially eliminated in the design and construction of the third bundle for the THTF. Bundle 3 FRSs (see idealized cross section in Fig. 1.2) were constructed with (1) a single outside sheath (rather than the dual sheath of Bundles 1 and 2), (2) BN insulator preforms to minimize eccentricity, and (3) multiple-sheath thermocouples per axial level (as compared with one in Bundle 1). HEATING5 analysis of this FRS design showed the surface heat flux to be perturbed by only _ of the mean flux. X rays and cross sections of prototypical Bundle 3 FRS revealed negligible eccentricity. Furthermore, the Bundle 3 FRS incorporated a flat power profile (i.e., no

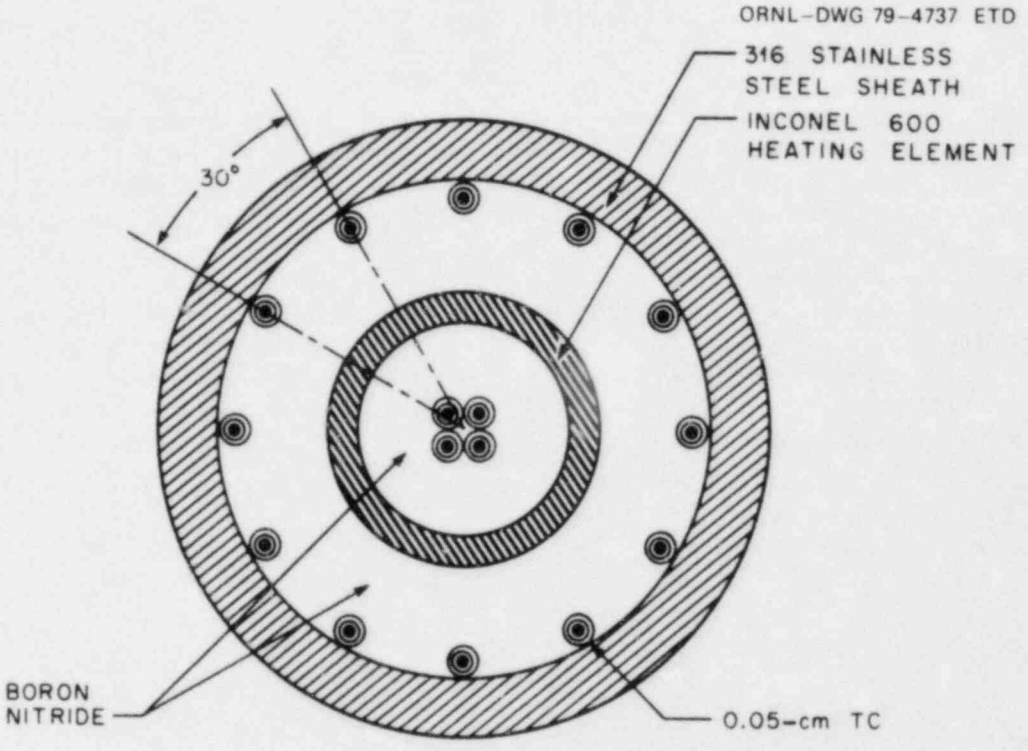

Fig. 1.2. Cross section of THTF Bundle 3 FRS.

changes in the power generation rate except at the ends of the 3.66-m heated length). These Bundle 3 FRSs were as nearly axisymmetric as possible using state-of-the-art manufacturing processes.

Assembly of Bundle 3 was completed June 19, 1979. The bundle is an 8 x 8 square array with 60 FRSs 9.5 mm (0.374 in.) in diameter and 4 unpowered positions. Bundle 3 was installed in the THTF June 26, 1979.

2. OBJECTIVE

The THTF Bundle 3 is one of the most extensively instrumented bundles ever used in light-water reactor safety research. Not counting spacer-grid and shroud-wall thermocouples, each FRS contains 16 thermocouples for a total of 960 thermocouples just in the FRSs. Additionally, there have been two major refurbishments of bundle 3 (once in March-April 1980 and again in July-August 1980). This report documents the thermal measurement sites in the original and refurbished Bundle 3 and provides supplemental information (such as FRS radial dimensions and heating element resistance) needed for thermal analysis of the FRS responses obtained during THTF testing. Also, a historical account of the THTF Bundle 3 since June 26, 1979, will be given.

3. ORIGINAL THTF BUNDLE 3

3.1 Core Configuration and Instrumentation

The original Bundle 3 was installed in the THTF test section on June 26, 1979. The FRS test assembly was an 8 x 8 square array containing 60 FRSs with a 9.5-mm OD (0.374-in.) on a 12.73-mm (0.501-in.) square pitch with a 3.66-m (12-ft) heated length having a flat power profile. Four unpowered rods (two thermocouple rods, one level rod, and one dummy rod) had an outside diameter of 10.2 mm (0.401 in.). A cross section of the bundle (identifying the FRSs, subchannel locations, and inactive rods) is given in Fig. 3.1. Each FRS contained 16 thermocouples in groups

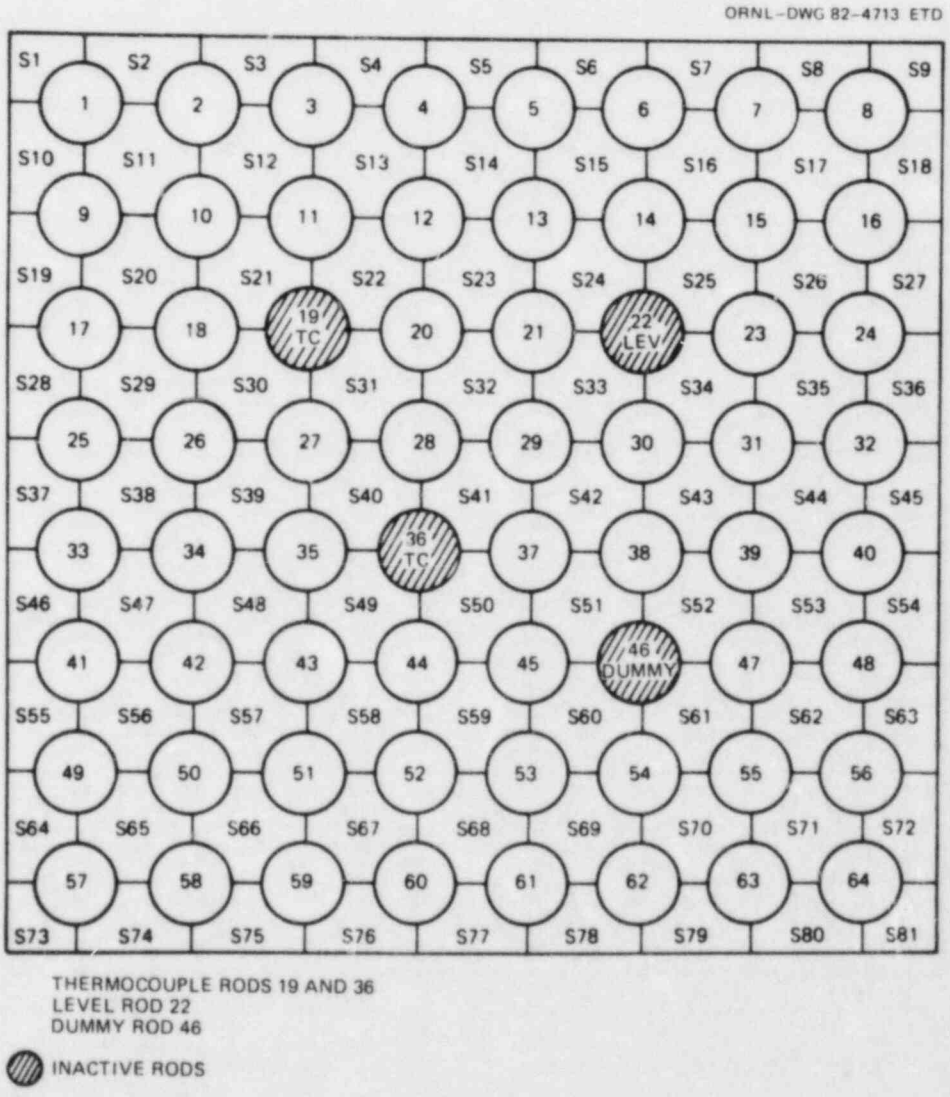

Fig. 3.1. Identification of THTF heater rods, subchannel locations, and inactive rods in THTF Bundle 3.

of four (one centerline and three sheath) at each of four axial levels. The axial levels monitored by each rod are indicated in Fig. 3.2; these axial levels are denoted by alphabetic letters, and the major level nominal locations (A–G) are presented, along with other critical points, in Fig. 3.3.

As in the case of Bundle 1, normal flow in the test section is upward through the bundle, and the temperature of the inter-rod flow channels

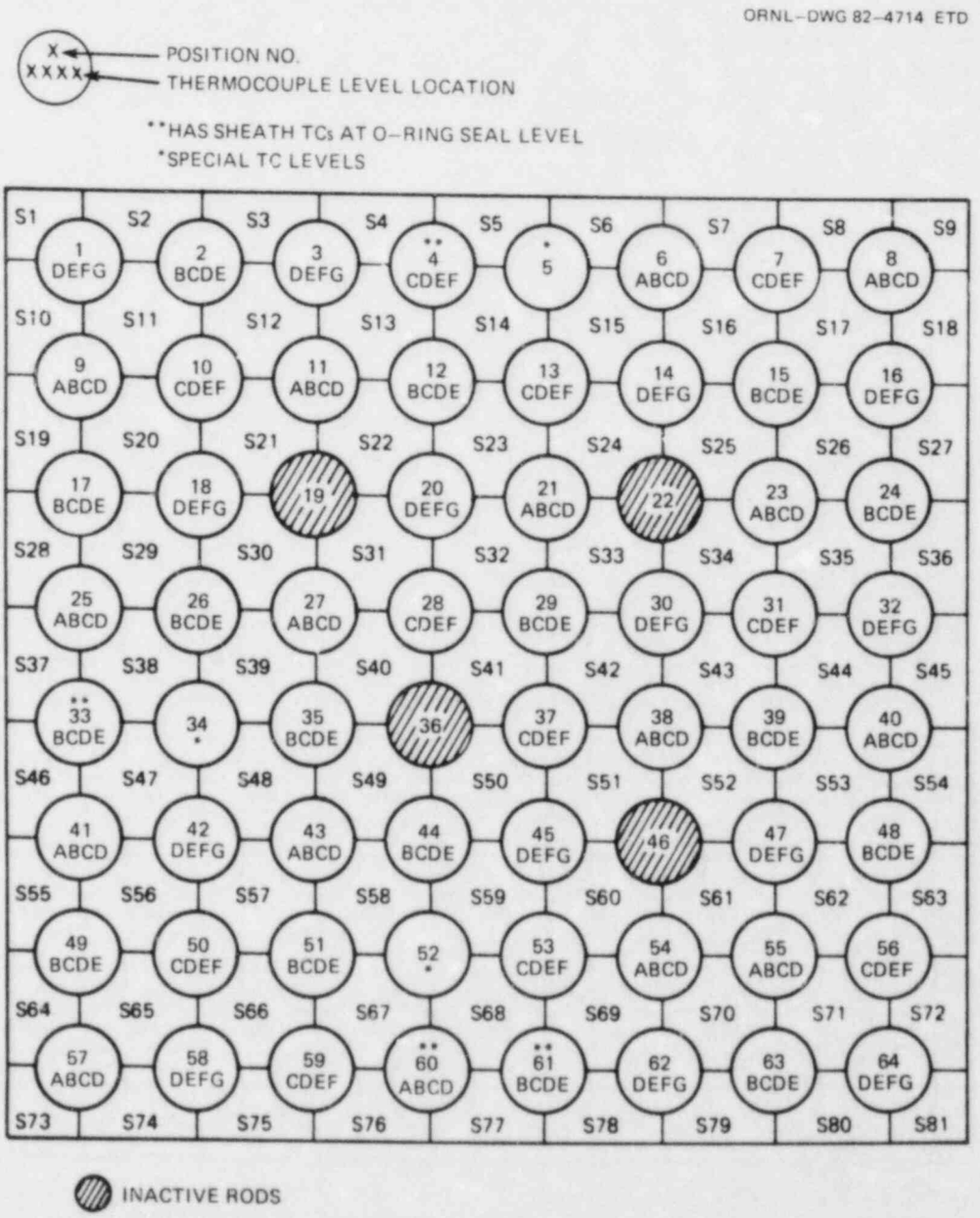

Fig. 3.2. Identification of THTF heater rods and axial thermocouple levels monitored by each rod in THTF Bundle 3.

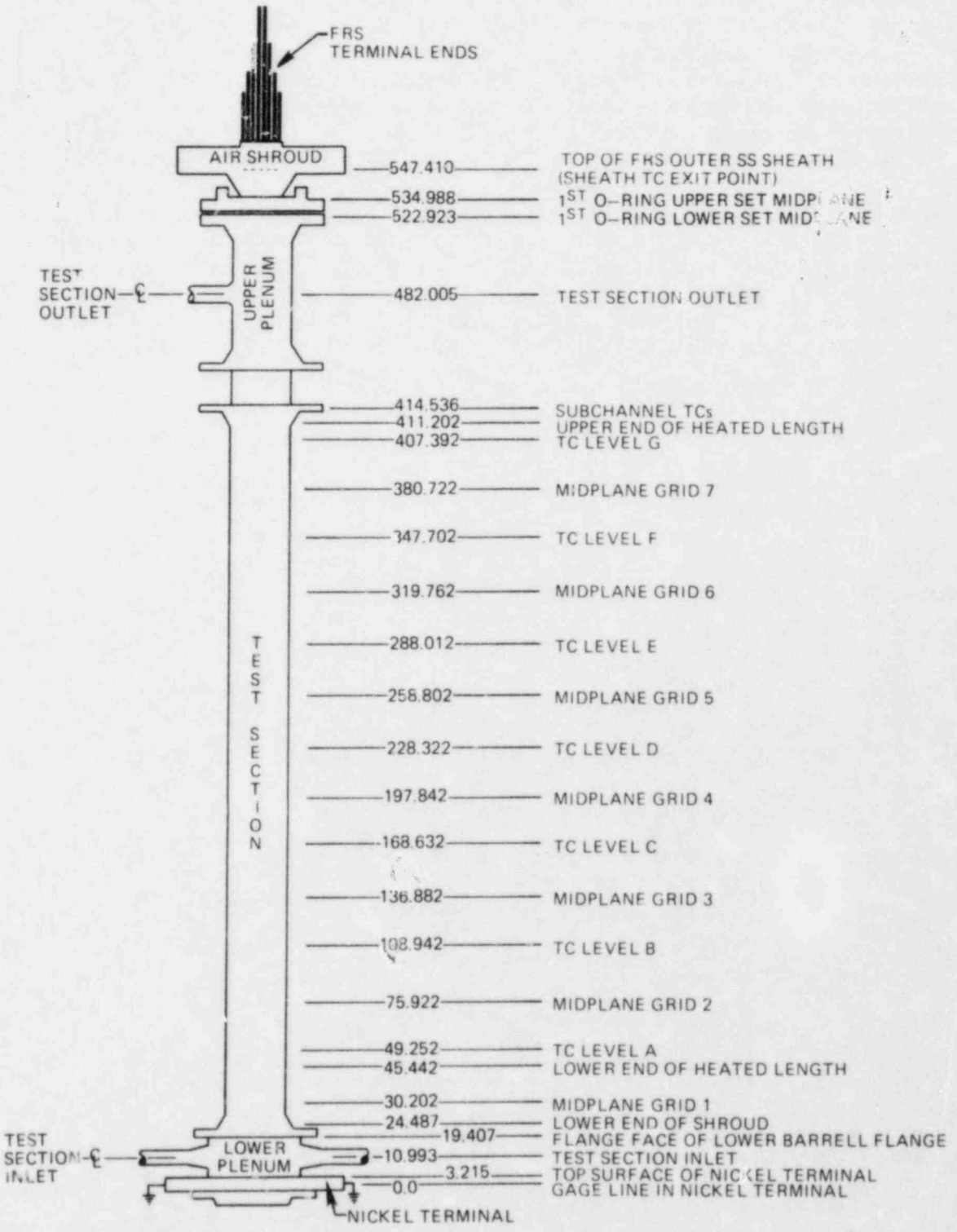

Fig. 3.3. Nominal location of critical points in THTF Bundle 3. All dimensions are in centimeters and are referenced to the gage line in the nickel terminal.

(subchannels) at the exit of the bundle heated length is monitored by thermocouples ~3.3 cm above the upper end of the heated zone. The inlet flow to Bundle 3 enters the bottom of the test section via an external downcomer (Fig. 3.4), whereas for Bundle 1 the flow entered at the upper end of the test section barrel and proceeded downward to the bundle inlet region by way of the annulus between the outside of the shroud box and the inside of the test section barrel. In the THTF configuration in Fig. 3.4, the old downcomer annulus is isolated from the bundle by means of a packing gland near the bottom of the shroud box.

The thermocouple level locations in Fig. 3.3 are nominal or design values and do not represent the actual "as-built" locations of the FRS thermocouples. The location of each thermocouple in each FRS in Bundle 3 was determined individually from x rays.[8] The compilation of these data is presented graphically in Figs. 3.5 and 3.6. Figure 3.5 is a schematic

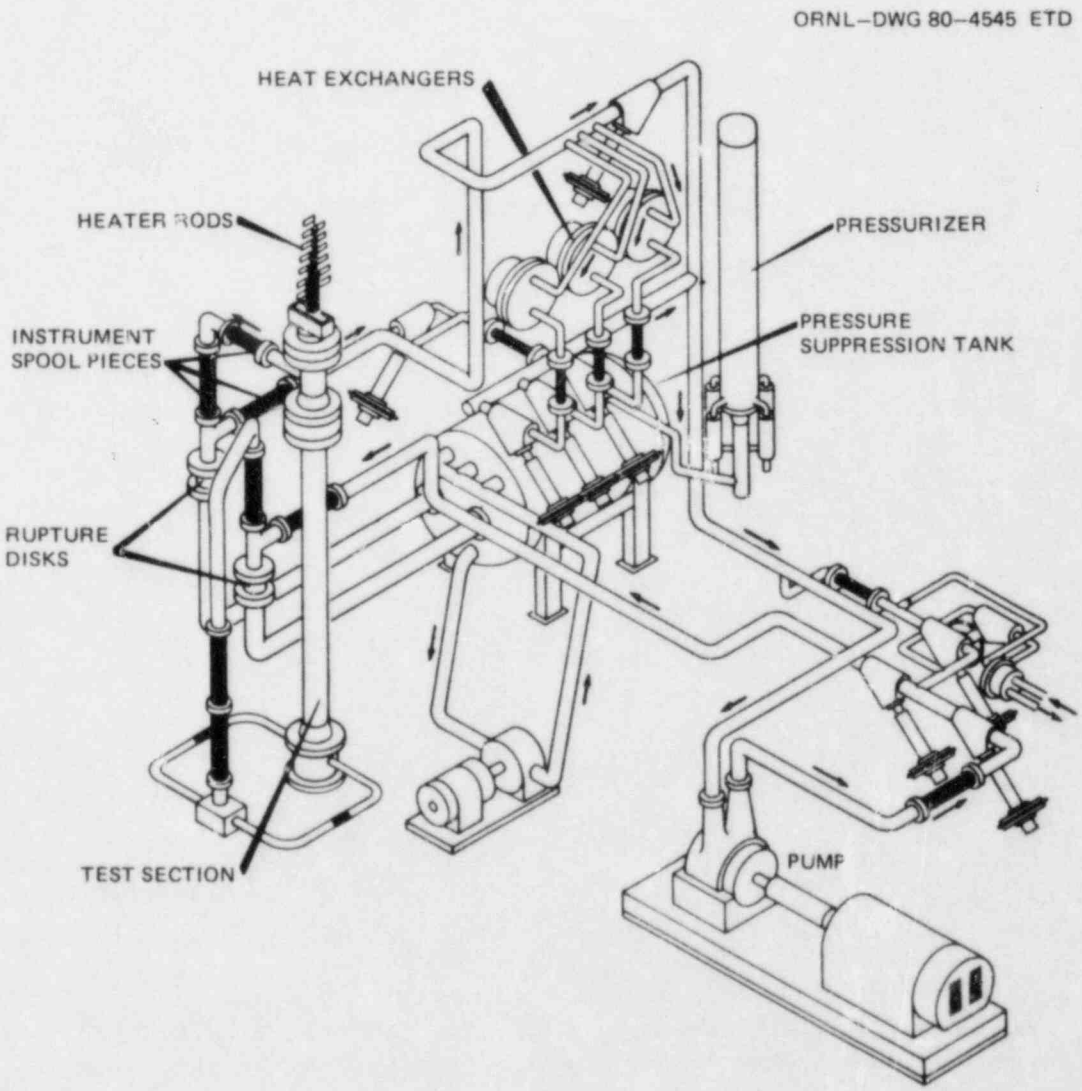

Fig. 3.4. THTF in standard configuration.

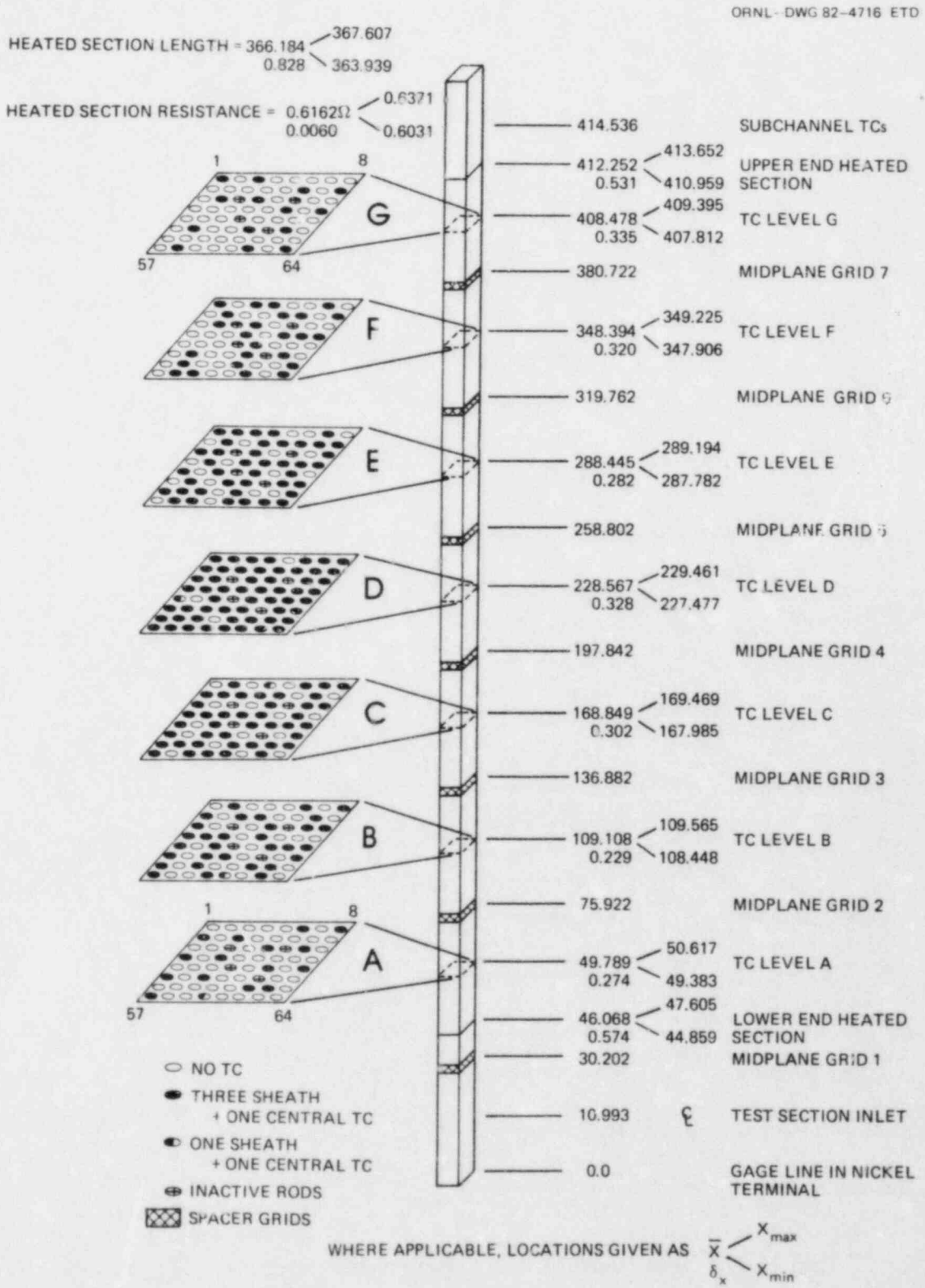

Fig. 3.5. Location of thermocouples in THTF Bundle 3. All dimensions are in centimeters and are referenced to the gage line in the nickel terminal.

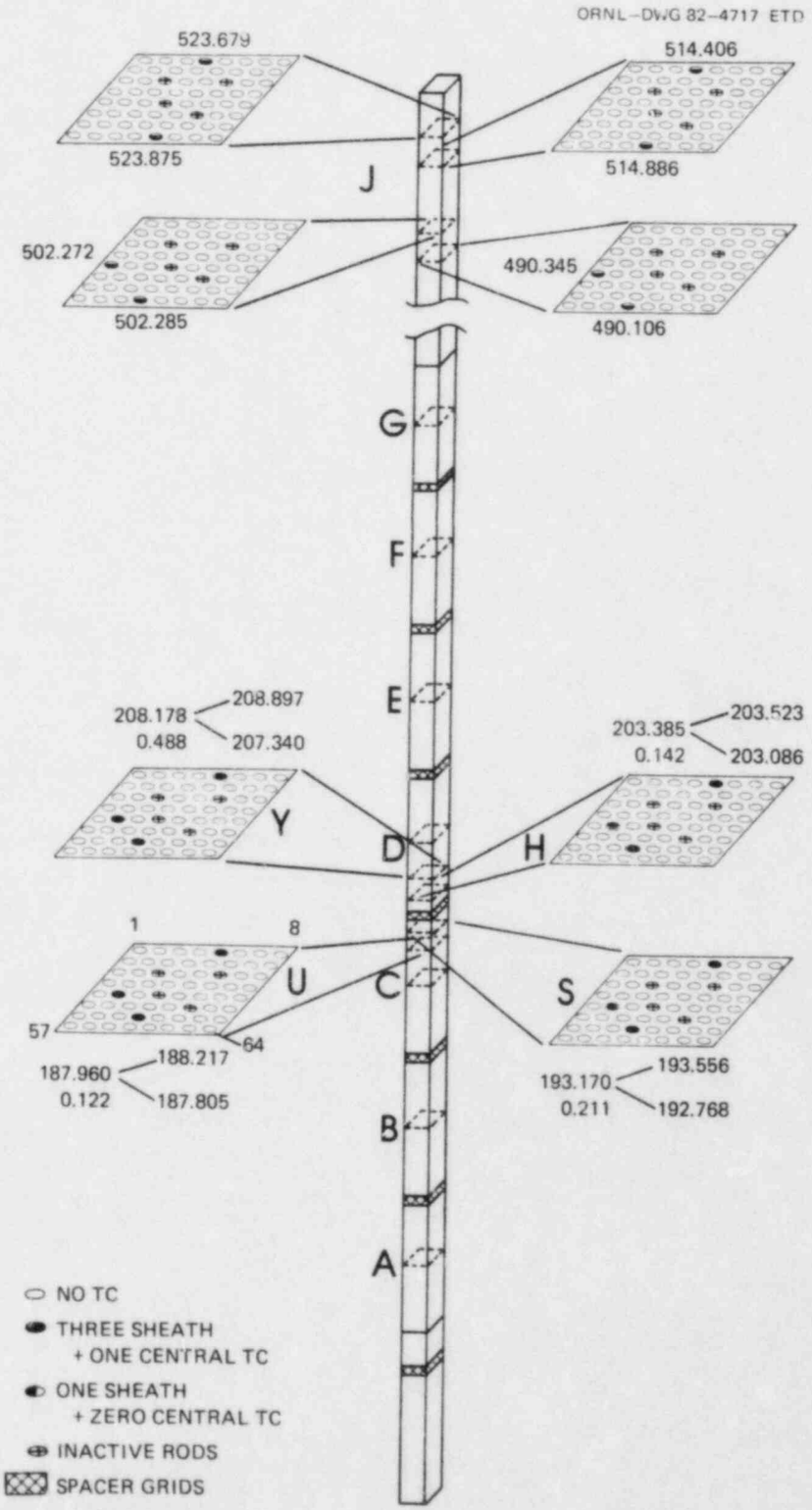

Fig. 3.6. Special thermocouple locations in THTF Bundle 3. All dimensions are in centimeters and are referenced to the gage line in the nickel terminal.

of Bundle 3 giving the location of all primary level FRS thermocouples (levels A–G) in the heated section. Figure 3.6 is a schematic of Bundle 3 illustrating the location of the special FRS thermocouples. These special locations include the Y, H, S, and U levels (rods 5, 34, and 52 grouped between C and D levels in the heated section) and O-ring thermocouples (designated as J level) in rods 4, 33, 60, and 61. Where applicable, locations are given as

$$\bar{X} \lessdot \begin{matrix} X_{max} \\ X_{min} \end{matrix} , \quad S_X$$

where

$\bar{X}$ = statistical mean,
S_X = standard deviation about the mean,
X_{max} = maximum variation about the mean,
X_{min} = minimum variation about the mean.

The nomenclature[9] for Bundle 3 FRS thermocouples takes the following form:

TE-3nnaL ,

where

nn = a number between 01 and 64 (inclusive) equal to the rod (grid) position number,
a = one of three letters (A, B, or C) designating the relative position of the sheath thermocouple to the other two thermocouples in that rod at the designated level. The three thermocouples at a level are labeled A, B, and C in a clockwise direction as viewed from the top of the rod. The centerline thermocouple is designated by the letter M.
L = the level of the thermocouple. A letter in the list A–G (heated section), J (O-ring area), or Y, H, S, and U (four levels grouped between C and D levels in the heated section).

An example of the FRS thermocouple naming convention applied to level F of rod 30 is given in Fig. 3.7.

In total, there are 960 (720 sheath and 240 centerline) FRS thermocouples. Due to a lack of Field Effect Transistor (FET) multiplexers for the computer-controlled data acquisition system (CCDAS), only ~60% of the total number of FRS thermocouples were monitored. As of January 8, 1980, those FRS thermocouples given in Table 3.1 were monitored by the CCDAS. Additionally, 50 FRS thermocouples were monitored by a visual multichannel temperature indicator (Metrascope) in the THTF control room; these thermocouples are not available for the CCDAS, and their responses are essentially lost unless noted visually and recorded by hand. The location and names of these Metrascope thermocouples are indicated in Fig. 3.8.

Table 3.1. In-service thermocouple listing for small-break LOCA test series (8-Jan-80)

Rod	Sheath angle level	Center level
1	AE,[a] AG, BF, CD	MD,[b] ME, MF, MG
2	AB, AE, BC, CD	MB, MC, MD, ME
3	BE, BF, CD, CG	MD, ME, MF, MG
4	AC, BD, BE, CF	MC, MD, ME, MF
5	AS, BH, BU, CY	MH, MS, MU, MY
6	AB, BA, BC, BD	MA, MC, MD
7	AC, AF, CE	MC, MD, ME, MF
8	AA, BC, BD, CB	MB, MC, MD
9	AC, AA, CB, CD	MA, MB, MC, MD
10	AF, BE, CC, CD	MC, MD, ME, MF
11	CA, CB, CC, CD	MA, MB, MC, MD
12	BC, BD, BE, CB	MB, MC, MD, ME
13	BC, BF, CD, CE	MC, MD, ME, MF
14	AD, AE, AF, AG BD, BE, BF, BG, CD, CE, CF	MD, ME, MF, MG
15	AB, AE, BC, CD	MB, MC, MD, ME
16	AD, BF, CE, CG	MD, ME, MF, MG
17	AE, CB, CC, CD	MB, MC, MD, ME
18	AD, AF, BE, BG	MD, ME, MF, MG
19	Rod 19 is unpowered	
20	AD, AE, AF, AG, BD, BE, BF, BG, CD, CE, CF, CG	MD, MF, MG
21	AA, AB, BC, CD	MA, MB, MD
22	Rod 22 is unpowered	
23	AD, BC, CB	MB, MC, MD
24	AC, BD, CB, CE	MC, MD, ME
25	AA, AB, AC, BA, BB, BC, BD, CA, CB, CC, CD	MA, MB, MC, MD
26	AC, BB, BD, CE	MB, MC, MD, ME
27	AA, AB, AC, AD, BA, BB, BC, BD, CA, CB, CC, CD	MA, MB, MC, MD
28	AC, AD, AE, AF, BC, BD, BE, BF, CC, CD, CE, CF	MC, MD, ME, MF
29	AB, AC, AD, AE, BB, BC, BD, BE, CB, CD, CE	MB, MC, MD, ME
30	BF, BG, CD, CE	MD, ME, MF, MG
31	AC, CD, CE, CF	MC, MD, ME, MF
32	AE, AD, AF, AG, BE, BG, CD, CE, CF, CG	MD, ME, MG
33	AC, AD, CB, CE	MB, MC, MD, ME
34	AH, AS, AU, AY, BH, BS, BU, BY, CH, CS, CU, CY	MH, MS, MY
35	AC, BB, BE, CD	MB, MC, MD, ME
36	Rod 36 is unpowered	
37	AE, BC, BD, CF	MC, MD, ME, MF
38	AB, BA, BC, BD	MA, MB, MC, MD
39	AC, BB, BD, BE	MB, MC, MD, ME
40	BC, BD, CA, CB	MA, MB, MC, MD
41	AB, BA, BD, CC	MA, MB, MC, MD
42	BD, BE, CF, CG	MD, ME, MF, MG
43	BA, BB, BC, CD	MA, MB, MC, MD
45	AD, AE, AF, AG, BD, BE, BF, BG, CD, CE, CF, CG	MD, ME, MG
46	Rod 46 is unpowered	
47	AD, AE, AG, BF	MD, ME, MF, MG
48	BC, BD, CB, CE	MB, MC, MD, ME
49	CB, CC, CD, CE	MB, MC, MD, ME
50	AC, AD, AE, AF, BC, BD, BE, BF, CC, CD, CE, CF	MC, MD, ME, MF
51	AB, AE, BC, BD	MB, MC, MD, ME
52	AH, AS, AU, AY, BH, BS, BU, BY, CH, CS, CU, CY	MH, MS, MU, MY
53	AD, AE, AF, CC	MC, MD, ME, MF
54	AD, CA, CB, CC	MA, MB, MC, MD
55	AA, AD, BC, CB	MA, MB, MC, MD
56	AD, AF, BE, CC	MC, MD, ME, MF
57	AA, AB, AC, AD, BA, BB, BC, BD, CA, CB, CC, CD	MA, MB, MC, MD
58	BE, CD, CF, CG	MD, ME, MF, MG
59	AD, AE, CC, CF	MC, MD, ME, MF
60	AA, AB, AC, AD	MA, MB, MC, MD
61	AB, AC, AD, CE	MB, MC, MD
62	AD, AE, AF, CG	MD, ME, MF, MG
63	AD, BC, BE, CB	MB, MC, MD, ME
64	AD, AE, AF, AG, BD, BE, BF, BG, CD, CE, CF, CG	MD, MF, MG

[a] Thermocouple TE-301AE is a sheath thermocouple in rod 1 at angle A on level E.

[b] Thermocouple TE-301MD is a centerline thermocouple (M) in rod 1 at level D.

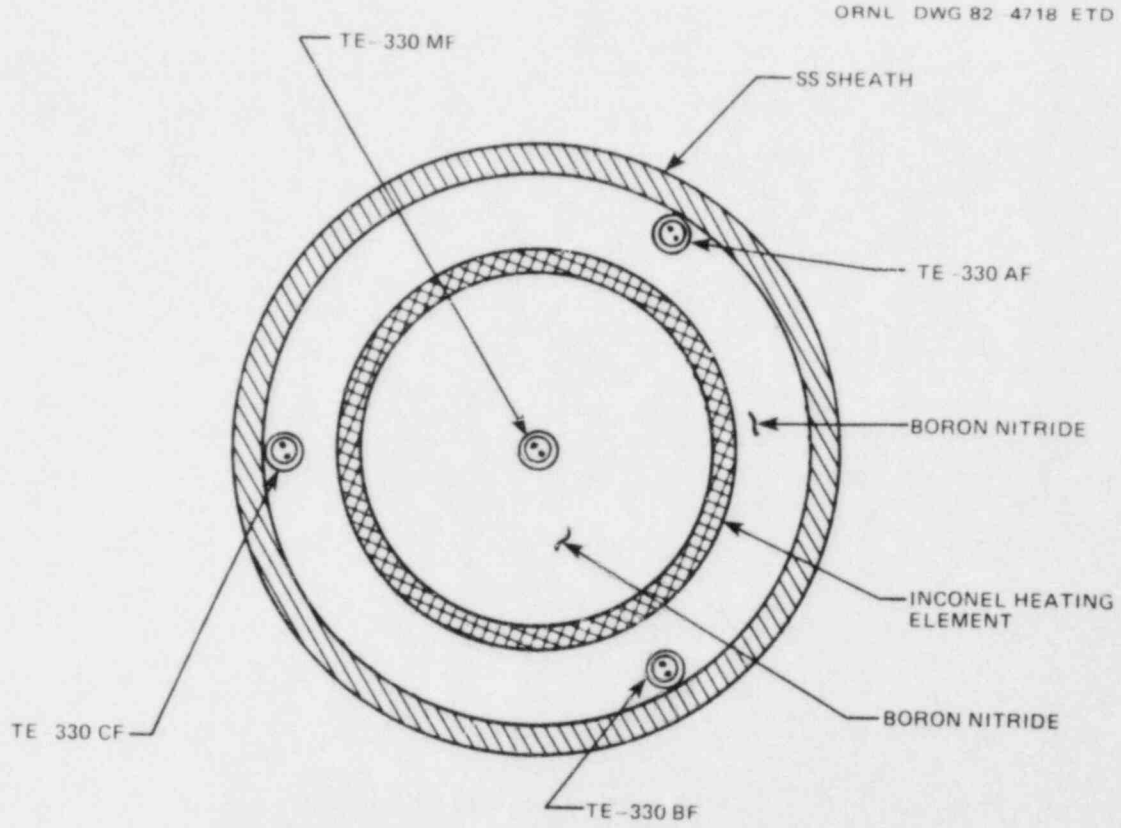

Fig. 3.7. Example of FRS thermocouple nomenclature.

In addition to the FRS thermocouples, the TFTF Bundle 3 instrumentation also monitors the core fluid temperature. Figure 3.9 is a schematic of Bundle 3 giving the axial and subchannel location of the *fluid* thermocouples in the core. In this sense, "fluid" encompasses all the subchannel, grid, shroud-box, and thermocouple-array rod thermocouples. Because distinguishing subchannels in Fig. 3.9 is somewhat difficult, more detailed location figures and the naming convention for the core fluid thermocouples are presented in Appendix A.

The remaining instrumentation of note in Bundle 3 was a liquid level rod occupying position 22 in the grid. This liquid level detector system, purchased from EG&G Idaho, Inc., for use in the BDHT Program,[10] consists of an assembly of 19 sensing elements mounted in a probe (rod) plus an electronics package that provides signal conditioning, signal readout, and an output signal for the CCDAS. The probe sensing elements consist of small electrodes surrounded by cylindrical ground planes. The presence or absence of liquid at each sensing element is detected by measurement of the electrical conductivity between the electrode and the ground plane. The axial location of these 19 sensing elements in Bundle 3 is presented in Fig. 3.10 (Ref. 11).

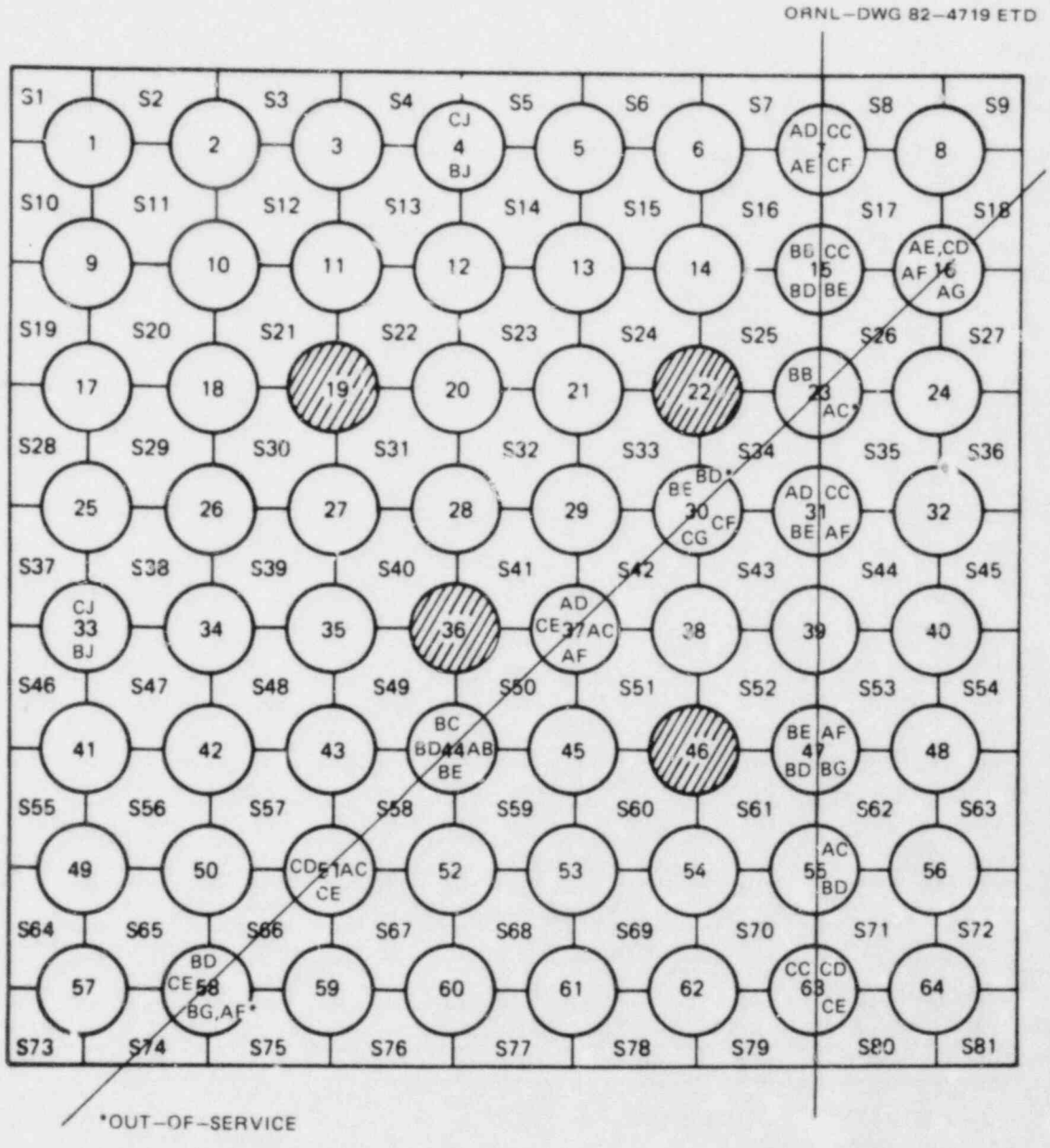

Fig. 3.8. Metrascope thermocouples.

3.2 Operating History

After installation of Bundle 3 in the THTF test section on June 26, 1979, the arduous tasks of modifying the THTF loop piping (to the configuration in Fig. 3.4) and instrumentation installation and verification remained. In addition, following the discovery of a leakage path between the test section core and the surrounding annulus, the bundle was raised out of the test section and the shroud walls were seam-welded to reduce

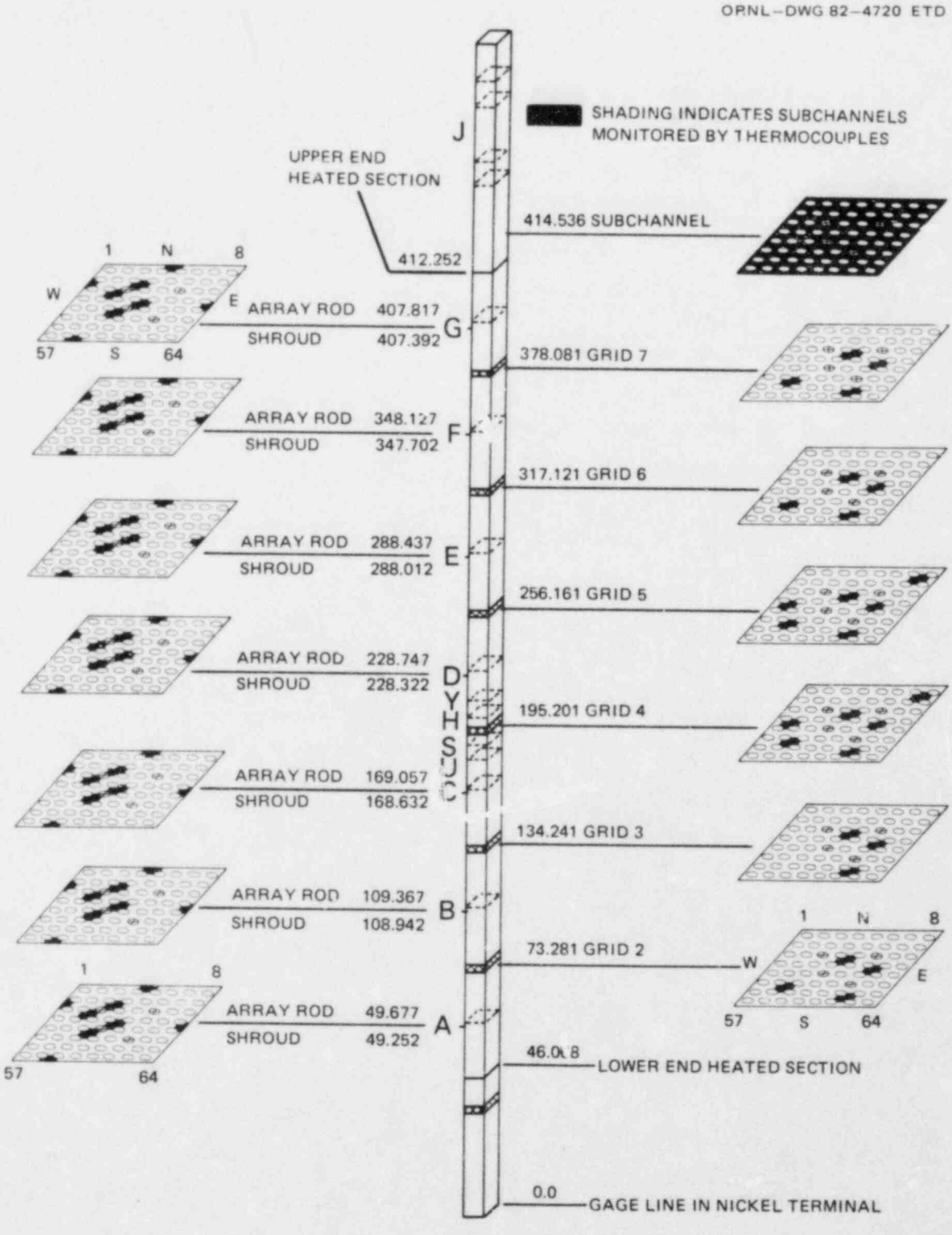

Fig. 3.9. Location of fluid thermocouples in THTF Bundle 3. All dimensions are in centimeters and are referenced to the gage line in the nickel terminal.

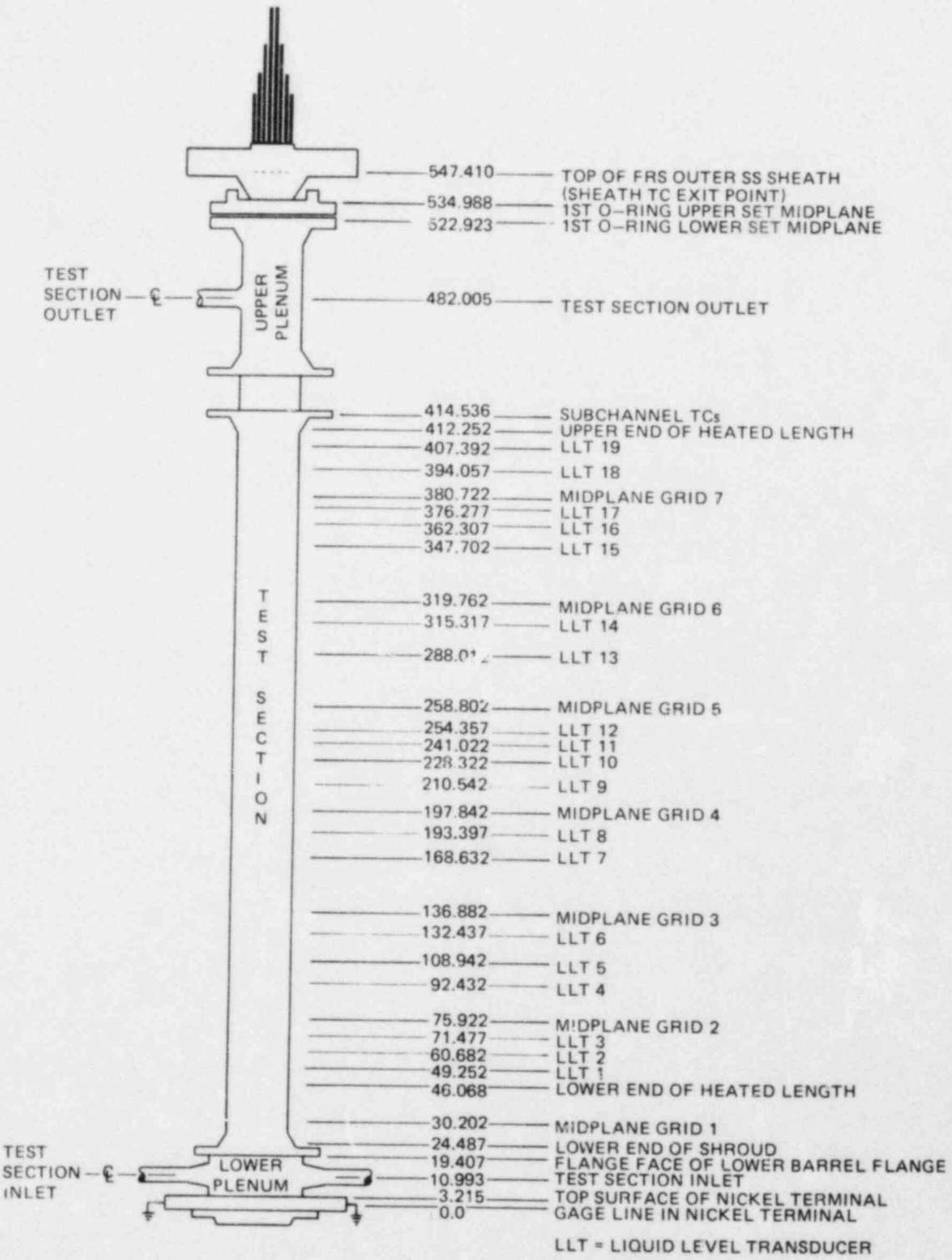

Fig. 3.10. Nominal location of critical points in THTF Bundle 3 and the axial position of the 19 liquid level sensing elements.

the leakage rate to <40 cm³/min [at a pressure differential of 0.34 MPa (50 psi) and room temperature]. The leakage rate prior to the welding fix was ~540 cm³/min.[12]

On November 2, 1979, the first test was conducted using Bundle 3 in the THTF. The test was a double-ended isothermal blowdown (test 3.01.5A) and was intended to be a shakedown for the new instrumentation and a source of information on the hydrodynamic response of the THTF with Bundle 3 installed. The approximate conditions at blowdown were (1) test section temperature of 478 K (400°F), (2) test section flow of 0.035 m³/s (500 gpm), and test section outlet pressure of 14.82 MN/m² (2150 psig). The break areas were 50% on the inlet and 60% on the outlet, where 100% refers to a nominal break area of 0.00125 m² (0.0135 ft²).[13]

Bundle characterization (calibration) tests were attempted on November 29 and December 11, 1979; however, neither test was successful. These tests, the first powered operation of Bundle 3, were designed to gain data that would allow in situ determination of the FRS thermal-physical properties as a function of temperature.[14] The tests were aborted on each occasion because of a trip of the crowbar system (bundle protection). The crowbar system involves fault detection devices that remove voltage from each FRS if any overcurrent condition develops. These trips were apparently spurious (i.e., not caused by an unsafe condition); modifications and testing of the crowbar system were initiated to eliminate the trip problem but still ensure safe power operations with the bundle.

After the bundle characterization test on December 11, the THTF loop configuration was changed for the small-break LOCA test series. A schematic of the THTF for these tests is presented in Fig. 3.11. The first of these tests was conducted on December 21, and the bundle was uncovered for a total of ~39 min. Further tests were completed on January 9, 1980, with the bundle being uncovered for ~187 min. A test series summary is presented in Table 3.2.

On completion of the small-break LOCA test series, the loop piping was changed to its standard configuration (Fig. 3.4), and another attempt was made to run the bundle classification tests. At this time, the bundle inner-seal coolant pressure [O-ring intermediate coolant cavity at the terminal end of the FRS (Fig. 3.3)] tracked the primary system pressure, thus indicating inner O-ring failure, possibly due to the severe conditions encountered in the small-break LOCA tests. The bundle characterization test was performed on February 15, 1980; at a power level of ~80 kW per rod (the highest power yet attained in the bundle), the crowbar system tripped on all generators. After the abort of the classification tests, power was applied to each individual rod to determine the cause of the crowbar problem. During these individual rod power tests on February 19 and 20, the outer O-rings began leaking badly, and system pressure could not be maintained; also 4 of the 60 FRSs were unable to reach full power without a fault condition (crowbar) occurring.

On February 26, the THTF operations staff began removing FRSs from the bundle to replace the damaged O-rings. It was found that severe electrical arcing had occurred in the FRS terminal end "Christmas tree;" in fact, rod 54 and the dummy rod in 46 had to be removed at the same time because they were welded together. All rods were removed from the test section by March 13.

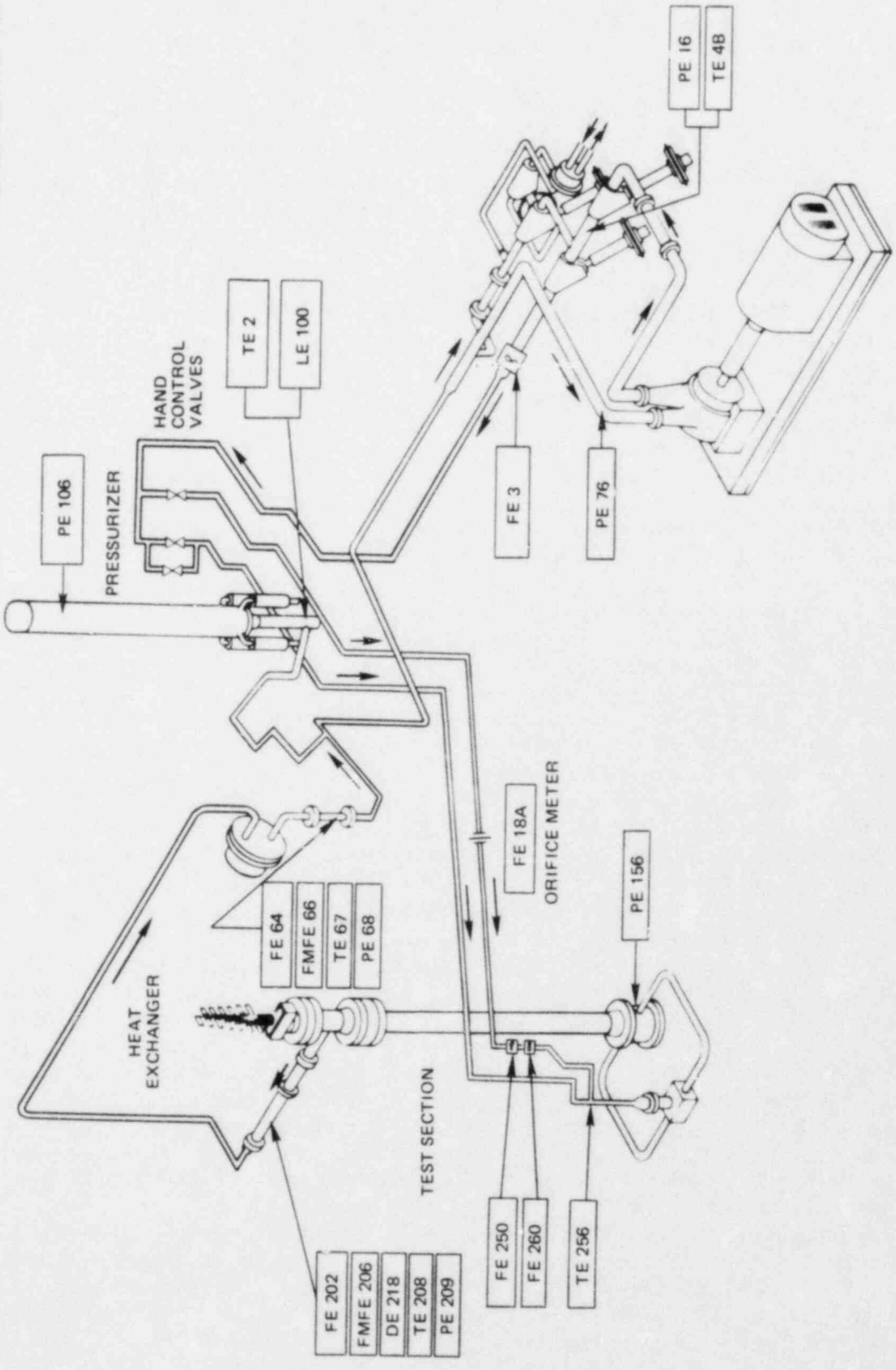

Fig. 3.11. THTF configuration for the small-break LOCA test series.

Table 3.2. Small-break LOCA test series summary

Power [kW/m (kW/ft)]	Pressure [MN/m^2 (psia)]	Maximum rod surface temperature [K (°F)]	Maximum steam temperature [K (°F)]	Maximum surface to steam ΔT [K (°F)]	Inlet temperature [K (°F)]	Outlet temperature [K (°F)]	Flooding rate [cm/s (in./s)]	Quench front velocity [cm/s (in./s)]		Initial collapsed liquid level [m (in.)]	Uncovery height [m (in.)]
								E-F	F-G		
1.050 (0.320)	6.96 (1010)	991 (1325)	889 (1140)	103 (185)	520 (476)	555 (540)	16.18 (6.37)	7.16 (2.82)	[a]	[b]	2.134 ± 0.3 (84 ± 12)
0.656 (0.200)	4.55 (660)	981 (1306)	813 (1003)	168 (303)	478 (400)	566 (560)	21.44 (8.44)	7.01 (2.76)	[a]	[b]	2.134 ± 0.3 (84 ± 12)
1.312 (0.400)	2.90 (420)	1024 (1383)	797 (975)	227 (408)	467 (381)	696 (794)	20.32 (8.00)		3.30 (1.30)	1.854 (73)	2.743 ± 0.3 (108 ± 12)
0.974 (0.297)	4.27 (620)	1044 (1419)	894 (1150)	149 (269)	464 (375)	714 (825)	16.00 (6.30)	7.16 (2.82)	4.90 (1.93)	1.740 (68.5)	2.134 ± 0.3 (84 ± 12)
1.444 (0.440)	4.27 (620)	1070 (1466)	846 (1064)	223 (402)	482 (408)	740 (872)	22.86 (9.00)		6.86 (2.70)	1.753 (69)	2.743 ± 0.3 (108 ± 12)
0.951 (0.290)	7.03 (1020)	1046 (1423)	879 (1122)	167 (301)	513 (464)	678 (761)	2.79 (1.10)		1.63 (0.64)	1.956 (77)	2.134 ± 0.3 (84 ± 12)
1.319 (0.402)	6.95 (1008)	1058 (1444)	839 (1050)	219 (394)	514 (466)	746 (883)	7.75 (3.05)	2.62 (1.03)	3.43 (1.35)	1.798 (70.8)	2.134 ± 0.3 (84 ± 12)
1.476 (0.450)	2.41 (350)	1047 (1425)	823 (1021)	224 (404)	460 (368)	658 (725)	5.84 (2.30)	2.31 (0.91)	2.69 (1.06)	1.313 (51.7)	2.134 ± 0.3 (84 ± 12)

[a] Not applicable.

[b] Not applicable because of injection of seal cooling water.

3.3 Postscript[15]

Initial visual examination of the FRSs after removal from the THTF indicated that some had been overheated in the O-ring seal region. Several rods exhibited local swelling of the clad and had severely burned O-rings. All rods were transferred to the FRS Technology Development Laboratory (TDL) for further investigation.

Meanwhile, investigation of the terminal arcing problem revealed flaws in the FRS crowbar circuits that apparently caused voltage feedback and interference. These flaws were corrected. Additionally, it was decided that the FRS terminal ends would be electrically insulated prior to reinsertion in the THTF to provide further assurance against future arcing.

A schematic of the upper test section in the THTF Bundle 3, illustrating the O-ring locations, is given in Fig. 3.12. Because the FRSs are bolted to the nickel terminal in the bottom of the test section, thermal expansion of the rods is allowed via the arrangement shown in Fig. 3.12. Details of the O-ring set construction are shown in Fig. 3.13. The grooves for the O-rings are formed by slip-on ferrules; each ferrule is attached to the FRS stainless steel sheath in four places by a tungsten-inert gas (TIG) weld. Several rods were damaged in the O-ring region as evident in the visual examination. By isolating the FRS sheath from the Inconel heating element, the electrical resistance of the BN insulation could be measured; thus, it was possible to determine how many of the FRSs were damaged and how severe the damage was. The results of the tests are summarized in Table 3.3. Sixty percent of the FRSs had insulation resistances below the acceptance criteria (considered damaged), while 33% measured $<10^3$ Ω and were thus considered severely damaged. To determine the

Table 3.3. Results of annular insulation resistance checks on FRS removed from the THTF Bundle 3

Insulation resistance (Ω)	Number of rods	
	Originally	After removal
$>10^{12}$	8	2
$>10^9$	52	22
$>10^6$	0	7[a]
$>10^3$	0	8[a]
$<10^3$	0	21[a]
Total	60	60

[a]Damaged.

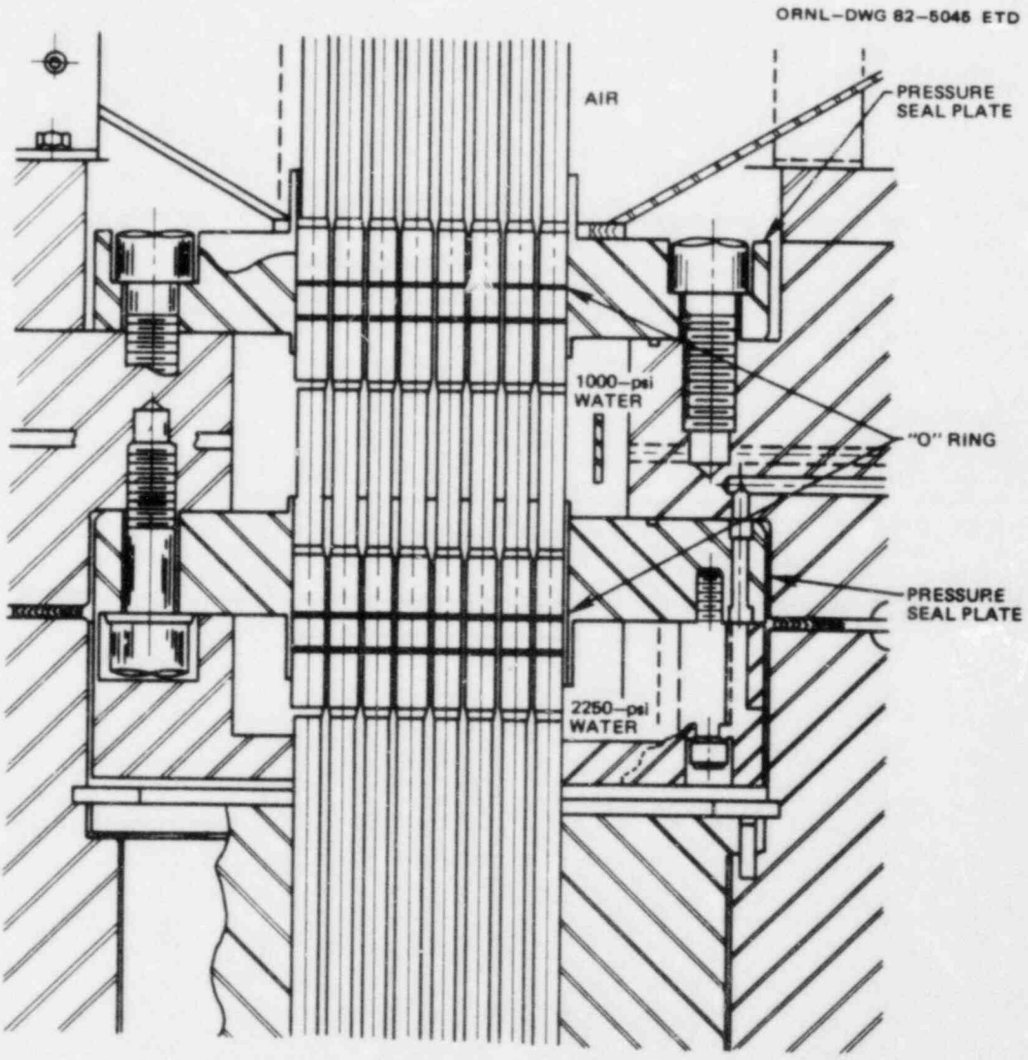

Fig. 3.12. Upper test section of the THTF Bundle 3.

location of the short circuit in the FRS, a variable power source was connected across the BN insulation (i.e., between the heating element and the sheath); thus, those regions that were low in insulation resistance would permit current flow and localized heating. All severely damaged rods exhibited heating in the O-ring region adjacent to one or more sets of the ferrule welds. In fact, BN and steam and water spewed from some of the welds as they were heated; thus, many of the TIG welds obviously had punctured the sheath, exposing the annular BN insulation to water.

Techniques were developed by the FRS TDL to dehydrate the FRSs; as a result, 52 of the original 60 Bundle 3 FRSs were salvaged. Eight permanently damaged FRSs were replaced with spare simulators. Also, a new single-piece O-ring oversleeve (instead of the six separate ferrules) was designed, fabricated, and installed on all FRSs (Fig. 3.14). An inspection and *safe* braze process were used, and helium leak, dye penetrant, and electrical checks were incorporated to assure reliable FRS repair.

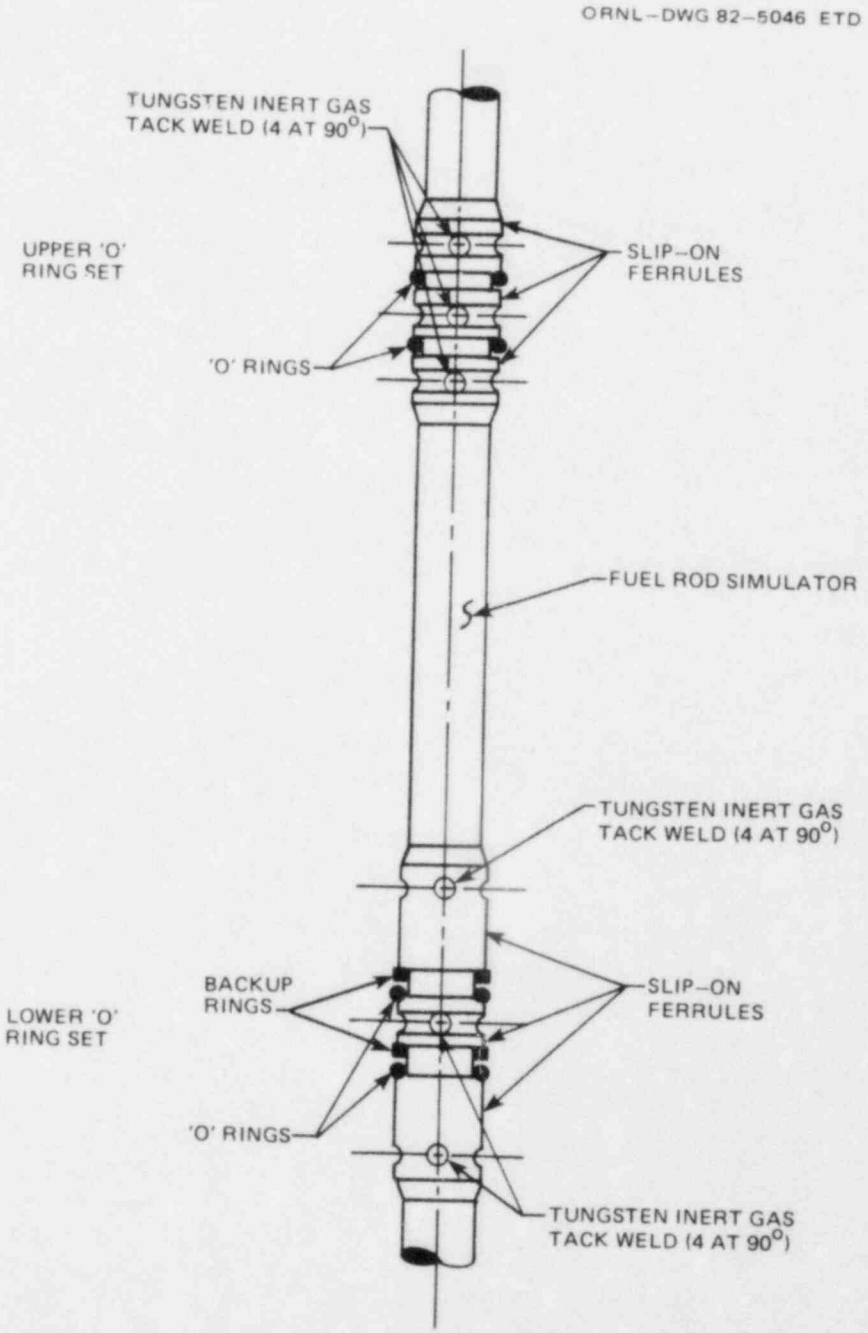

Fig. 3.13. Details of THTF Bundle 3 FRS O-ring region.

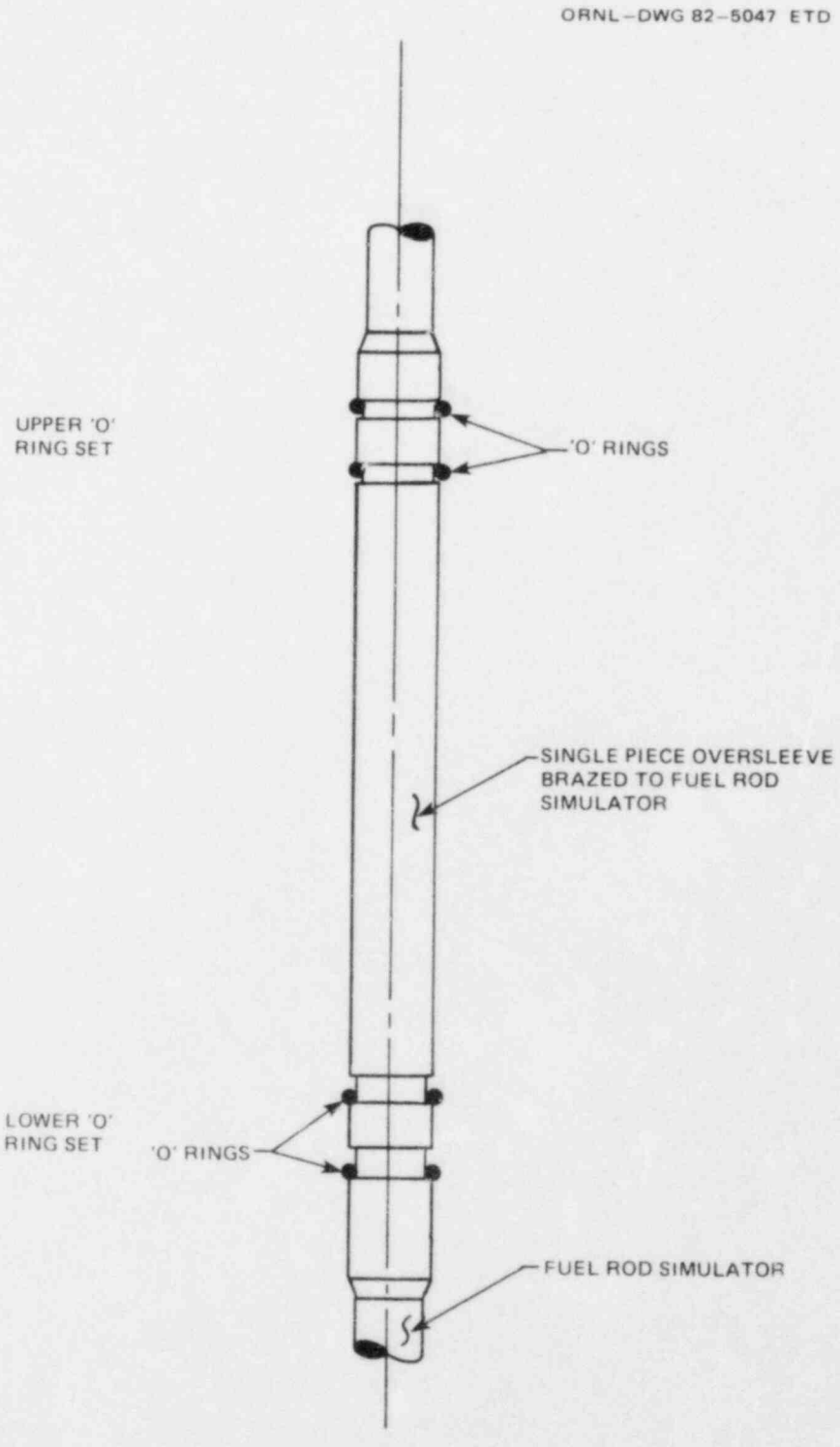

Fig. 3.14. Refurbished THTF Bundle 3 FRS O-ring region.

An additional advantage of this O-ring oversleeve was realized when the THTF pressure seal plates (Fig. 3.12) were examined. The rod penetration holes in the seal plate had been chrome plated to provide a smooth surface for movement of the O-rings during rod thermal expansion; however, the chrome plating either had not adhered properly or had been damaged by high temperature. The oversleeves increased the O-ring OD sufficiently to permit reaming and polishing of the seal plate holes, thus removing all traces of chrome plating while still permitting a pressure seal.

4. REFURBISHED THTF BUNDLE 3 (March-July 1980)

4.1 Core Configuration and Instrumentation

The BDHT operations staff began installing the refurbished FRSs in the THTF test section on April 17, 1980; this task was completed on April 25. As stated previously, eight of the original Bundle 3 FRSs had been severely damaged and could not be repaired by the FRS TDL. Therefore, these simulators were replaced with back-up simulators. Seven of these replacement FRSs were preproduction models of the original Bundle 3 rods; these FRSs contain ten thermocouples (six sheath and four centerline) divided between four axial levels (level D has the normal contingent of one centerline and three sheaths and the remaining three levels have a centerline-sheath pair only). The eight replacement rod positions are cross-hatched in Fig. 4.1. The axial levels monitored by each rod are indicated in Fig. 4.2.

A schematic[16] of the refurbished Bundle 3 giving the location of all primary level (A-G) FRS thermocouples is presented in Fig. 4.3; also, the location of the special FRS thermocouples (levels Y, H, S, U, and J) in the refurbished bundle are given in Fig. 4.4. The naming convention for these FRS thermocouples is the same as that given in Sect. 3.1. As of May 2, 1980, those FRS thermocouples presented in Table 4.1 were monitored by the CCDAS.

The core fluid temperatures are also monitored by thermocouples; the axial and subchannel location of all fluid thermocouples in the refurbished core are presented in the schematic in Fig. 4.5. The only changes in the locations given in Figs. 4.5 and 3.9 (and Appendix A) are the loss of the subchannels monitored by the thermocouple-array rod thermocouples in grid position 36 in the original bundle. One of the original thermocouple-array rods was damaged beyond repair and was replaced in the grid by a dummy rod.

In addition, pressure taps were installed along the test section during this time. This modification was primarily intended to provide improved test section instrumentation for the second small-break LOCA test series. The locations will be described in Sect. 5 along with additional instrumentation improvements.

4.2 Operating History

A week after the installation of the refurbished Bundle 3 in the THTF test section, the first successful high-powered test using Bundle 3 was completed. On May 3, a power-drop calibration test (from 90 kW/rod) was run, and ~2 weeks later (May 15) a second power-drop calibration test (from 120 kW/rod) was completed. These tests, the first powered operation of the refurbished Bundle 3, were designed to gain data that would allow in situ determination of the FRS thermal-physical properties as functions of temperature. The approximate test conditions for the May 3 and May 15 power drops are presented in Table 4.2.

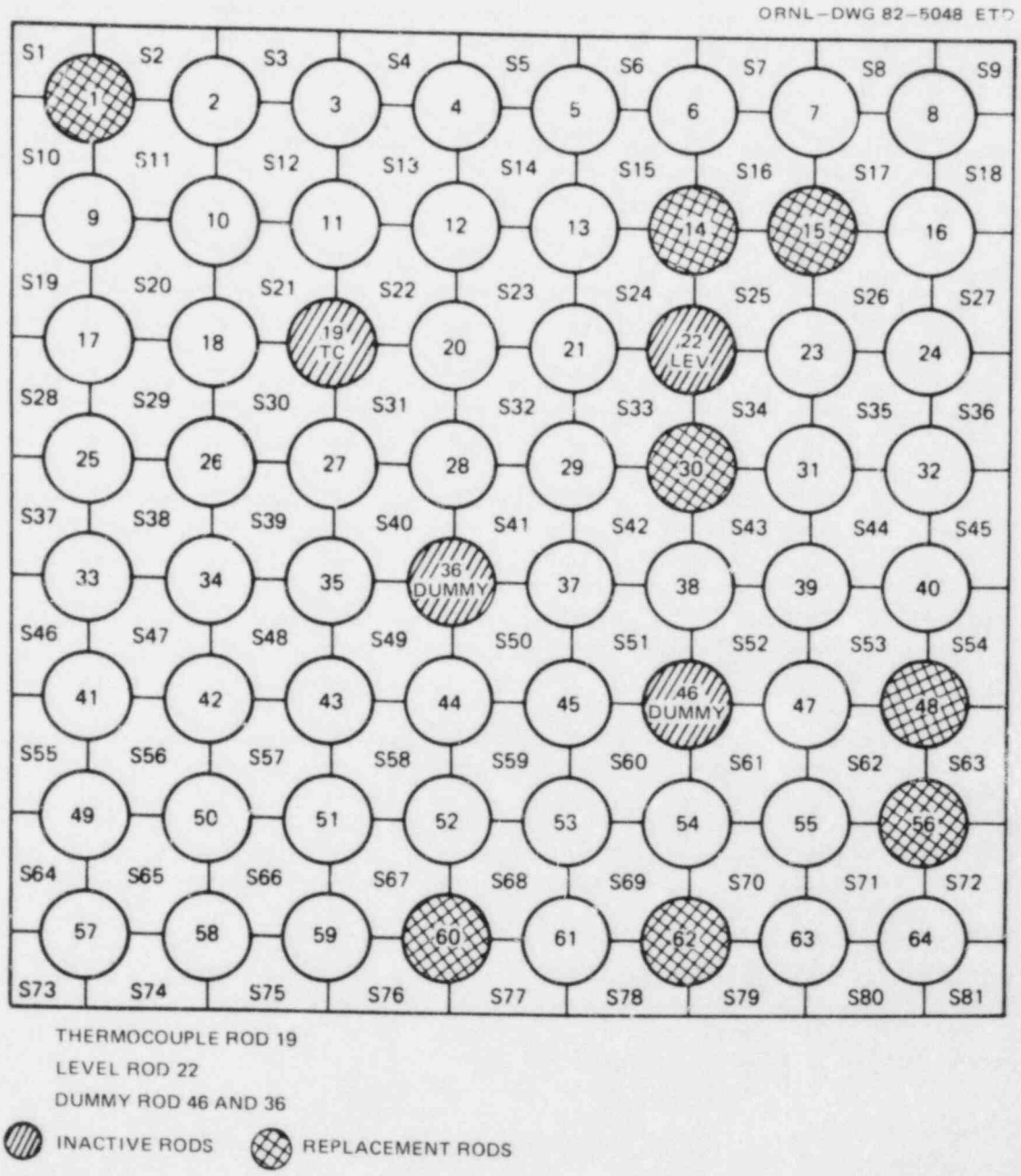

Fig. 4.1. Identification of THTF heater rods, subchannel locations, and inactive rods in refurbished THTF Bundle 3 (March–July 1980).

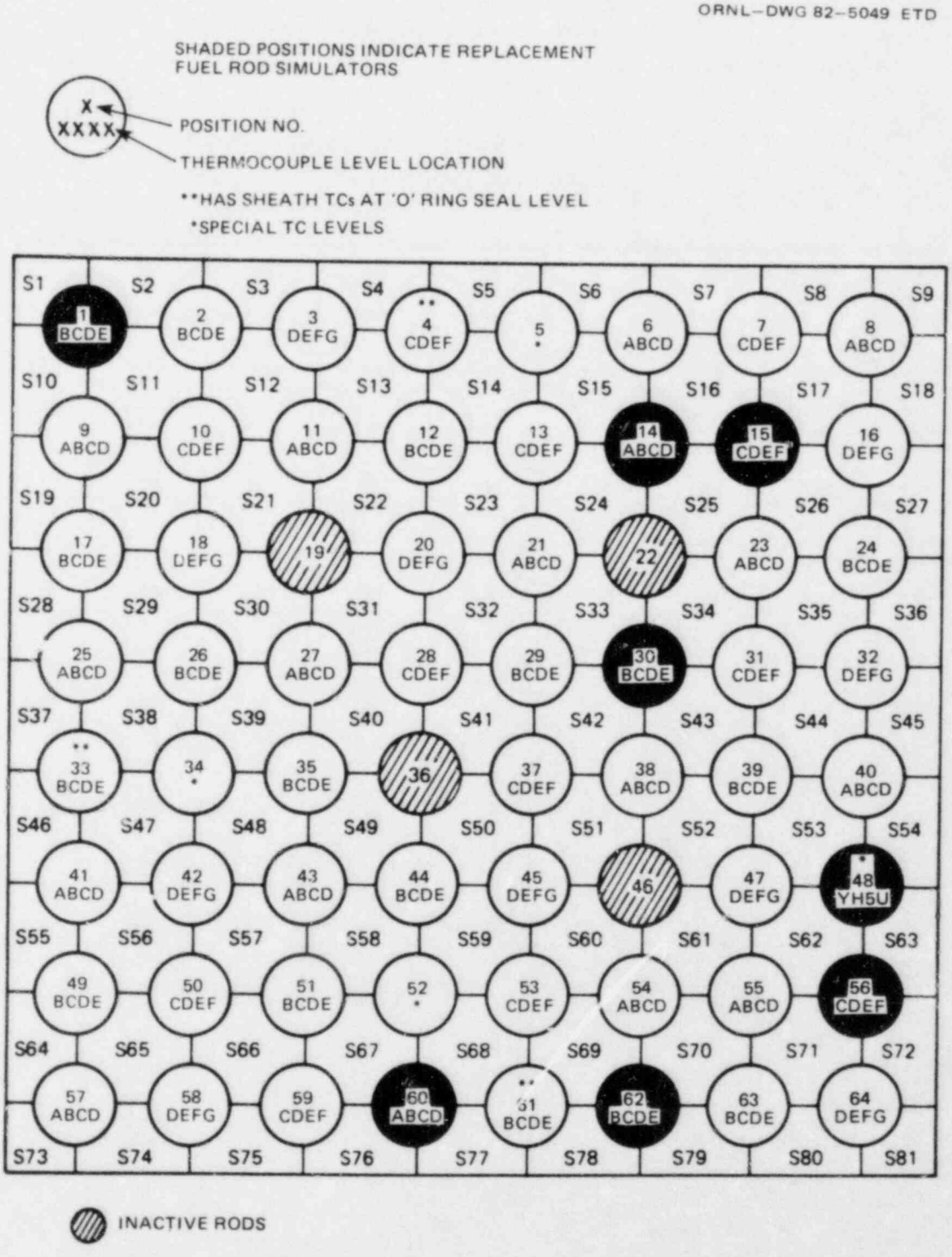

Fig. 4.2. Identification of THTF heater rods and axial thermocouple levels monitored by each rod in the refurbished THTF Bundle 3 (March–July 1980).

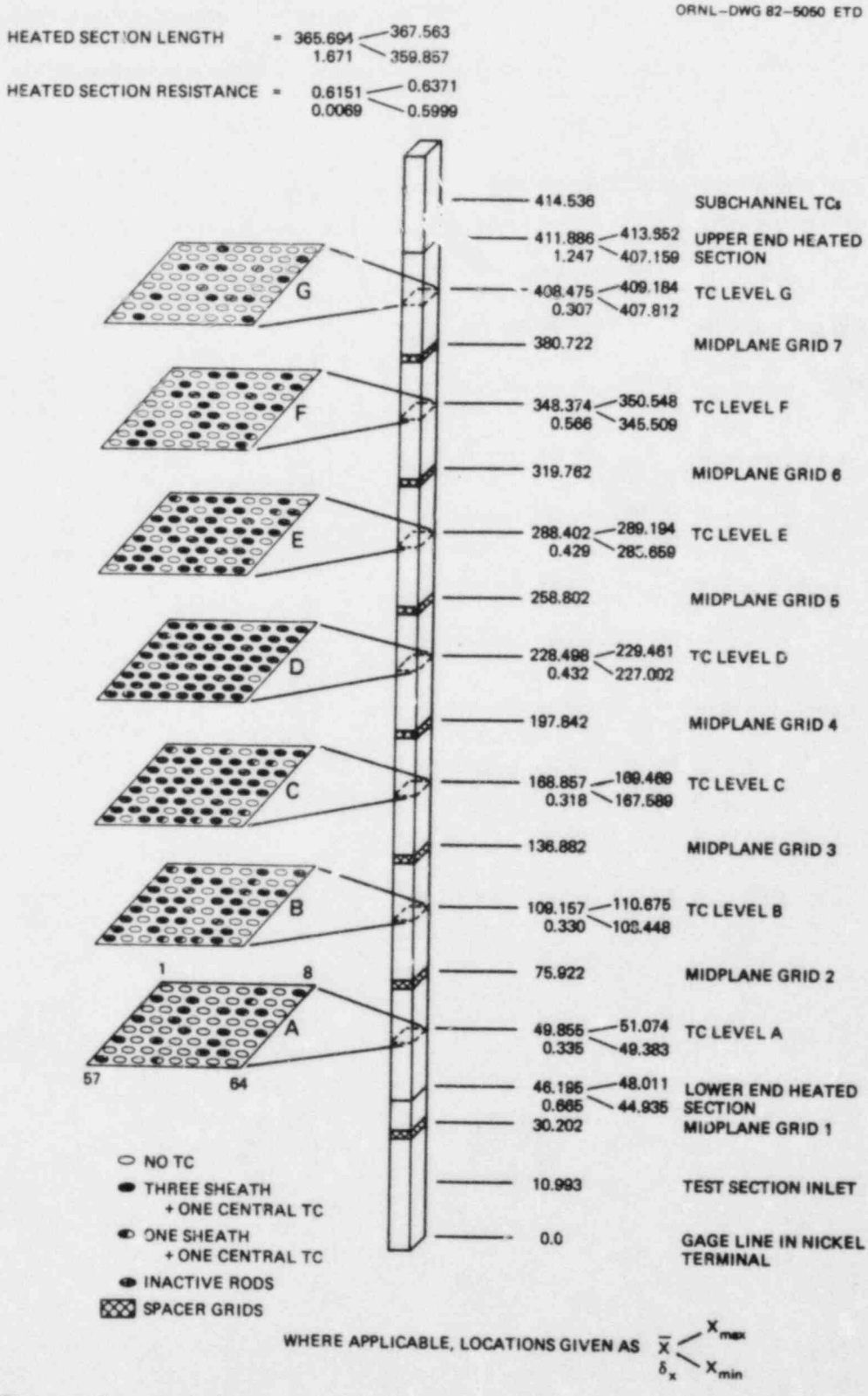

Fig. 4.3. Location of thermocouples in refurbished THTF Bundle 3 (March-July 1980). All dimensions are in centimeters and are referenced to the gage line in the nickel terminal.

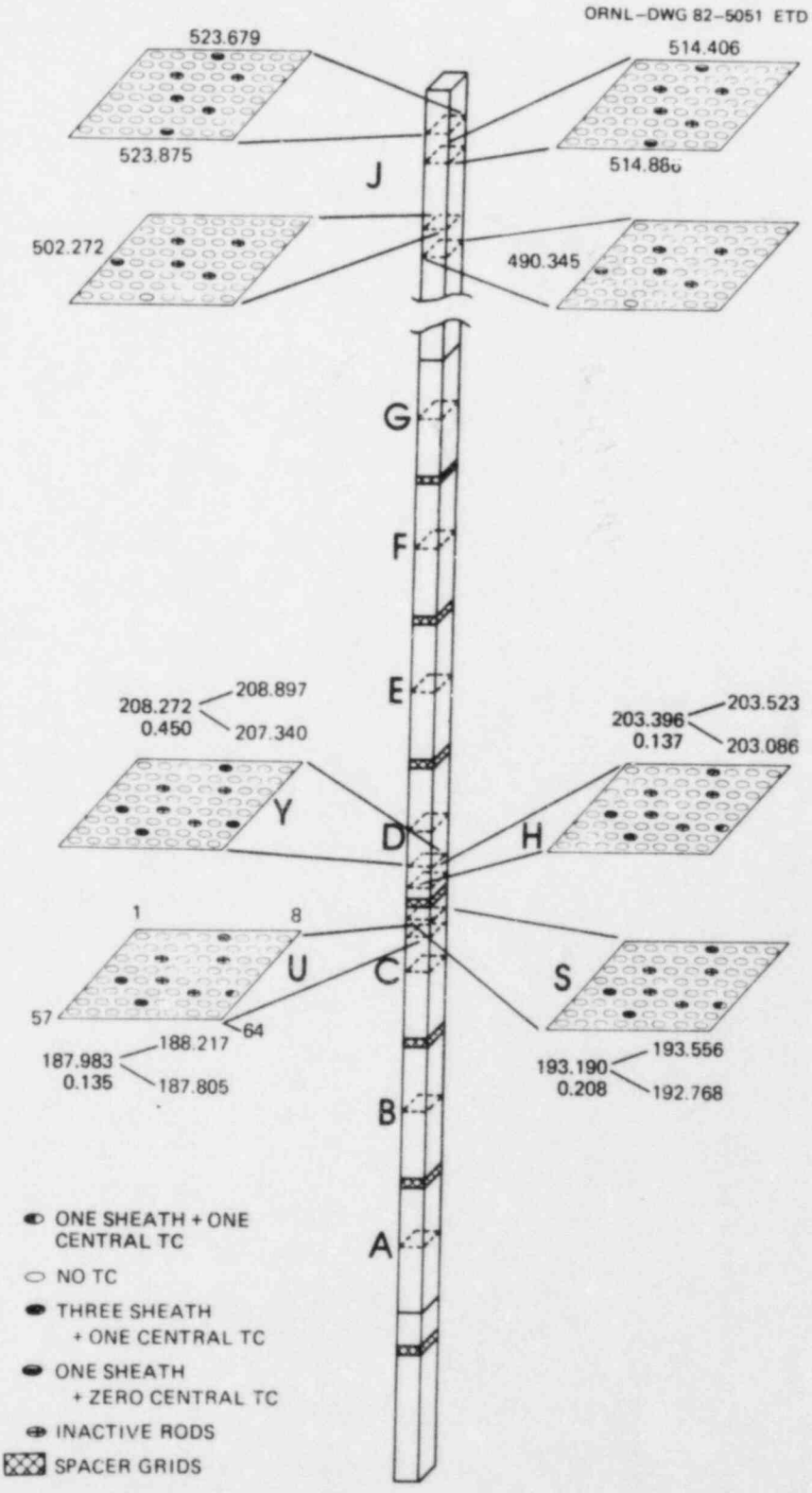

Fig. 4.4. Special thermocouple locations in refurbished THTF Bundle 3 (March–July 1980). All dimensions are in centimeters and are referenced to the gage line in the nickel terminal.

Table 4.1. In-service thermocouple listing for Bundle 3 power-drop test (02-May-80)

Rod	Sheath angle level	Center level
1	AB, AD, AC, AE	MB, MC, MD, ME
2	AB, AD, AE, BC	MB, MC, MD, ME
3	BE, BF, CD, CG	MD, ME, MF, MG
4	AC, BD, BE, BF	MC, MD, ME, MF
5	AS, BH, BU, CY	MH, MS, MU, MY
6	AA, AB, BC, BD	MA, MC, MD
7	AC, AF, CE	MC, MD, ME, MF
8	BB, BC, BD, CB	MB, MC, MD
9	AC, BA, CB, CD	MA, MB, MC, MD
10	AF, BE, CC, CD	MC, MD, ME, MF
11	AA, AD, CB, CC	MA, MB, MC, MD
12	AD, AE, BC, CB	MB, MC, MD, ME
13	BC, BF, CD, CE	MC, MD, ME, MF
14	AA, AB, AC, BD	MA, MB, MC, MD
15	AC, AD, AE, AF	MC, MD, ME, MF
16	AD, BF, CE, CG	MD, ME, MF, MG
17	AE, CB, CC, CD	MB, MC, MD, ME
18	AD, AF, BE, BG	MD, ME, MF, MG
19	Rod 19 is unpowered	
20	AD, AE, AF, AG, BD, BE, BF, BG, CD, CE, CF, CG	MD, MF, MG
21	AA, AB, BC, CD	MA, MB, MD
22	Rod 22 is unpowered	
23	AA, AD, BC, CB	MB, MC, MD
24	AC, BD, CB, CE	MC, MD, ME
25	AA, AB, AC, BA, BB, BC, BD, CA, CB, CC, CD	MA, MB, MC, MD
26	AC, BB, BD, CE	MB, MC, MD, ME
27	AA, AB, AC, AD, BA, BB, BC, BD, CA, CB, CC, CD	MA, MB, MC, MD
28	AC, AD, AE, AF, BC, BD, BE, BF, CC, CD, CE, CF	MC, MD, ME, MF
29	AB, AC, AD, AE, BB, BC, BD, BE, CB, CD, CE	MB, MC, MD, ME
30	CB, CC, CD, CE	MB, MC, MD, ME
31	AC, CD, CE, CF	MF
32	AD, AF, AG, BE, BG, CD, CE, CF, CG	MD, ME, MG
33	AC, AD, CB, CE	MB, MC, MD, ME
34	AH, AS, AU, AY, BH, BS, BU, BY, CH, CS, CU, CY	MH, MS, MY
35	AC, BB, BE, CD	MB, MC, MD, ME
36	Rod 36 is unpowered	
37	AE, BC, BD, CF	MC, MD, ME, MF
38	AB, BA, BC, BD	MA, MB, MC, MD
39	AC, BB, BD, BE	MB, MC, MD, ME
40	BC, BD, CA, CB	MA, MB, MC, MD
41	AB, BA, BD, CC	MA, MB, MC, MD
42	BD, BE, CF, CG	MD, ME, MF, MG
43	BA, BB, BC, CD	MA, MB, MC, MD
44	CB, CC, CD, CE	MB, MC, ME
45	AD, AE, AF, AG, BD, BE, BF, BG, CD, CE, CF, CG	MD, ME, MG
46	Rod 46 is unpowered	
47	AD, AE, AG, BF	MD, ME, MF, MG
48	AH, AS, AU, AY	MH, MS, MU, MY
49	CB, CC, CD, CE	MB, MC, MD, ME
50	AC, AD, AE, AF, BC, BD, BE, BF, CC, CD, CE, CF	MC, MD, ME, MF
51	AB, AE, BC, BD	MB, MC, MD, ME
52	AH, AS, AU, AY, BH, BS, BU, BY, CH, CS, CU, CY	MH, MS, MU, MY
53	AD, AE, AF, CC	MC, MD, ME, MF
54	AD, CA, CB, CC	MA, MB, MC, MD
55	AA, AD, BC, CB	MA, MB, MC, MD
56	AC, AE, AF, CD	MC, MD, ME, MF
57	AA, AB, AC, AD, BA, BB, BC, BD, CA, CB, CC, CD	MA, MB, MC, MD
58	BE, CD, CF, CG	MD, ME, MF, MG
59	AD, AE, CC, CF	MC, MD, ME, MF
60	AB, AC, AD, CD	MA, MB, MC, MD
61	AB, AC, AD, CE	MB, MC, MD
62	AB, AC, AE, CD	MB, MC, MD, ME
63	AD, BC, BE, CB	MB, MC, MD, ME
64	AD, AE, AF, AG, BD, BE, BF, BG, CD, CE, CF, CG	MD, MF, MG

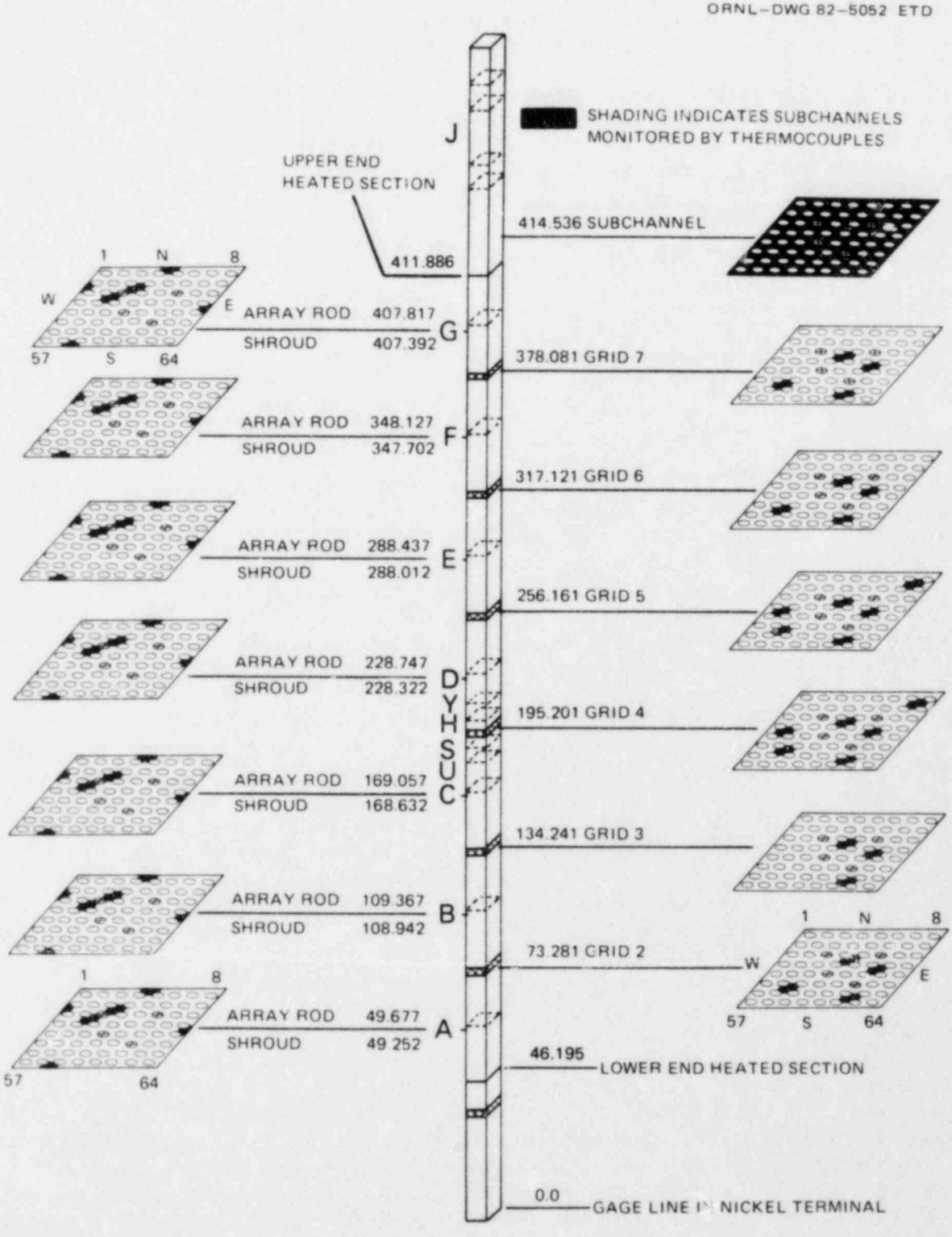

Fig. 4.5. Location of fluid thermocouples in refurbished THTF Bundle 3 (March-July 1980). All dimensions are in centimeters and are referenced to the gage line in the nickel terminal.

Table 4.2. Power-drop bundle characterization test conditions

Test section	May 3	May 15
Average rod power, kW	89.2	119.2
Flow, m^3/s (gpm)	0.022 (350)	0.019 (304)
Inlet temperature, K (°F)	496.8 (434.6)	460.8 (369.9)
Outlet temperature, K (°F)	553.2 (536.1)	549.7 (529.8)
Outlet pressure, MN/m^2 (psia)	13.29 (1928)	13.91 (2018)

With the THTF in standard configuration (Fig. 3.4), the first attempt at a powered blowdown occurred on May 15 (test 3.03.6A) after the power-drop test. Because of a premature trip in rod power, the test was not successful. This test was repeated a week later on May 21 and was successful. The initial conditions for test 3.03.6AR are presented in Table 4.3. The purposes[17] of the experiment were to: (1) obtain transient heat transfer data for film boiling in rod bundle geometry to be used in assessing or developing film boiling heat transfer correlations for use in transient reactor analysis codes, (2) obtain data in the high-flow film boiling data ranges requested by the Nuclear Regulatory Commission (NRC) Office of Nuclear Reactor Regulation, and (3) provide a benchmark for transient reactor analysis codes. The upflow film boiling data ranges are presented in Table 4.4.

On June 19, the second transient film boiling test (3.04.7R) was performed.[18] The purposes of the experiment were the same as previously described; however, the core phenomena were different from 3.03.6AR. Where 3.03.6AR was predominantly upflow film boiling, test 3.04.7R was designed for film boiling in downflow. The initial conditions for test 3.04.7R are presented in Table 4.5. Overall, the test was marginally successful. Critical heat flux (CHF) was achieved throughout the lower part of the bundle; however, the lateness of CHF onset, followed almost immediately by a rewet, severely limited the amount of post-CHF data obtained.

On July 3, a relatively high-powered double-ended blowdown loss-of-coolant experiment (test 3.05.5B) was conducted in the THTF.[19] The objectives of the test were to: (1) measure times to departure-from-nucleate-boiling (DNB) and investigate the possibility of return-to-nucleate-boiling (RNB) in a hydraulic environment similar to that predicted to exist in a PWR during a loss-of-coolant accident (LOCA) and (2) provide a benchmark for transient reactor analysis codes. The initial conditions for test 3.05.5B are presented in Table 4.6.

Test 3.05.5B was the last test conducted using the refurbished Bundle 3. To meet future needs of planned small-break LOCA tests, more FRS thermometry[20-23] would be needed at the D-G bundle thermocouple levels; also there was a special NRC request to determine the effects of the

Table 4.3. Initial conditi' for Test 3.03.6AR

Total bundle power, MW	3.96
Average rod power, kW	65.9
Flow	
Volumetric, m^3/s (gpm)	0.018 (285)
Mass, kg/s (lb_m/s)	14.1 (31.0)
Inlet temperature, K (°F)	540 (512)
Outlet temperature, K (°F)	590 (602)
Outlet pressure, MN/m^2 (psia)	14.1 (2065)

Table 4.4. THTF upflow film boiling data ranges – Test 3.03.6AR

	NRC requested	Obtained in Test 3.03.6AR
Mass flux, $kg/s \cdot m^2$ ($lb_m/h \cdot ft^2$)	270–4070 (2×10^5–3×10^6)	203–543 (1.5×10^5–4×10^5)
Quality, %	0–100	30–100
Pressure, MN/m^2 (psi)	4.14–18.61 (600–2700)	5.17–9.7 (750–1400)
Heat flux, W/m^2 ($Btu/h \cdot ft^2$)	3×10^4–3×10^6 (10^4–10^6)	15.7×10^4–6.3×10^5 (5×10^4–2×10^5)

Table 4.5. Initial conditions for Test 3.04.7R

Total bundle power, MW	2.18
Average rod power, kW	36.4
Flow	
Volumetric, m^3/s (gpm)	0.0128 (203)
Mass, kg/s (lb_m/s)	9.34 (20.6)
Inlet temperature, K (°F)	571.4 (568.9)
Outlet temperature, K (°F)	605.6 (630.4)
Outlet pressure, MN/m^2 (psia)	13.76 (1996)

Table 4.6. Initial conditions for Test 3.05.5B

Total bundle power, MW	7.52
Average rod power, kW	125.3
Flow	
Volumetric, m^3/s (gpm)	0.032 (506)
Mass, kg/s (lb_m/s)	24.44 (53.88)
Inlet temperature, K (°F)	549.7 (529.7)
Outlet temperature, K (°F)	601.7 (623.4)
Outlet pressure, MN/m^2 (psia)	14.64 (2124)

bundle grid spacers on the FRS heat transfer during core recovery. Additionally, it was preferable to replace the less sophisticated preproduction FRSs (substituted for failed rods) with new rods. Therefore, after test 3.05.5B, the THTF was again taken down not only to replace the FRSs but also to improve the instrumentation in the core by adding an in-bundle densitometer and thermocouples in the test section shroud wall.

5. REFURBISHED THTF BUNDLE 3
(August 1980 to Present)

5.1 Core Configuration and Instrumentation

The refurbishment of THTF Bundle 3 was completed by August 15, 1980. During the down-time between test 3.05.5B and August 15, ten new FRSs were fabricated and installed in the THTF Bundle 3 (the FRS locations are shown in Fig. 5.1). Additionally, FRSs number 15, 56, and 62 were removed and replaced with the FRSs from positions 50, 34, and 17, respectively. Thus, only two of the replacement rods from the first refurbishment of the bundle were left (positions 30 and 48). The axial levels monitored by each rod are indicated in Fig. 5.2.

A schematic[24] of the refurbished Bundle 3 giving the location of all primary level (A-G and Y, H, S, and U) FRS thermocouples is presented in Fig. 5.3. The location of special FRS thermocouples between primary levels F and G is illustrated in Fig. 5.4. Also, special FRS thermocouples are located between primary levels E and F as shown in Fig. 5.5. The naming convention for these special (or super-level) thermocouples is different from that given in Sect. 3.1 and is illustrated in Table 5.1.

Table 5.1. Naming convention for super-level FRS thermocouples[a]

Level axial position[b] (cm)	al
297.292	E1
304.366	E2
312.511	E3
329.966	E6
335.514	E7
343.172	E8
358.107	F1
365.849	F2
373.377	F3
380.528	F4
385.763	F5
391.246	F6
396.208	F7
403.664	F8

[a] General form: TE-3nnal, where nn is a number between 01 and 64 equal to the rod or grid position number, and al is a combination of a letter (E or F) and a number (1-8). This combination is given along with the level axial position.

[b] Figures 5.4 and 5.5.

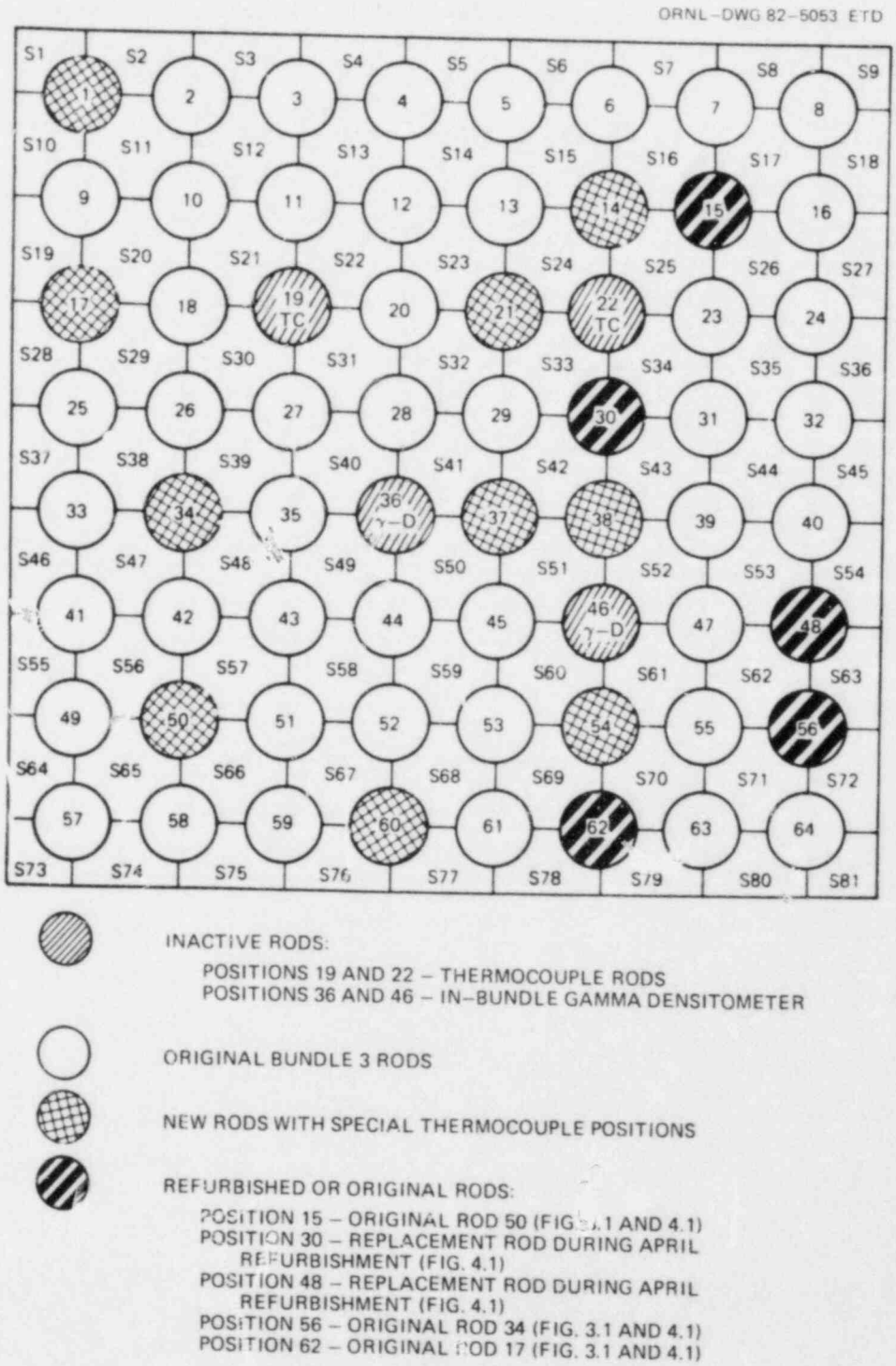

Fig. 5.1. Identification of THTF heater rods, subchannel locations, and inactive rods in the refurbished THTF Bundle 3 (August 1980 to present).

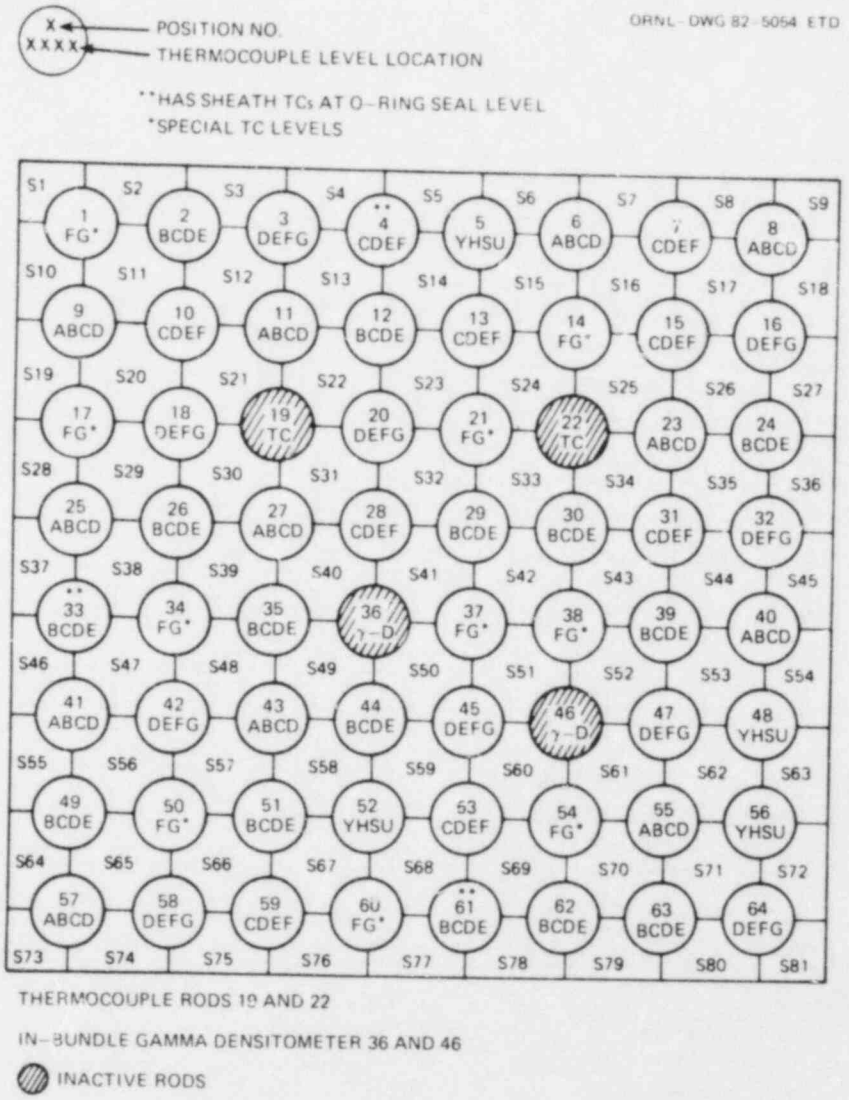

Fig. 5.2. Identification of THTF heater rods and axial thermocouple levels monitored by each rod in the refurbished THTF Bundle 3 (August 1980 to present).

As of August 29, 1980, those FRS thermocouples presented in Table 5.2 were monitored by the CCDAS.

The core-fluid temperature measurement sites are indicated in Fig. 5.6. The location of subchannel, spacer grid, and shroud-fluid sites remain the same as in Figs. 3.9, 4.5, and Appendix A. The thermocouple-array rod that was in position 19 in the refurbished bundle was removed and discarded. (It was theorized that the thermocouple extensions into the fluid were bent back into the rod during reassembly of the refurbished bundle, and as a result no longer measured the bulk fluid temperature.) Two new thermocouple-array rods were constructed (with measurement sites at D, E, F, and G levels) and installed in the refurbished bundle in grid positions 19 and 22.

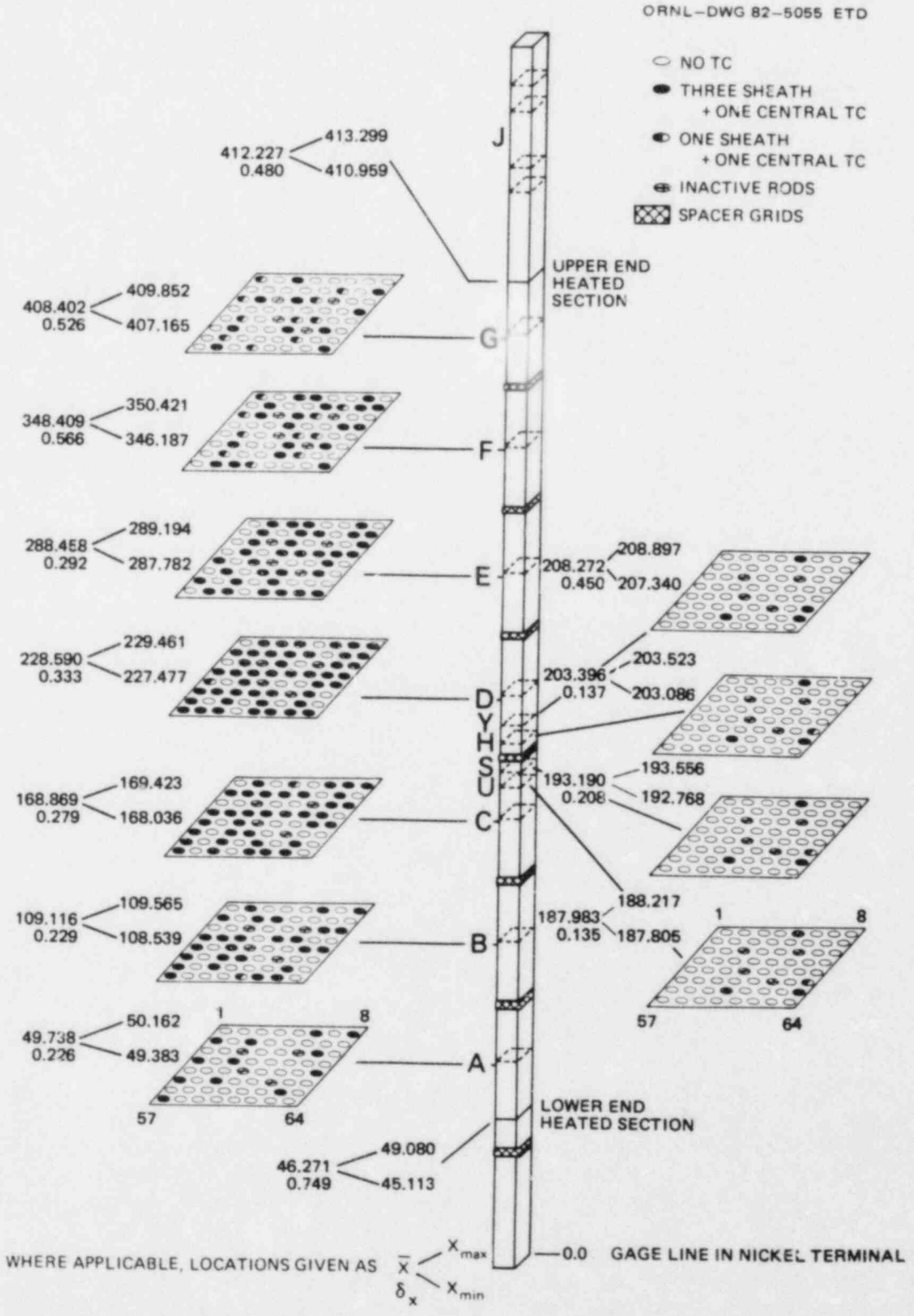

Fig. 5.3. Location of primary FRS thermocouples in the refurbished THTF Bundle 3 (August 1980 to present). All dimensions are in centimeters and are referenced to the gage line in the nickel terminal.

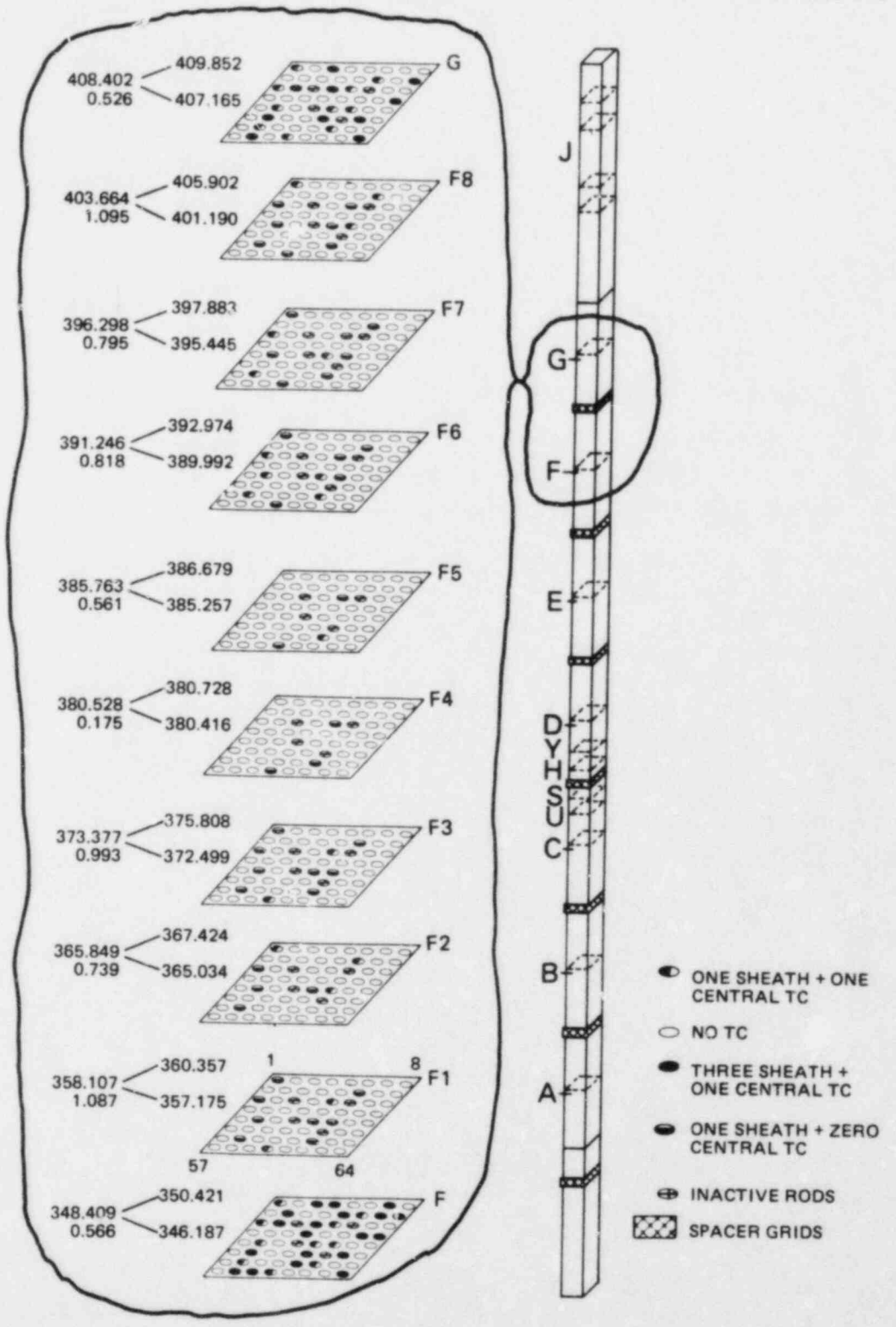

Fig. 5.4. Location of special FRS thermocouples (between primary levels F and G) in the refurbished THTF Bundle 3 (August 1980 to present). All dimensions are in centimeters and are referenced to the gage line in the nickel terminal.

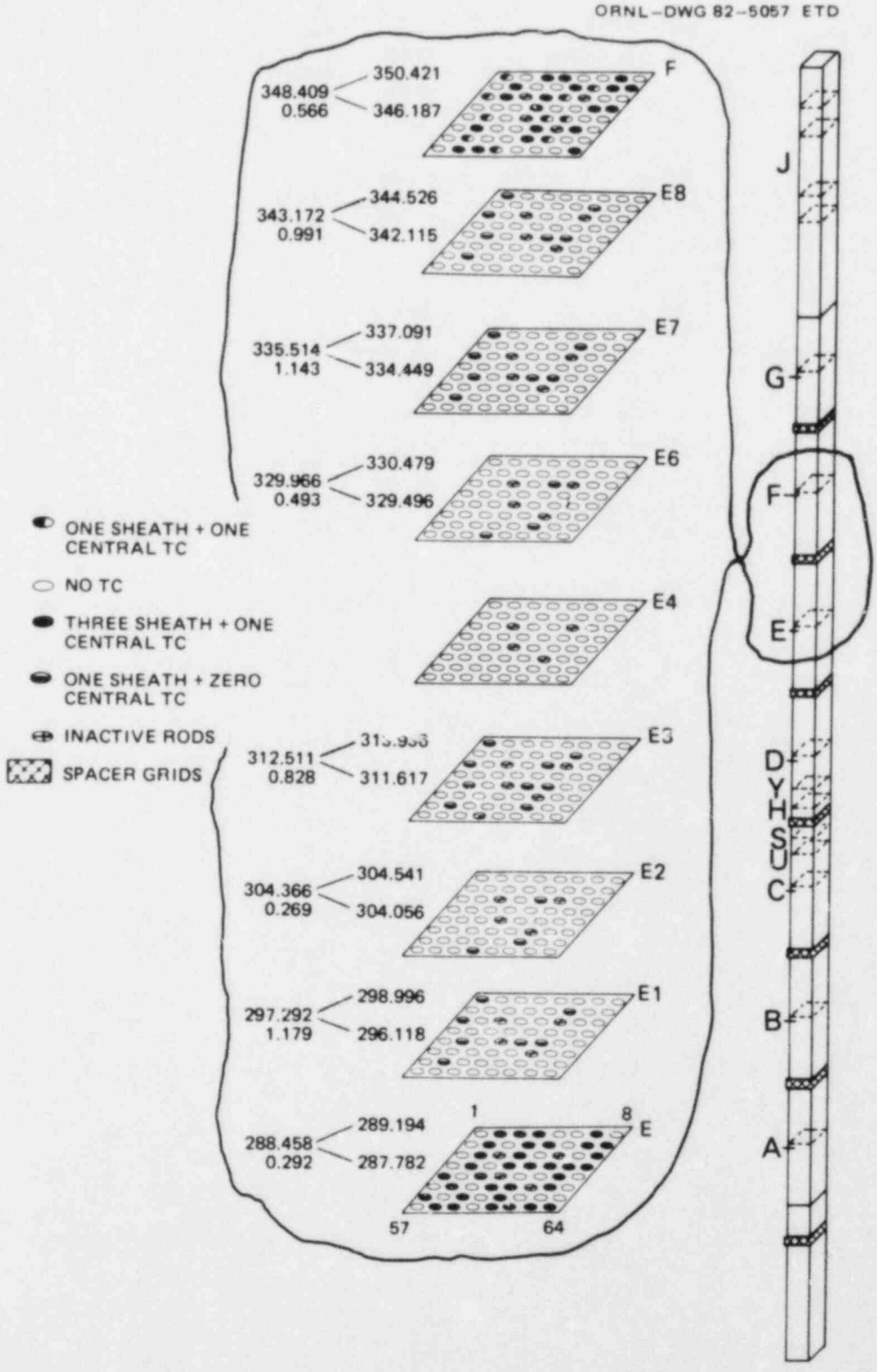

Fig. 5.5. Location of special FRS thermocouples (between primary levels E and F) in the refurbished THTF Bundle 3 (August 1980 to present). All dimensions are in centimeters and are referenced to the gage line in the nickel terminal.

Table 5.2. In-service thermocouple listing for Test 3.06.6B (29-Aug-80)

Rod	Sheath angle level	Center level
1	AF, AG, E1, E3, E7, E8, F1, F2, F3, F6, F7, F8	MF, MG, M2, M8
2	AB, BC, AD, AE	MB, MC, MD
3	CD, BE, CE, BF, CG	MD, ME, MF, MG
4	AC, AD, BE, AF	MC, MD, ME, MF
5	BU, AS, BH, CY	MU, MS, MH, MY
6	AA, AB	MA
7	AC, BE, CE, AF, BF	MC, ME, MF
8	CB, BC, AD, CD	MB, MC, MD
9	CB, AC, CD	MB, MC
10	CC, BD, CD, BE, AF, BF, CF	MC, MD, ME
11	AA, AB, CC	MA, MC
12	CB, BC, CD, AE	MB, MC, MD, ME
13	BC, CD, AE, CE, BF, CF	
14	AF, AG, E1, E3, E7, E8, F2, F3, F6, F7, F8	MF, MG, M2, M8
15	AC, AD, BD, BE, CE, AF	MC, MD, ME, MF
16	AD, BE, CE, BF, BG, CG	MD, ME, MF, MG
17	AF, AG, E3, F1, F2, F3, F6, F7, F8	MF, MG, M6, M7
18	BD, CD, AE, BE, CE, AF, CF, AG, BG, CG	MD, ME, MF
19	Rod 19 is unpowered	
20	AD, BD, CD, AE, BE, CE, AF, BF, CF, AG, BG, CG	MD, MG
21	AF, AG, E2, E3, E6, F1, F3, F4, F5, F6, F7, F8	MF, MG, M1, M3
22	Rod 22 is unpowered	
23	AA, BC	
24	AB, AC, BD, AE, CE	MC, MD, ME
25	CA, CB, BC, CC, BD, CD	MA, MB, MC, MD
26	BB, AC, AD, BD, CD, AE, BE, CE	MC, MD, ME
27	BA, CB, AC, CC, AD, BD, CD	MB
28	AC, CC, AD, BD, CD, AE, CE, AF, BF, CF	MC, MD, ME, MF
29	CB, AC, BC, AD, BD, CD, AE, BE, CE	MB, MC, MD, ME
30	CB, AC, AD, AE, BE	MB, MC, ME
31	CD, CE, BF, CF	MF
32	CD, AE, CE, CF, CG	MD, ME, MG
33	AC, AD, AE, BE, CE	MC
34	AF, AG, E3, E7, E8, F1, F2, F3, F6, F7, F8	MF, M6
35	BB, BD, BE	MB, MD, ME
36	Rod 36 is unpowered	
37	AF, AG, E3, E7, E8, F1, F6, F7, F8	MF, MG, M6, M7
38	AF, AG, E1, E3, E7, E8, F1, F2, F3, F6, F7, F8	MF, MG, M2, M8
39	BB, AC, BD	MB, MC, MD
40	CA, CB, BC, BD	MA, MB, MC
41	AB	MB
42	BD, BE, BF, AG, BG, CG	
43	BA, BB, BC, AD, BD	
44	CB, CC, CD, AE, CE	MB, MC, ME
45	AD, BD, AE, BE, AF, BF, CF, AG, BG, CG	MD, ME, MG
46	Rod 46 is unpowered	
47	CF, CG	MF, MG
48	AH, AY	MH, MY
49	CB, CC, CD, AE, BE, CE	MB, MC, MD, ME
50	AG, E1, E3, E7, F1, F2, F3, F6, F7, F8	M6, M7
51	AB, BC, BD, AE, BE	MC
52	AU, BU, CU, AS, BS, CS, AH, BH, CH, AY, BY, CY	MU, MS, MH, MY
53	CC, AE, BE, BF	MC, ME
54	AF, AG, E2, E3, E6, F1, F3, F4, F5, F6, F7, F8	MF, MG, M5, M6
55	AA, CB, BC, CD	MA, MB, MC, MD
56	BU, BS, CH, AY	MS, MH
57	BA, CB, AC, BC, BD, CD	MA, MB, MC, MD
58	AD, CD, AE, BE, BF, CG	MD, ME, MF, MG
59	CC, AD, AE, BE, CE, AF, BF, CF	MC, ME, MF
60	AF, AG, E2, E3, E6, F3, F4, F5, F6, F7, F8	MF, MG, M3
61	AB, AC, AD, AE, BE, CE	MB, MC, MD
62	BB, AC, AD, CE	
63	CB, BC, AE, BE	MB, MC, ME
64	AD, BD, CD, AE, BE, AF, BF, CF, AG, CG	MD, MF, MG

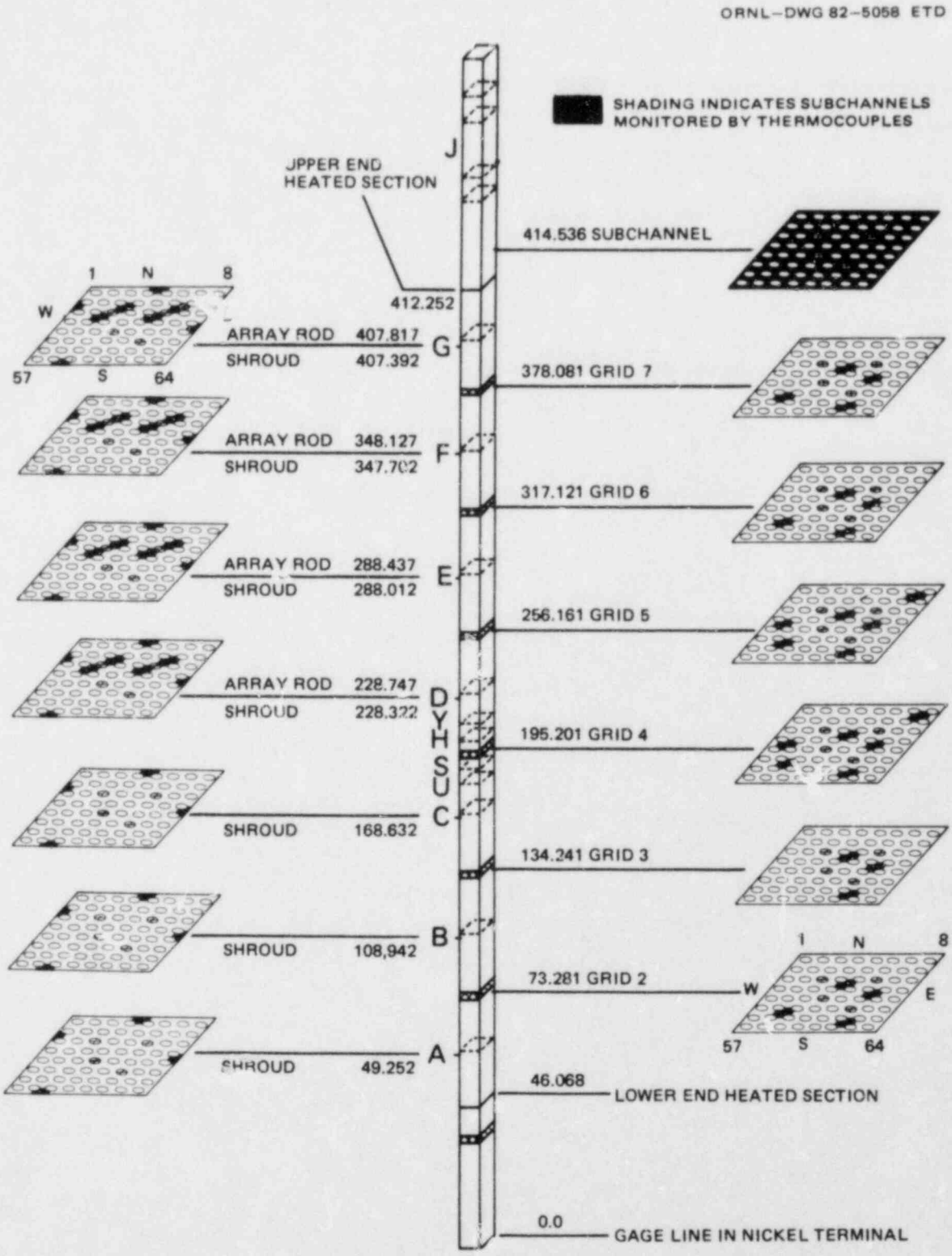

Fig. 5.6. Location of fluid thermocouples in the refurbished THTF Bundle 3 (August 1980 to present). All dimensions are in centimeters and are referenced to the gage line in the nickel terminal.

During the refurbishment of the THTF bundle, considerable improvements in the in-core instrumentation were being made:

1. installation of shroud-wall thermocouples at 13 test section locations,
2. fabrication and installation of 2 new in-bundle gamma densitometers and a motor drive system.

The locations of the pressure taps installed during the first refurbishment and the shroud-wall thermocouples[25] are shown in Fig. 5.7. Figure 5.8 illustrates the assembly of the shroud thermocouples in the east and south walls of the shroud. Table 5.3 contains the location of the inside

Table 5.3. Location of shroud-wall thermocouples relative to the core side of the shroud

Location No.	Level and wall	Thermocouple assembly IAN	Location of inside thermocouple bead[a] [cm (in.)]	Location of outside thermocouple bead[b] [cm (in.)]
1	0E	TE-270AE[a] TE-270BE[b]	0.2769 (0.1090)	1.8669 (0.7350)
2	1E	TE-271AE TE-271BE	0.3376 (0.1329)	1.7777 (0.6999)
3	2E	TE-272AE TE-272BE	0.2875 (0.1132)	1.7976 (0.7077)
4	3E	TE-273AE TE-273BE	0.1575 (0.0620)	1.6576 (0.6526)
6	5E	TE-275AE TE-275BE	0.4394 (0.1730)	2.0594 (0.8108)
7	6E	TE-276AE TE-276BE	0.3744 (0.1474)	1.9042 (0.7497)
8	7E	TE-277AE TE-277BE	0.4061 (0.1599)	1.9461 (0.7662)
9	8E	TE-278AE TE-278BE	0.4544 (0.1789)	2.1245 (0.8364)
10	9E	TE-279AE TE-279BE	0.2032 (0.0800)	1.7033 (0.6706)
11	2S	TE-272AS TE-272BS	0.4747 (0.1869)	2.1549 (0.8484)[c]
12	5S	TE-275AS TE-275BS	0.2489 (0.0980)	1.7689 (0.6964)
13	9S	TE-279AS TE-279BS	0.4016 (0.1581)	1.9715 (0.7762)[c]

[a] Inside thermocouple.

[b] Outside thermocouple.

[c] Location of outside thermocouple is in the purge stream, not in the shroud wall.

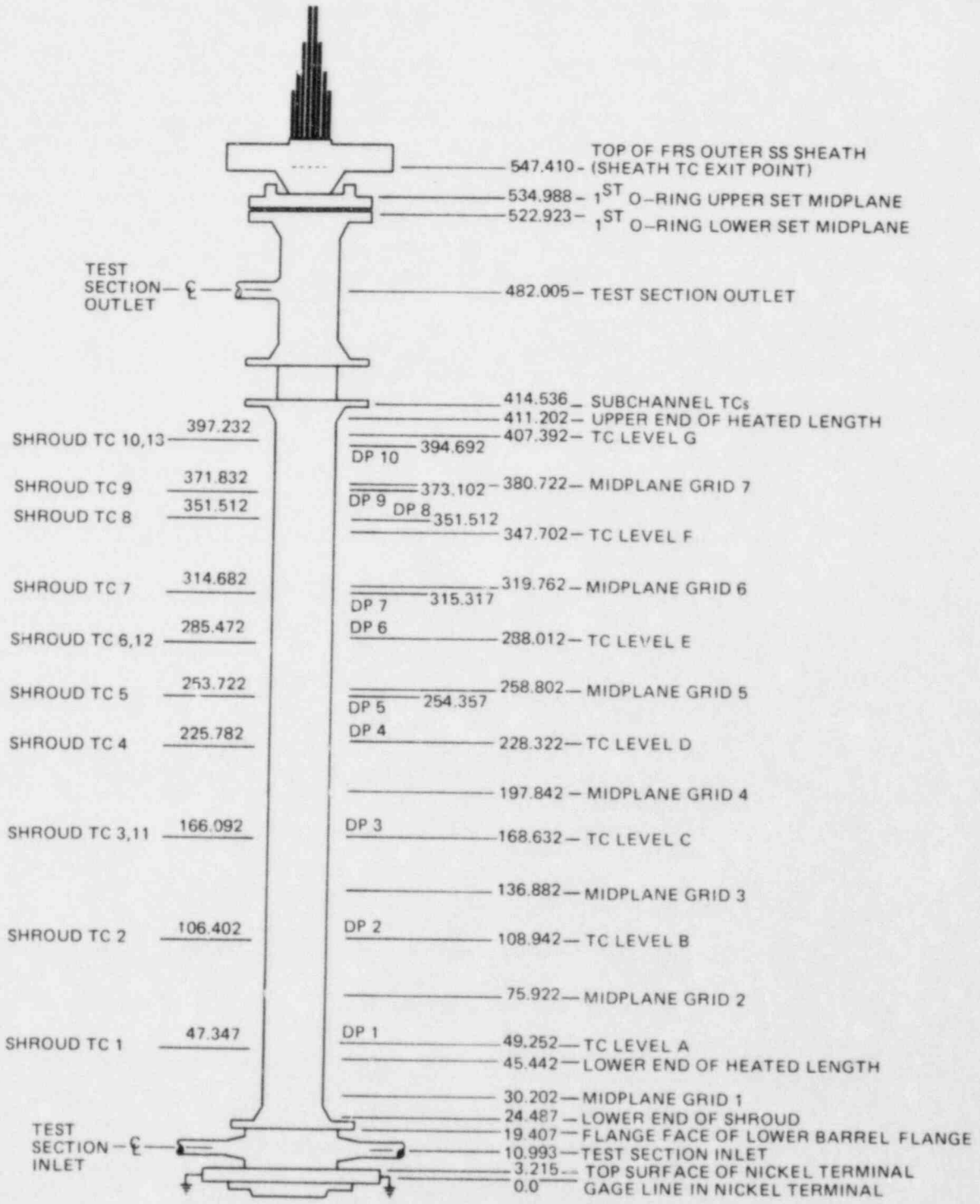

Fig. 5.7. Nominal location of critical points in THTF Bundle 3 including location of shroud-wall thermocouples and test section differential-pressure measurement devices.

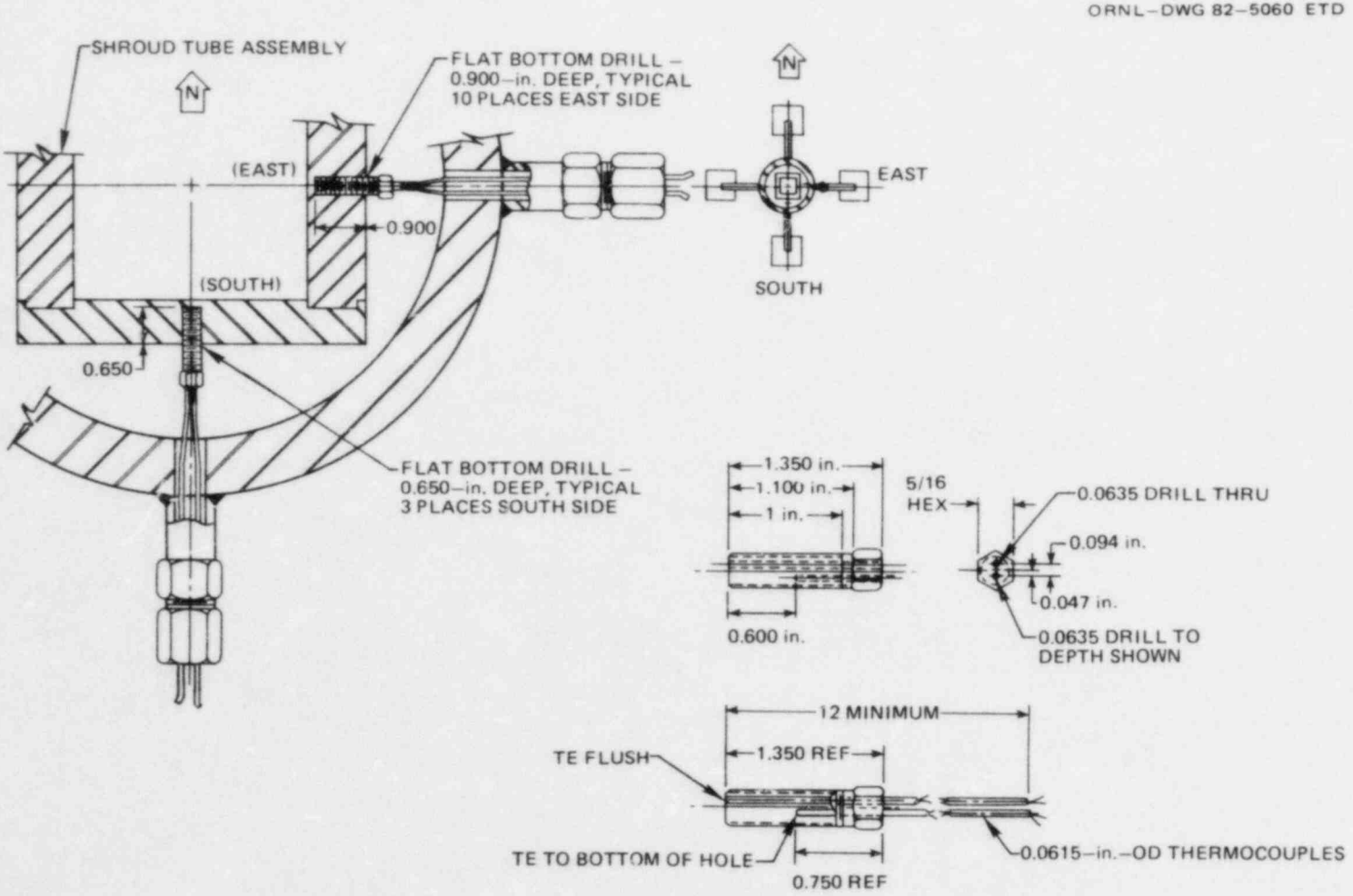

Fig. 5.8. Shroud-wall thermocouple assembly. Dimensions are in inches (1 in. = 2.54 cm).

and outside thermocouple beads at each location relative to the core side of the shroud wall. Note that at two positions (11 and 13), the outside bead is not in the shroud wall. The nomenclature used for these thermocouples has the following form:

TE-27abc ,

where

TE-27 is the same for all positions,
a = level (0–9),
b = the letter A or B (A indicates the inside thermocouple, and B indicates the outside thermocouple),
c = the letter E (east wall) or S (south wall).

The in-bundle gamma densitometer[26-28] uses low-energy gamma sources and high-temperature ion chambers positioned in two of the instrumented rods. A line-of-sight path that crosses two subchannels exists between unheated instrument rod positions 36 and 46. The design concept is the determination of in-bundle void fraction by measurement of the variation in the attenuation of the source across the subchannel path length. A detail of the source-detector radial geometry is shown in Fig. 5.9. The

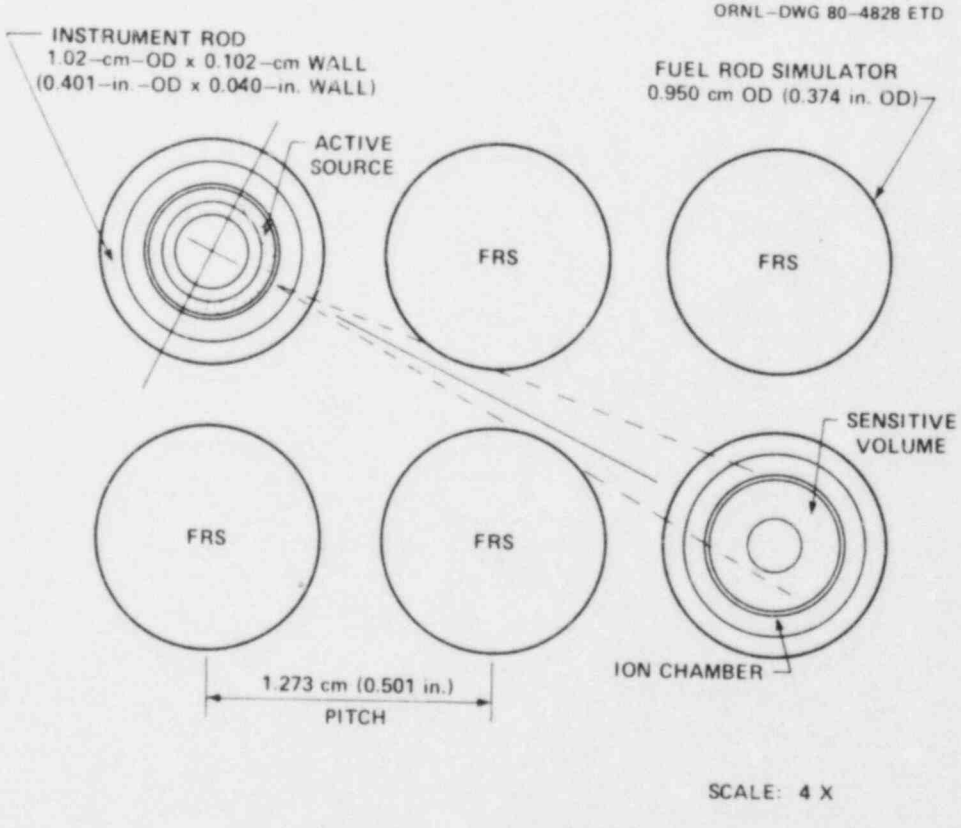

Fig. 5.9. In-bundle densitometer geometry.

annular source design was chosen to allow placement of two source-detector systems using only two instrument rod positions. For the instrument rod where the source is located above the detector (Fig. 5.10), the detector cable passes through the source annulus and out of the instrument rod tube. The source and detector assemblies in each of the rods are attached to a motor drive system for axial positioning. The two measurement sites are fixed with respect to each other; but variation of the axial position of the two measurement sites over the heated length of the bundle is made possible with the aid of the positioning motor drive.

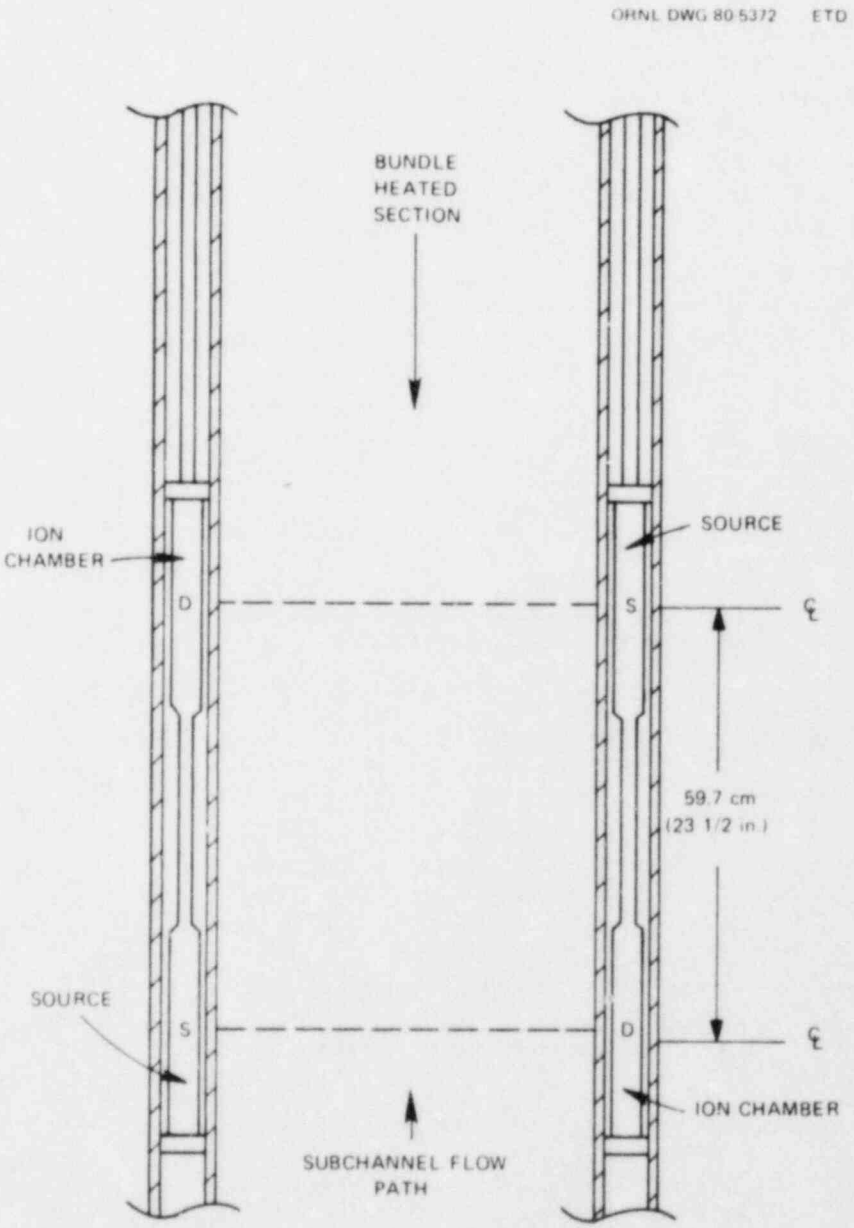

Fig. 5.10. Axial positioning of the source-detector measurement location.

All of these instrumentation improvements were intended for the next series of small-break LOCA tests.

5.2 Operating History

On August 29, 1980, a power-drop calibration test (from ~129 kW/rod) was completed. As stated before, this test was designed to obtain data that would allow in situ determination of the FRS thermal-physical properties as functions of temperature. This test was essential because there were ten new rods in the refurbished bundle. The approximate test conditions for the August 29 power drop are presented in Table 5.4.

On the same day of the power drop, the second upflow film boiling test (3.06.6B) was attempted and completed with the THTF in standard configuration (Fig. 3.4). The initial conditions for test 3.06.6B are presented in Table 5.5. The purposes of the experiment were the same as for test 3.03.6AR (Sect. 4.2). The upflow film boiling data ranges[29] requested by NRC and obtained in test 3.06.6B are presented in Table 5.6.

Table 5.4. August 29 power-drop/bundle characterization test conditions

Average rod power, kW	129.1
Flow	
Volumetric, m^3/s (gpm)	0.0177 (280)
Mass, kg/s (lb_m/s)	15.19 (33.5)
Inlet temperature, K (°F)	487.5 (417.8)
Outlet temperature, K (°F)	587.7 (598.2)
Outlet pressure, MN/m^2 (psia)	13.61 (1974)

Table 5.5. Initial conditions for Test 3.06.6B

Total bundle power, MW	2.26
Average rod power, kW	37.7
Flow	
Volumetric, m^3/s (gpm)	0.0079 (125)
Mass, kg/s (lb_m/s)	6.04 (13.3)
Inlet temperature, K (°F)	547 (526)
Outlet temperature, K (°F)	610.2 (638.7)
Outlet pressure, MN/m^2 (psia)	14.98 (2173)

Table 5.6. THTF upflow film boiling data ranges – Test 3.06.6B

	NRC requested	Obtained in Test 3.06.6B
Mass flux, kg/s·m² (lb_m/h·ft²)	270–4070 (2×10^5–3×10^6)	135–340 (1×10^5–2.5×10^5)
Quality, %	0–100	15–100
Pressure, MN/m² (psi)	4.14–18.61 (600–2700)	6.03–12.4 (875–1800)
Heat flux, W/m² (Btu/h·ft²)	3×10^4–3×10^6 (10^4–10^6)	15.7×10^4–4.7×10^5 (5×10^4–1.5×10^5)

Between September 11 and October 1, 1980, a series of steady-state experiments[30] (test series 3.07.9) were conducted in the THTF. These experiments provided steady-state rod bundle film boiling data over a range of flow conditions. These tests provided a means of obtaining data in the high-flow film boiling data ranges requested by the NRC. These tests were conducted with the THTF slightly altered from its standard configuration (Fig. 3.4); that is, the pressurizer connection was located in the pump bypass line rather than just beyond the horizontal outlet spool piece. Conditions for these tests are shown in Table 5.7. The FRS in grid position 32, normally a heated rod, failed on October 1 about halfway through the testing on that date.

At the end of the steady-state testing on October 1, a transient film boiling heat transfer experiment (test 3.08.6C) was conducted in the THTF. The test objectives were the same as in the previous upflow film boiling tests. The initial conditions for test 3.08.6C are given in Table 5.8. The upflow film boiling data ranges[31] requested by NRC and obtained in test 3.08.6C are given in Table 5.9.

On October 8, the rod in grid position 32 was replaced with FRS-051. On October 22 and 30, the second series of small-break LOCA tests (3.09.10I-N) were attempted. Posttest analysis indicated that large pressure differentials across the core shroud wall resulted in steam leakage through the shroud (from the core to the test section annulus). Because of the large uncertainty in the core outlet mass flow, these tests were labeled unsuccessful and were rescheduled for November (after modifications to the loop to eliminate the large pressure differentials across the shroud wall).

Using the loop configuration illustrated in Fig. 5.11, the second attempt to run tests 3.09.10I-N was made on November 25, 1980. These tests were designed to complement the first small-break LOCA test series conducted in December 1979 and January 1980. The November series may be broken down into four separate categories: (1) transient boiloff tests (total of five), (2) steady-state bundle uncovery tests (total of six),

Table 5.7. THTF steady-state upflow film boiling data ranges, test series 3.07.9a (a = test letter)[a]

Date	Test (a)	Mass flux [kg/s·m² (lb_m/h·ft²)]	Heat flux [W/m² (Btu/h·ft²)]	Core exit quality	Pressure [MN/m² (psia)]
September 11	K	225 (1.7×10^5)	4.41×10^5 (1.4×10^5)	1.1	4.38 (635)
	H	257 (1.9×10^5)	4.10×10^5 (1.3×10^5)	1.08	8.89 (1290)
	I	362 (2.7×10^5)	5.68×10^5 (1.8×10^5)	1.09	9.19 (1332)
	L	529 (3.9×10^5)	7.88×10^5 (2.5×10^5)	1.005	8.30 (1203)
	M	657 (4.8×10^5)	8.82×10^5 (2.8×10^5)	0.94	8.57 (1242)
	N	800 (5.9×10^5)	9.45×10^5 (3.0×10^5)	0.82	8.52 (1234)
	O	307 (2.3×10^5)	5.36×10^5 (1.7×10^5)	1.09	5.98 (867)
	X	339 (2.5×10^5)	5.99×10^5 (1.9×10^5)	1.13	6.01 (872)
	P	520 (3.8×10^5)	8.19×10^5 (2.6×10^5)	1.02	6.03 (874)
September 18	Q	326 (2.4×10^5)	5.68×10^5 (1.8×10^5)	1.12	6.53 (947)
	R	366 (2.7×10^5)	6.46×10^5 (2.0×10^5)	1.13	6.57 (952)
October 1	T	240 (1.8×10^5)	3.15×10^5 (1.0×10^5)	1.03	11.89 (1723)
	U	242 (1.8×10^5)	3.15×10^5 (1.0×10^5)	1.01	11.69 (1694)
	V	250 (1.8×10^5)	3.15×10^5 (1.0×10^5)	0.99	12.04 (1745)
	G	248 (1.8×10^5)	3.15×10^5 (1.0×10^5)	1.0	12.54 (1818)
	W	257 (1.9×10^5)	3.78×10^5 (1.2×10^5)	1.17	12.55 (1820)
	F	255 (1.9×10^5)	3.78×10^5 (1.2×10^5)	1.18	12.62 (1830)
	C	334 (2.5×10^5)	5.67×10^5 (1.8×10^5)	1.32	12.46 (1805)
	D	517 (3.8×10^5)	6.93×10^5 (2.2×10^5)	1.05	12.75 (1847)
	E	593 (4.4×10^5)	6.93×10^5 (2.2×10^5)	0.95	13.2 (1908)
	J	733 (5.4×10^5)	7.56×10^5 (2.4×10^5)	0.82	13.37 (1937)
	B	705 (5.2×10^5)	9.14×10^5 (2.9×10^5)	1.04	12.76 (1849)

[a]Data ranges requested by NRC:

Mass flux 270–4070 kg/s·m² (2×10^5–3×10^6 lb_m/h·ft²),

Heat flux 3×10^4–3×10^6 W/m² (10^4–10^6 Btu/h·ft²),

Pressure 4.14–18.61 MN/m² (600–2700 psia).

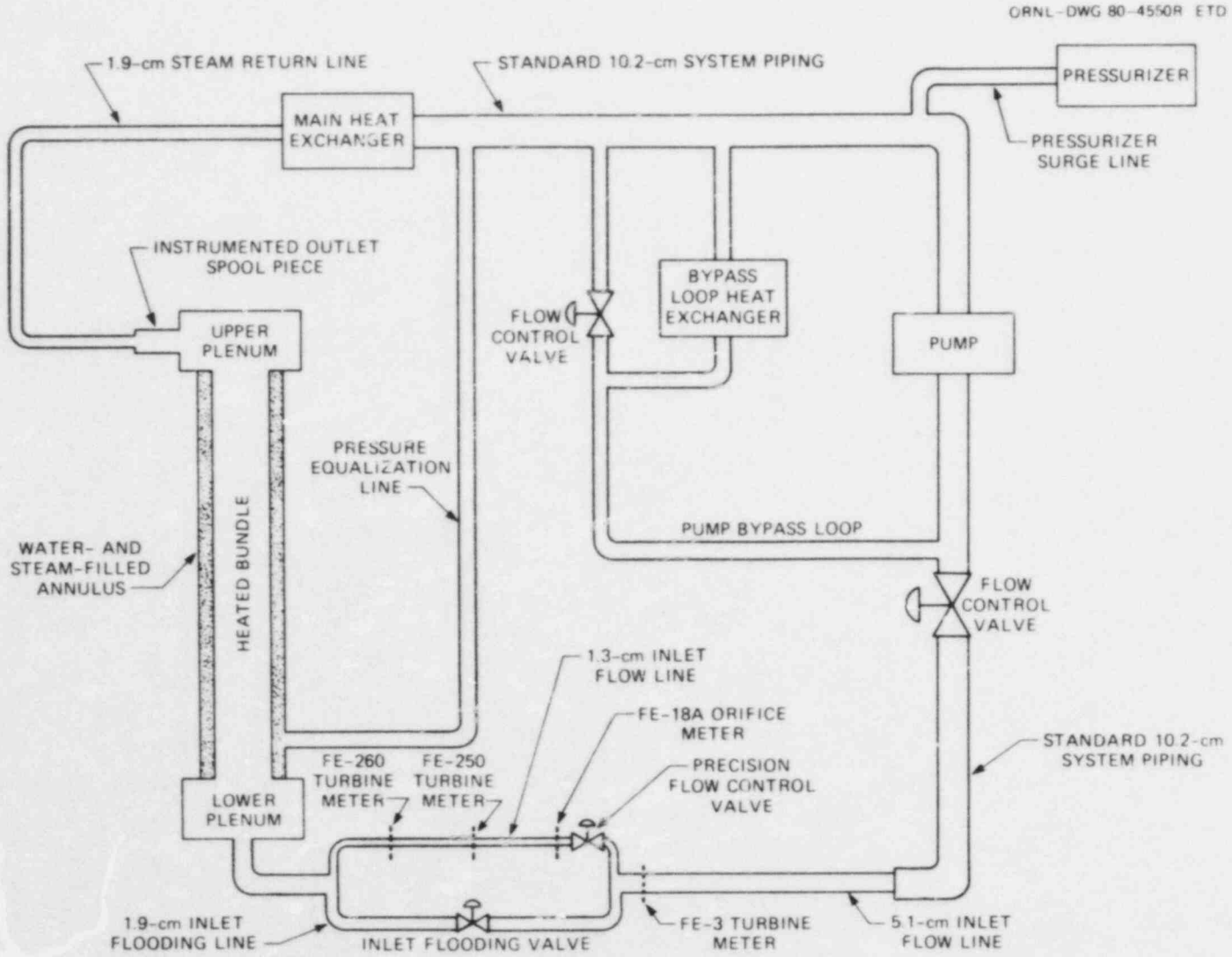

Fig. 5.11. Schematic of THTF for November 1980 small-break LOCA test series.

Table 5.8. Initial conditions for Test 3.08.6C

Total bundle power, MW	2.4
Average rod power, kW	40.6
Flow	
Volumetric, m^3/s (gpm)	0.0082 (130)
Mass, kg/s (lb_m/s)	6.39 (14.1)
Inlet temperature, K (°F)	538 (519)
Outlet temperature, K (°F)	598 (618)
Outlet pressure, MN/m^2 (psia)	12.9 (1870)

Table 5.9. THTF upflow film boiling data ranges – Test 3.08.6C

	NRC requested	Obtained in Test 3.08.6C
Mass flux, $kg/s \cdot m^2$ ($lb_m/h \cdot ft^2$)	270–4070 (2×10^5–3×10^6)	200–1085 (1.5×10^5–8×10^5)
Quality, %	0–100	35–100
Pressure, MN/m^2 (psi)	4.14–18.61 (600–2700)	6.55–11.72 (950–1700)
Heat flux, W/m^2 ($Btu/h \cdot ft^2$)	3×10^4–3×10^6 (10^4–10^6)	4.73×10^5–1.1×10^6 (1.5×10^5–3.5×10^5)

(3) transient reflood tests (total of five), and (4) mixture level swell tests (total of twelve).

A summary[32] of the main features of the transient boiloff tests along with the test designations is presented in Table 5.10. The steady-state bundle uncovery tests are summarized in Table 5.11, and the transient reflood tests are summarized in Table 5.12.

The last official run in the THTF Bundle 3 was made on February 3, 1981. These tests were aimed at mass flux and power conditions intermediate to the 3.07.9 and 3.09.10 test series. At this time, these tests have not been analyzed.

Table 5.10. THTF transient boiloff tests, November 1980 (preliminary)

Test	Test duration (s)	Average rod linear power [kW/m (kW/ft)]	Depressurization [MN/m² (psia)]		Maximum bundle uncovering (%)	
			Desired	Observed	Desired	Observed
3.09.10T	200	0.95 (0.29)	6.2–4.14 (900–600)	5.79–3.45 (840–500)	80	70
3.09.10U	60	1.90 (0.58)	7.93–6.2 (1150–900)	8.00–5.52 (1160–800)	70	70
3.09.10V	135	0.66 (0.20)	7.93–6.2 (1150–900)	7.58–5.52 (1100–800)	70	70
3.09.10W	100	0.62 (0.19)	7.93–6.2 (1150–900)	7.86–5.86 (1140–850)	70	45
3.09.10X	280	0.33 (0.10)	8.62 (1250)	8.55–8.34 (1240–1210)	60	70

Table 5.11. THTF steady-state bundle uncovery tests, November 1980

Test	Pressure [MN/m² (psia)]	Power [kW/m (kW/ft)]	Mixture level [m (ft)]	Maximum temperature [K (°F)]
3.09.10I	4.14 (600)	2.23 (0.68)	2.67 (8.75)	1050 (1430)
3.09.10J	4.14 (600)	0.98 (0.30)	2.92 (9.58)	905 (1170)
3.09.10K	4.14 (600)	0.36 (0.11)	2.13 (7.00)	980 (1320)
3.09.10L	7.58 (1100)	2.20 (0.67)	2.74 (9.00)	997 (1335)
3.09.10M	6.89 (1000)	1.05 (0.32)	2.54 (8.33)	1011 (1360)
3.09.10N	7.24 (1050)	0.49 (0.15)	2.13 (7.00)	1044 (1420)

Table 5.12. THTF reflood tests, November 1980 (preliminary)

Test	Pressure [MN/m² (psia)]	Power [kW/m (kW/ft)]	Flooding rate [cm/s (in./s)]
3.09.10O	4.14 (600)	1.97 (0.6)	15.24 (6)
3.09.10P	4.14 (600)	0.98 (0.3)	7.62 (3)
3.09.10Q	4.14 (600)	0.98 (0.3)	2.54 (1)
3.09.10R	7.58 (1100)	1.97 (0.6)	7.62 (3)
3.09.10S	7.58 (1100)	0.98 (0.3)	7.62 (3)

6. FRS RADIAL DIMENSIONS

One of the primary requirements of the BDHT program is the determination of transient FRS surface temperatures and surface heat fluxes from the FRS internal-sheath thermocouples (Fig. 6.1) during a transient test in the THTF. This requires the solution of the inverse heat conduction problem that is accomplished at ORNL by the computer codes ORINC (Ref. 2) and ORMDIN (Ref. 33). These codes along with the FRS calibration codes (ORTCAL) (Ref. 14) require that the FRS radial dimensions be known as precisely as possible. This should not imply that these codes would fail if these dimensions are not precise and accurate but that the uncertainties in the computed results would be less (hopefully) or at least could be estimated. Unfortunately, these dimensions are not readily available primarily because of the manufacturing technique used for the construction of the FRS. The best method to determine these dimensions is to (1) destructively cross-section an FRS, (2) mount and polish the cross sections, (3) photograph the cross sections at magnification, and (4) then make the measurements using a tool maker's microscope (at 100X magnification). The estimated accuracy of these measurements is $\pm$0.0025 mm (0.0001 in.). There are disadvantages to this method; namely, an expensive FRS is no longer available (except in 25-mm sections), and the assumption must be made that the cross-sectioned FRS is representative of the bundle.

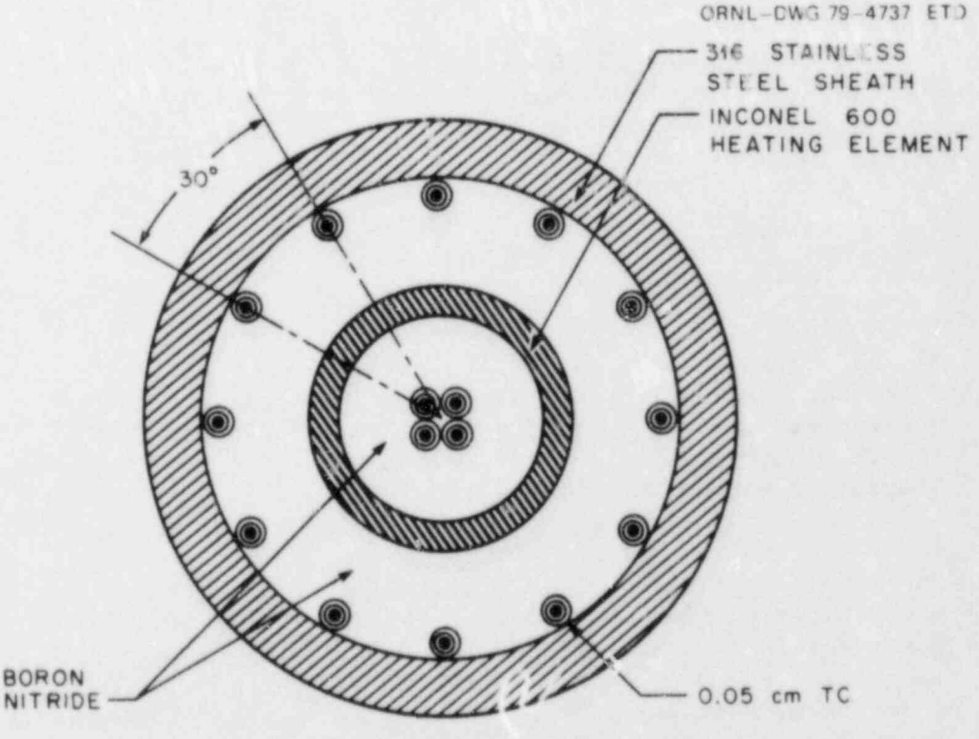

Fig. 6.1. Cross section of THTF Bundle 3 FRS.

Prior to the assembly of the original Bundle 3 (June 1979), BDHT FRS-038 was cross-sectioned and measured by the Y-12 Development Division Metallurgical Department.[34] FRS-038 (an original Bundle 3 FRS) was never placed in a BDHT loop and thus never power-cycled; in fact, this rod failed an electrical check during construction, which was the primary reason the rod was cross-sectioned. The electrical failure was caused by metal inclusions in the BN annular insulator that resulted in arcing between the heating element and the FRS cladding during the electrical check. Other than the metal inclusions, FRS-038 was typical of the original Bundle 3 FRSs (noncycled, that is). Table 6.1 contains the results[35] of a statistical analysis performed on the FRS-038 measurements. The radial results (determined from diametric measurements) are independent of those for the thicknesses (the dimensions cross-check). Estimates of the uncertainties (one standard deviation) in the radii and thicknesses are included in Table 6.2.

The dimensional stability of preproduction Bundle 3 FRSs is indicated in Table 6.3. These measurements were compiled from four rods prior and subsequent to testing in the BDHT single-rod loop. Even though the diametric change in Table 6.3 was small, it was decided to cross-section a THTF-cycled FRS when one became available.

After the refurbishment of Bundle 3 (July-August 1980), four FRSs formerly in grid positions 21, 37, 38, and 54 of the original Bundle 3 were placed in storage. These rods had experienced the first series of small-break LOCA tests and THTF testing during May and June 1980. One of these rods, FRS-058B (grid position 37) was acquired for testing in the

Table 6.1. Bundle 3 FRS sublayer radii and thicknesses

Sublayer	Outer radius [mm (in.)]	Thickness [mm (in.)]
	Heated length	
Stainless steel clad	4.7523 (0.1871)	0.4801 (0.0189)
Outer boron nitride	4.2723 (0.1682)	1.1557 (0.0455)
Heater element	3.1166 (0.1227)	0.3505 (0.0138)
Inner boron nitride	2.7661 (0.1089)	2.0523 (0.0808)
Thermocouple bundle	0.7137 (0.0281)	
	Terminal end	
Stainless steel clad	4.7371 (0.1865)	0.4724 (0.0186)
Outer boron nitride	4.2647 (0.1679)	1.1760 (0.0463)
Heater element	3.0886 (0.1216)	0.3556 (0.0140)
Copper tubing	2.7330 (0.1076)	0.8865 (0.0349)
Inner boron nitride	1.8466 (0.0727)	1.1303 (0.0445)
Thermocouple bundle	0.7163 (0.0282)	

Table 6.2. Bundle 3 FRS sublayer radius and thickness uncertainties (1 standard deviation)

Sublayer	Outer radius uncertainty[a] [mm (in.)]	Thickness uncertainty[b] [mm (in.)]
	Heated length	
Stainless steel clad	0.0076 (0.0003)	0.0102 (0.0004)
Outer boron nitride	0.0102 (0.0004)	0.0356 (0.0014)
Heater element	0.0152 (0.0006)	0.0076 (0.0003)
Inner boron nitride	0.0152 (0.0006)	0.0406 (0.0016)
Thermocouple bundle	0.0356 (0.0014)	

[a] 150 observations.

[b] 300 observations.

Table 6.3. Stability statistics for loop-cycled rods

Rod No.	Before loop testing [mm (in.)]		After loop testing [mm (in.)]		Change[a] (%)
	Mean value of rod diameter	Standard deviation	Mean value of rod diameter	Standard deviation	
40A	9.4945 (0.3738)	0.0127 (0.0005)	9.5352 (0.3754)	0.0178 (0.0007)	0.4
18A	9.4920 (0.3737)	0.0102 (0.0004)	9.5199 (0.3748)	0.0203 (0.0008)	0.3
10A	9.4996 (0.3740)	0.0076 (0.0003)	9.4996 (0.3740)	0.0102 (0.0004)	0.0
6A			9.5631 (0.3765)	0.0178 (0.0007)	

[a] Relative to rod diameter before testing.

FRS TDL (Sects. 7 and 8) and subsequent cross-sectioning and measurement by the Y-12 Development Division Metallurgical Department. FRS-058B should be representative of a cycled THTF rod, and the change in the rod's outer diameter (0.3–0.4%) agrees very well with the preproduction Bundle 3 rods (Table 6.3) cycled in the BDHT single-rod facility.

Presented in Table 6.4 are the internal dimensions for the cycled Bundle 3 FRS. (Sublayer radius and thickness uncertainties are included in Table 6.5.) These dimensions are the result of a statistical analysis[36] performed on measurements[37] from BDHT FRS-058B. The radial results (determined from diametric measurements) are independent of those for the thicknesses.

Comparisons of the sublayer radii in Tables 6.1 and 6.4 show apparent dimensional changes. The direction of these diametric changes in the interfaces is indicated in Fig. 6.2. Apparently, the FRS has stress-relieved itself. Considering the FRS manufacturing process, the relief is in the correct direction. Roughly the manufacturing process takes the

Table 6.4. Cycled Bundle 3 FRS sublayer radii and thicknesses

Sublayer	Outer radius [mm (in.)]	Thickness [mm (in.)]
Stainless steel clad	4.7630 (0.18752)	0.4636 (0.01825)
Outer boron nitride	4.2997 (0.16928)	1.1763 (0.04631)
Heater element	3.1227 (0.12294)	0.3345 (0.01317)
Inner boron nitride	2.7882 (0.10977)	2.1224 (0.08356)
Thermocouple bundle	0.6652 (0.02619)	

Table 6.5. Cycled Bundle 3 FRS sublayer radius and thickness uncertainties (1 standard deviation)

Sublayer	Outer radius uncertainty[a] [mm (in.)]	Thickness uncertainty[b] [mm (in.)]
Stainless steel clad	0.0038 (0.00015)	0.0117 (0.00046)
Outer boron nitride	0.0056 (0.00022)	0.0310 (0.00122)
Heater element	0.0060 (0.00024)	0.0089 (0.00035)
Inner boron nitride	0.0078 (0.00031)	0.0615 (0.00242)
Thermocouple bundle	0.0580 (0.00229)	

[a] 69 observations.

[b] 138 observations.

following scheme:

1. Four centerline thermocouples and a wire stiffener (Fig. 6.3) are inserted in a stainless steel tube (~2 mm in diameter).
2. This assembly is inserted into an Inconel-600 tube, and BN preforms are slipped over the thermocouple bundle and crushed until the tube is full. It is now called the active component assembly (ACA).
3. The ACA is swaged (outer diameter reduced) in a hammer mill to a specified outer diameter.
4. The ACA is inserted in the stainless steel clad (a jig holds the ACA, clad, and sheath thermocouples in the proper positions), and grooved BN preforms are slipped over the ACA and crushed until the assembly is full.
5. This completed assembly (FRS) is then swaged (outer diameter reduced) in a hammer mill until the outer diameter, the position of the sheath thermocouples, and active heated length are correct.

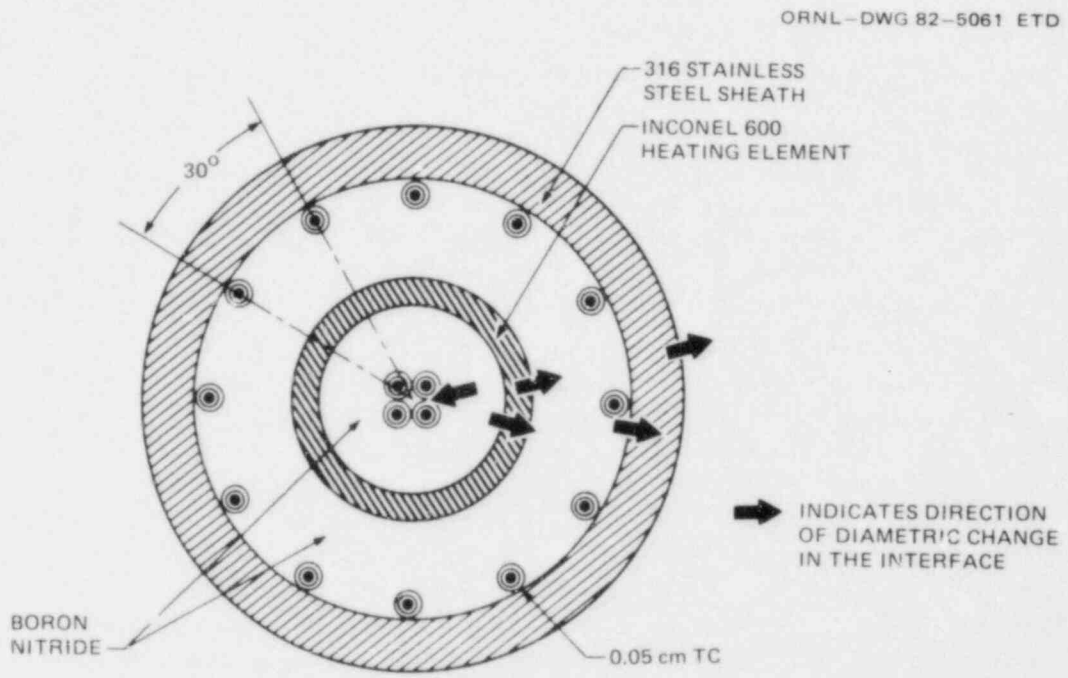

Fig. 6.2. Cross section of THTF Bundle 3 FRS with directional changes in the sublayer interfaces (uncycled FRS → cycled FRS).

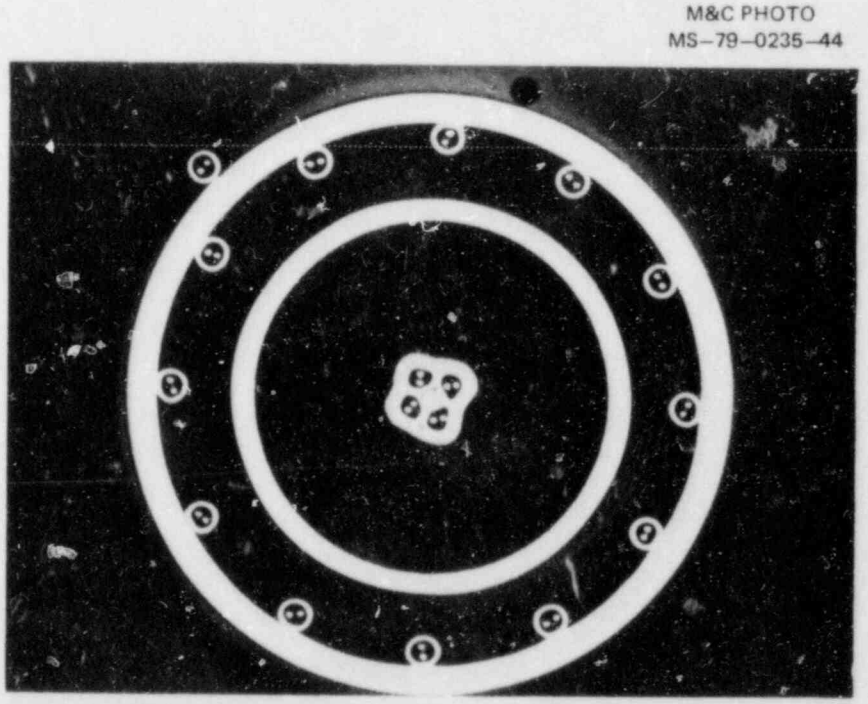

Fig. 6.3. Photograph of typical cross section of FRS-058B.

The procedure[38] is actually more complicated than outlined in the preceding paragraphs; but, generally the process follows this scheme. Thus, given the swaging process and the diametric reductions, expected stress relief would follow the directions shown in Fig. 6.2.

During the construction of the FRS, a strict inventory (weight) of the BN preforms used in the ACA and the annular FRS region is maintained. Thus, given the final FRS dimensions (length and diametric), the BN density can be determined. Using the dimensions from Table 6.1, the average BN core density for 61 rods was 2.215 g/cm³ (138.3 lb_m/ft^3) with a standard deviation of the observations of 0.013 g/cm³ (0.81 lb_m/ft^3); also, the average annular BN density was 2.175 g/cm³ (135.8 lb_m/ft^3) with a standard deviation of 0.019 g/cm³ (1.19 lb_m/ft^3). Now, using the cycled rod dimensions from Table 6.4, the average BN core density was 2.158 g/cm³ (134.7 lb_m/ft^3) with a standard deviation of 0.013 g/cm³ (0.8 lb_m/ft^3), and the average annular BN density was 2.135 g/cm³ (133.3 lb_m/ft^3) with a standard deviation of 0.019 g/cm³ (1.19 lb_m/ft^3). Comparisons of the as-constructed FRS BN densities and the BN densities after rod thermal cycling show further evidence that the rods underwent stress relief.

The discussion on rod radial dimensions has dealt exclusively with the original Bundle 3 rods. The rods that were cross-sectioned for the data in Tables 6.1 and 6.4 were original Bundle 3 rods. However, as noted in Sect. 4 (and Fig. 4.1) during the first refurbishment of the bundle, seven of the original rods were replaced with "preproduction" models (these units contained only ten thermocouples, six sheaths, and four centerlines). Using the dimensions from Table 6.1, it would be expected that the core BN density would be approximately the same as the production model with the annular density possibly less than the production model; this was observed to be the case. The cycled rod data in Table 6.4 includes that from a preprototype rod, two preproduction rods, and one production rod; thus, after cycling, these rods (and FRS-058B) exhibit similar diametric changes (~0.3–0.4%). Additionally, the new rods inserted in the bundle during the rerefurbishment phase (Sect. 5) were slightly different from the production models in that 0.4-mm (0.016-in.) thermocouples instead of 0.5-mm (0.020-in.) thermocouples were used. Neither a preproduction FRS or a new FRS have ever been cross-sectioned, photographed, and measured. Therefore, no internal dimensions are available for these rods. However, given that (1) the outer diametric changes are essentially the same, (2) the heating element (Inconel-600) electrical resistance per unit length is approximately equal, and (3) the relative density difference between the core and annular BN is the same as the production FRS, the internal radial dimensions and BN densities of the preproduction FRSs and the new FRSs can be estimated from the dimensions in Table 6.4. This has been done and the dimensions (and BN densities) for the three rod types are given in Table 6.6.

It is suggested that for all thermal analyses of THTF Bundle 3 rod response that the internal FRS radial dimensions and BN densities specified in Table 6.6 be used.

Table 6.6. Internal dimensions and boron nitride densities of Bundle 3 FRSs (for the original and refurbished bundles)

Sublayer	Preproduction FRS	Original or production FRS	New FRS
	Outer radius [mm (in.)]		
Stainless steel clad	4.7630 (0.18752)	4.7630 (0.18752)	4.7630 (0.18752)
Outer boron nitride	4.2997 (0.16928)	4.2997 (0.16928)	4.2997 (0.16928)
Heater element	3.1413 (0.12367)	3.1227 (0.12294)	3.1436 (0.12376)
Inner boron nitride	2.8090 (0.11059)	2.7882 (0.10977)	2.8116 (0.11069)
Thermocouple bundle	0.6652 (0.02619)	0.6652 (0.02619)	0.6652 (0.02619)
	Boron nitride density [g/cm³ (lb_m/ft^3)]		
Core	2.139 (133.5)	2.158 (134.7)	2.154 (134.5)
Annulus	2.117 (132.1)	2.135 (133.3)	2.131 (133.1)

7. FRS HEATING ELEMENT ELECTRICAL RESISTANCE

As mentioned in Sect. 6, accurate determination of the FRS radial dimensions is required for thermal analysis of the rods by ORINC, ORMDIN, and ORTCAL; however, the accuracy of the boundary conditions for these codes is much more important than the FRS radial dimensions.[39] The boundary conditions for ORINC and ORMDIN are the power generation rate in the heating element and the FRS sheath thermocouple response(s). The uncertainty in the BDHT FRS sheath thermocouple response is relatively well known;[40] however, during preliminary analysis of the THTF tests, the ability to compute the power input to the THTF core was only marginally accurate. For instance, the summed EI product [i.e., the sum for all rods of the product of the rod current (I) and the generator voltage (E)] was ~3 to 10% greater than the observed power delivery to the core fluid. Also, if the power to each rod was computed by using the rod current I and FRS heating element resistance R, where R is determined from literature data for Inconel-600 electrical resistivity and the cross-sectional area of the heating element, then the total power to the core was 2 to 4% greater than observed. These uncertainties in the computed power to each FRS (and the method of calculation) were totally unacceptable. Therefore, after the refurbishment of Bundle 3 (July–August 1980), FRS-058B (rod in grid position 37 in the refurbished bundle) was sent to the FRS TDL for tests to determine the in situ electrical resistance of the ACA (the FRS heating element) as a function of temperature.

S. D. Snyder of the Infrared Inspection Section of the FRS TDL has devised techniques for inspecting and characterizing FRSs.[41] The FRS is an electrical heating device, and, during its construction, the ability to measure accurately electrical parameters such as low and high resistance and leakage current is essential.[41] Low-resistance measurements are necessary to monitor the condition of the central heating element (the ACA). High-resistance and leakage-current measurements are necessary to determine the condition of the electrical insulation between the ACA and the sheath of the FRS and between the ACA and the FRS centerline thermocouples.

The circuit shown in Fig. 7.1 was assembled to measure the low-resistance value of the ACA with an accuracy of $\pm 0.5\%$. The FRS is heated to the desired temperature (as monitored by the FRS centerline thermocouples) by resistance heating of the FRS clad (the clad is electrically insulated from the ACA by the annular BN). Then, with the switch turned to position one, thus placing the dc voltmeter (DVM with a 0.1-mV sensitivity) across a 1.0000-Ω resistor, the power supply potential to the ACA is raised until the voltmeter reads 1.000 V. This establishes a 1.0000-A current through the ACA and resistor circuit. When the switch is moved to position two, the voltmeter reading is the ohmic value of the ACA resistance, because the current is 1.0000 A.

Using this technique, the ACA resistance curves vs temperature in Figs. 7.2–7.4 were generated. A comparison of four different runs is shown in Fig. 7.2. None of the four separate runs duplicated each other, and the extreme spread was ~3%. To provide a reason for this nonrepeatability, it is necessary to look at the run sequence and time frame for the tests. Run 1 (Fig. 7.2) was generated as the rod was heated up; the

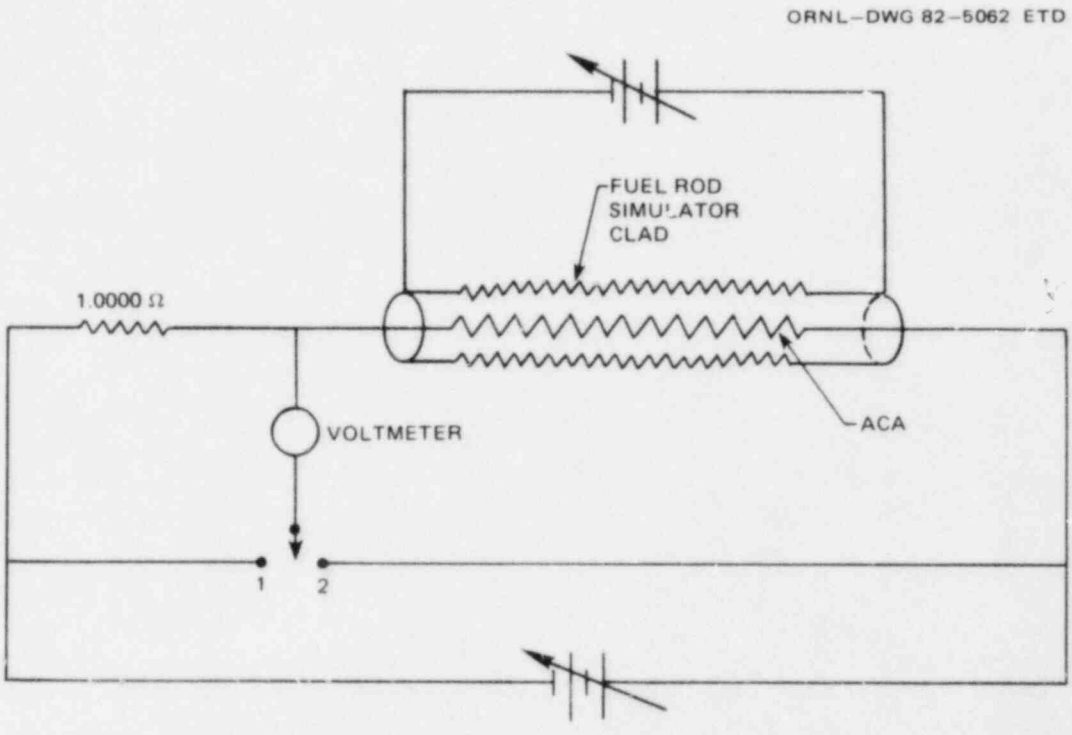

Fig. 7.1. ACA resistance measurement circuit.

starting point (condition) of the rod was as it was received from the THTF. The data for run 2 were obtained as the rod cooled down (after run 1), and the time required to complete run 2 was ~1 d (i.e., it was a very slow cool down). Two days elapsed between runs 2 and 3; after completing the test, the power to the FRS sheath was turned off, and the rod cooled to room temperature in ~1 h. Several ramped heating tests were made between runs 3 and 4, and these are indicated in Fig. 7.3. In these runs, the power to the sheath was turned on, the rod attained equilibrium conditions, data were taken, and then power was turned off. The cooling period in each case was 30 to 60 min. Run 4 was made after these ramp tests. The rod was cooled to room temperature in ~20 min by using a fan. Note that the ACA resistance at room temperature was repeatable when the rod had been previously cooled from >1000 K to room temperature in <1 h. Runs 1–4 and the ramp tests were made with the entire ACA; that is, the ACA consisted of the 3.672-m heated length and the terminal lead-in. After run 4, the terminal lead-in section of FRS-058B was cut-off, leaving just the 3.672-m heated length. The final run and run 4 are shown in Fig. 7.4. The difference between run 4 and the final run in Fig. 7.4 is the resistance of the ACA terminal lead-in section.

The resistance behavior illustrated by Fig. 7.2 is typical of alloys that can undergo order–disorder phenomenon. The order–disorder phenomenon has been extensively studied for Chromel (a nickel-chromium alloy)[43] because it is a common thermoelement material (type K thermocouples).

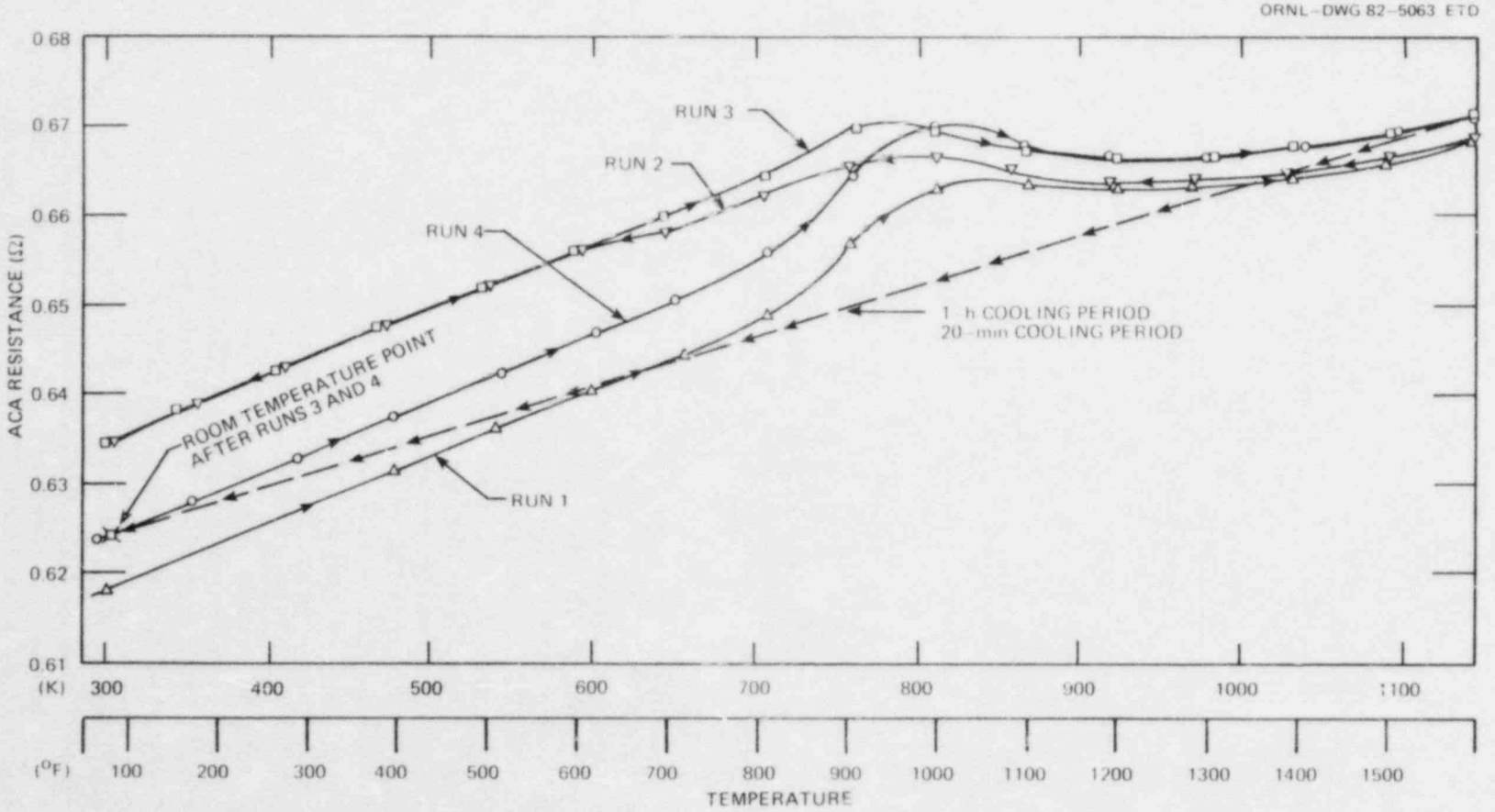

Fig. 7.2. ACA resistance vs temperature for entire ACA of FRS-058B.

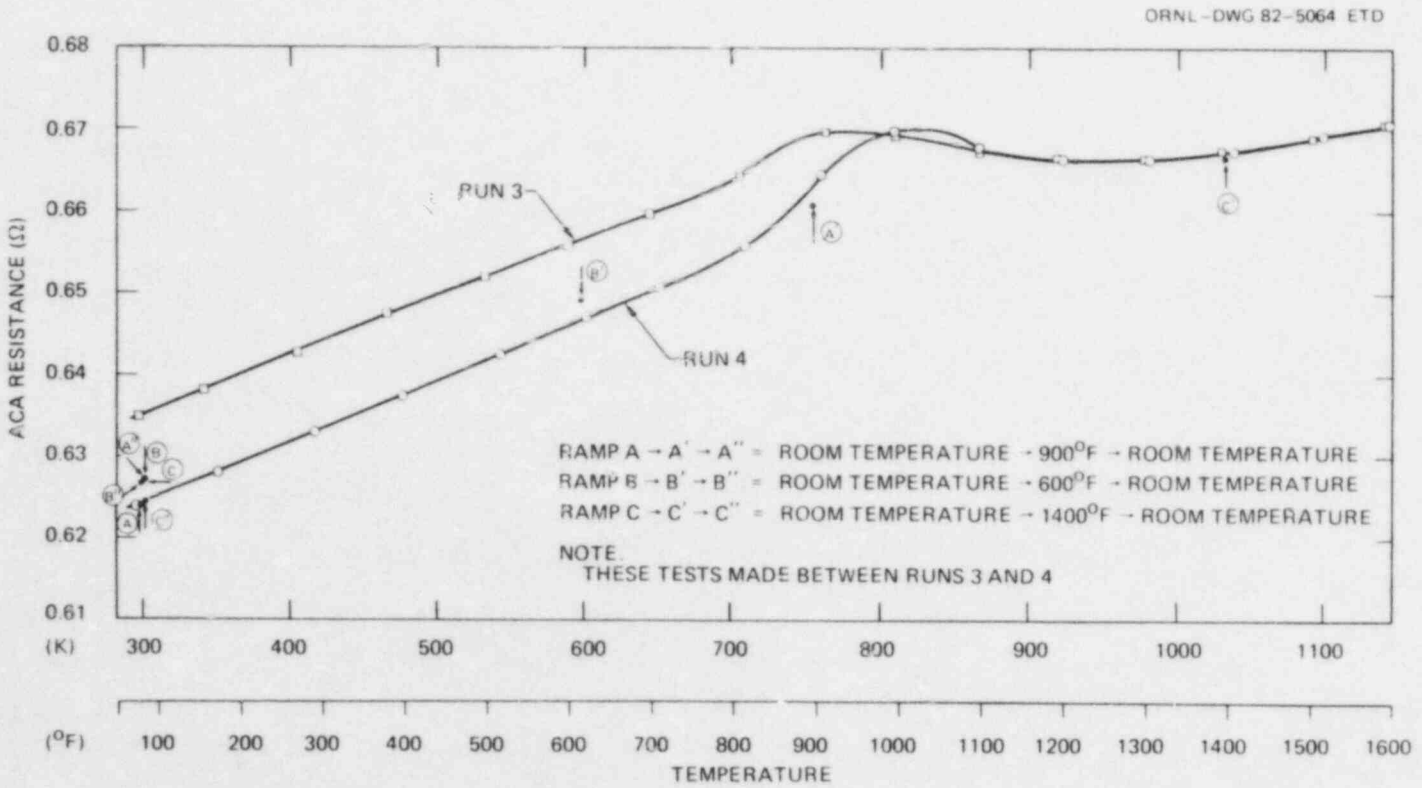

Fig. 7.3. ACA resistance vs temperature for entire ACA of FRS-058B (ACA heated by ramping sheath).

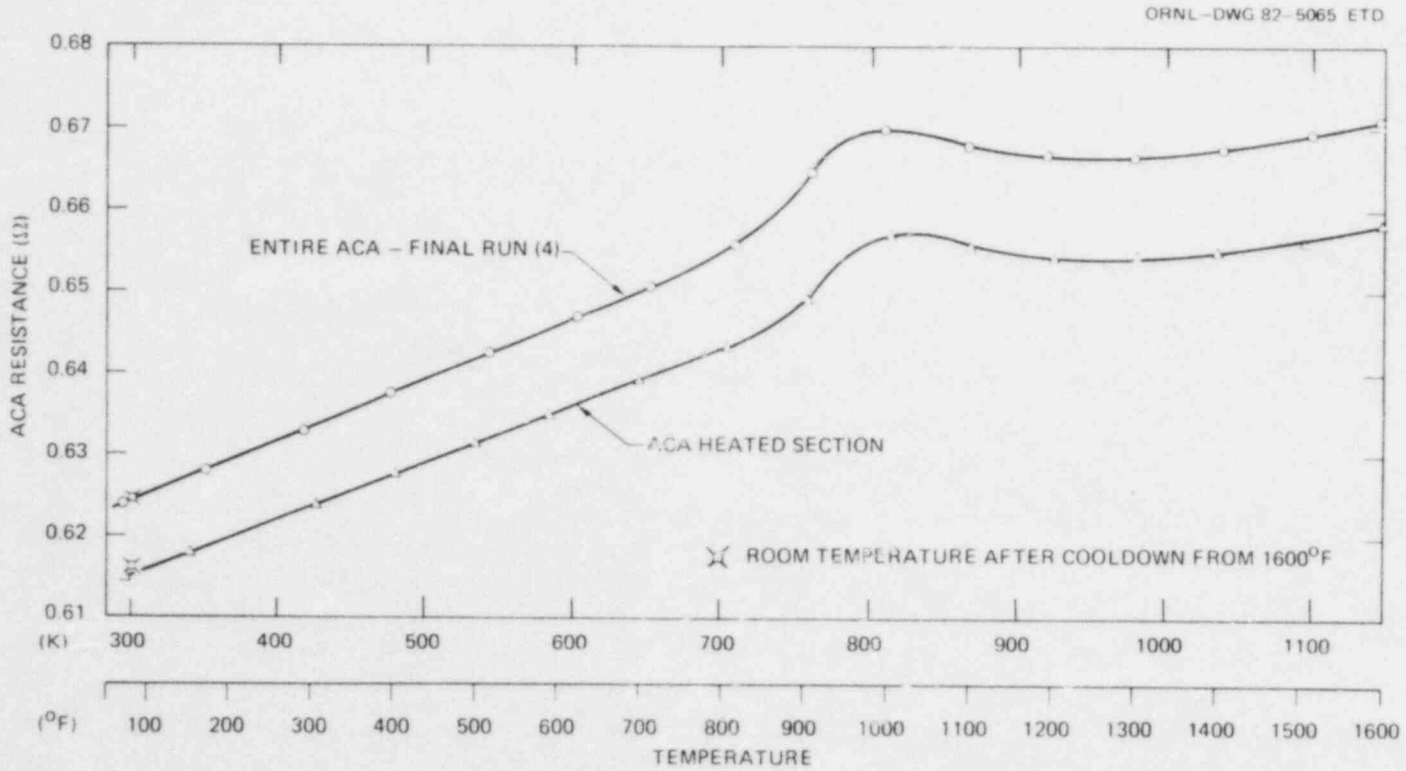

Fig. 7.4. ACA resistance vs temperature for heated section of FRS-058B.

Some of the pertinent points follow:

1. Between 475 and 875 K, the nickel and chromium atoms in Chromel tend to occupy specific sites in the crystal lattice (the ordered state).
2. Above 875 K, the atoms are distributed randomly among the lattice sites (the disordered state).
3. A change from the ordered to the disordered state or vice versa is reversible.
4. The rate and extent at which the ordered state is formed are time and temperature dependent.

McCulloch[44] has shown that the resistance change can approach +4% for Chromel. This background on Chromel has been given because the heating element in the BDHT rods consists of Inconel-600, which is a nickel, iron, and chromium alloy. Inconel-600 can undergo the same order-disorder phenomena as Chromel.

Referring to Fig. 7.2, the resistance curves for runs 1 and 2 (run 2 data were generated over an ~8-h cool-down period after run 1) start diverging (as the temperature decreases) at ~875 K. The ordering process appears to be complete at ~575 K, and the two runs are essentially parallel below that temperature with approximately +3% change in the resistance at room temperature. Run 3 resistance should track the run 2 results up to ~575 K, and above that temperature it should be greater than run 2 (at the corresponding temperature) because the degree of ordering is greater. In all runs subsequent to run 2, some degree of ordering (approximately +0.6% change in the resistance) appears even at temperatures >875 K. However, because the ordering is a time and temperature rate controlled process with faster cooling periods (as following run 3), the degree of ordering (and the resulting change in resistance) is less. Little difference appears in the resulting resistance (approximately +0.6%) at room temperature after cooling periods of 20 min and 1 h. Also, it must be stated that the laboratory cooling environment for FRS-058B is totally different from that in the THTF. Following a typical test in the THTF, the rod would be steam-cooled or water-quenched at a rate three orders of magnitude faster than the best rate obtained in the Infrared Laboratory.

The resistance curve generated in run 1 is assumed to be typical of Bundle 3 FRSs in the THTF. Run 1, however, included the entire ACA. Knowing the resistance of the heated section and the terminal lead-in separately would be preferable. The primary resistance in the ACA in the terminal lead-in section is in copper sleeves inside and outside of the Inconel-600 tube, and this resistance can be determined from Fig. 7.4. Thus, if the terminal end resistance is subtracted from the run 1 resistance curve, the resistance of the FRS-058B heated section as received from the THTF may be determined. This resistance along with the curves in Fig. 7.4 and run 1 are overlayed in Fig. 7.5.

If the ACA heated-section electrical resistance (lower curve in Fig. 7.5) is divided by the heated length (3.672 m for FRS-058B) and then multiplied by the heating element cross-sectional area (using dimensions from Table 6.6), the in situ Inconel-600 electrical resistivity is obtained. This is compared with literature data[45] in Figs. 7.6 and 7.7. The ACA heated-section electrical resistance per unit length for FRS-058B is shown in Fig. 7.8, and the ACA terminal end electrical resistance per unit

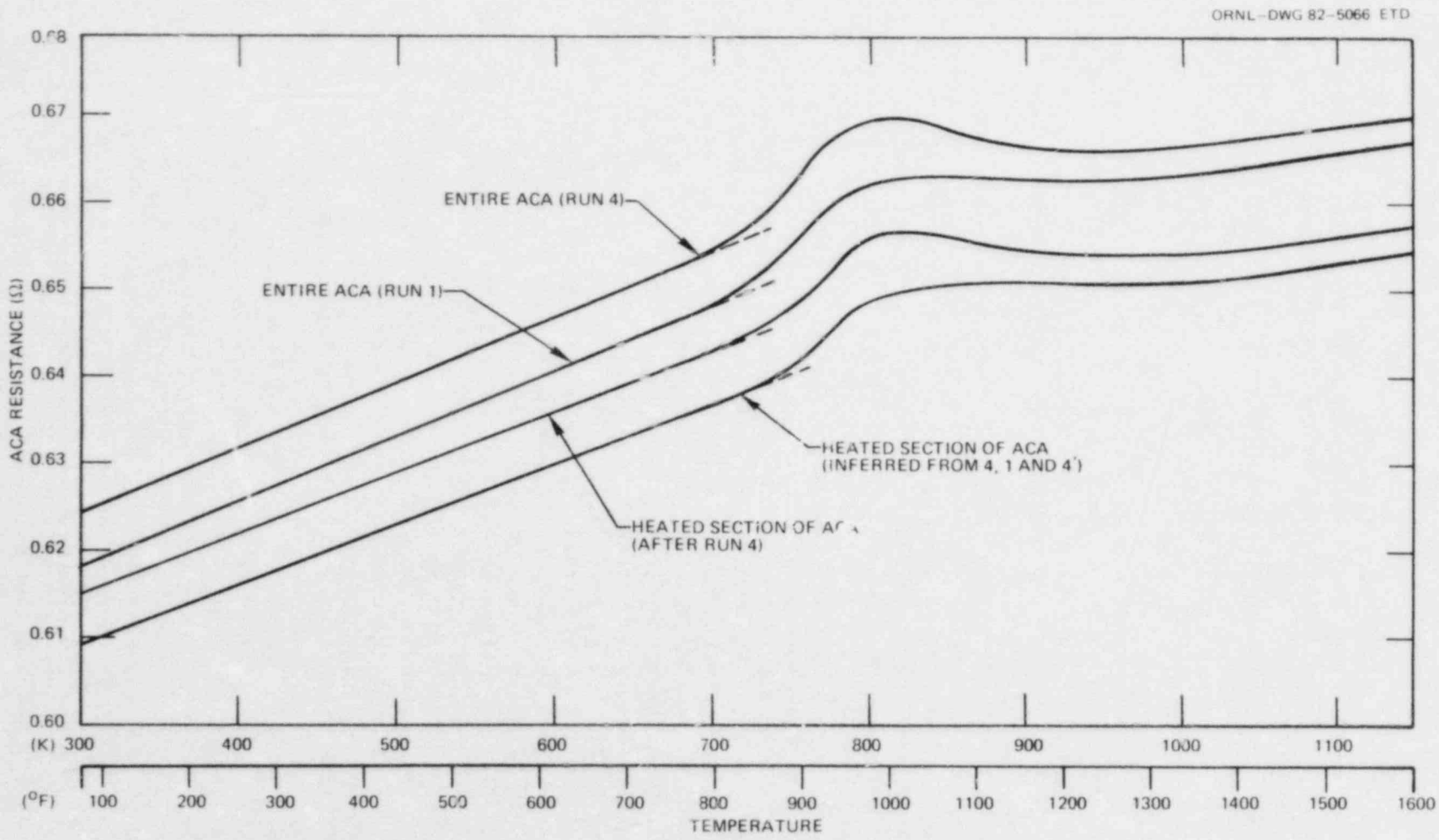

Fig. 7.5. ACA resistance vs temperature for heated section of FRS-058B.

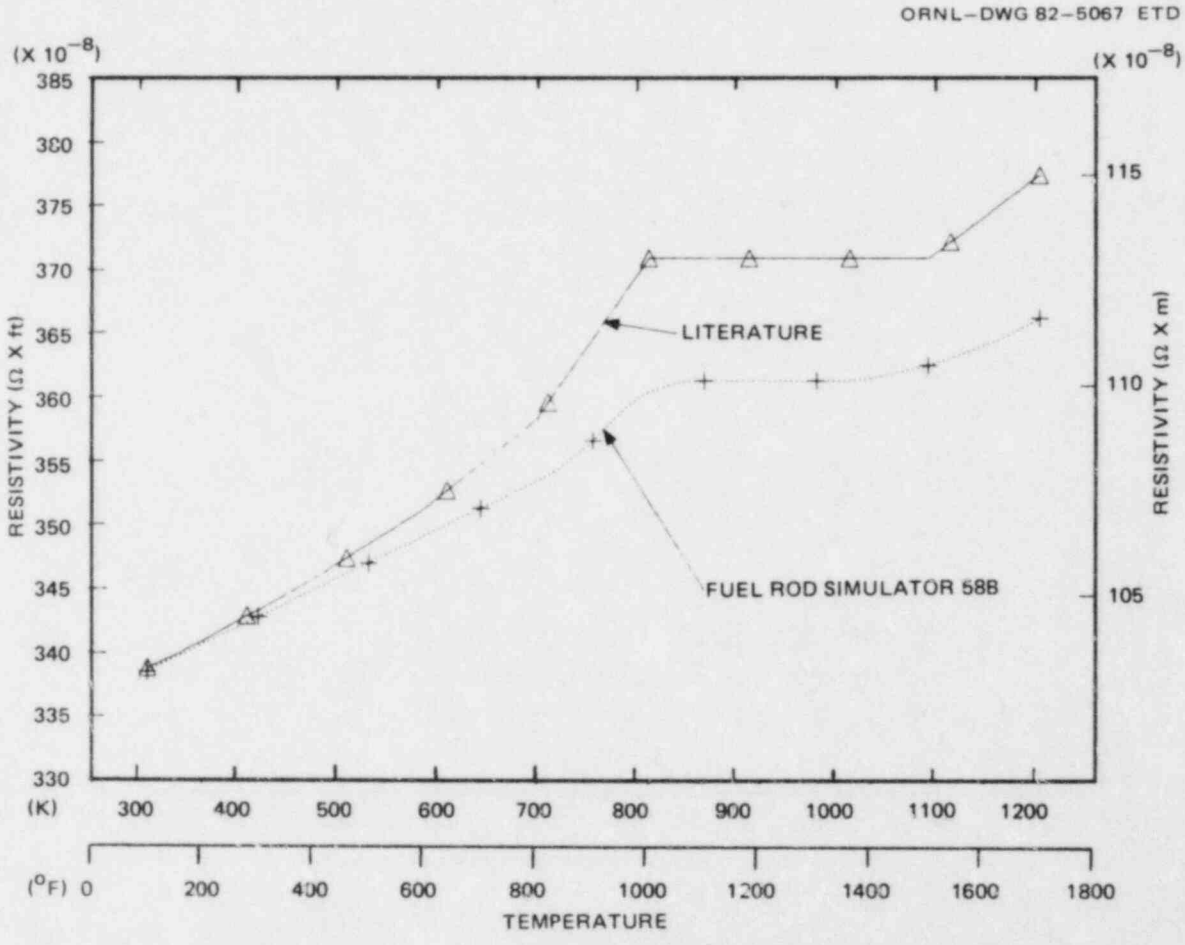

Fig. 7.6. Inconel-600 electrical resistivity comparison.

length for FRS-058B is shown in Fig. 7.9. Using a correction factor β_i defined by

$$\beta_i = \frac{\text{heated length of rod i}}{\text{heated length of FRS-058B}} ,$$

the electrical resistance of rod i in the THTF core can be determined from Fig. 7.8 and β_i by

$$R_i = R_{\text{FRS-0}} \times \beta_i ,$$

where R_i has units of ohm per unit length.

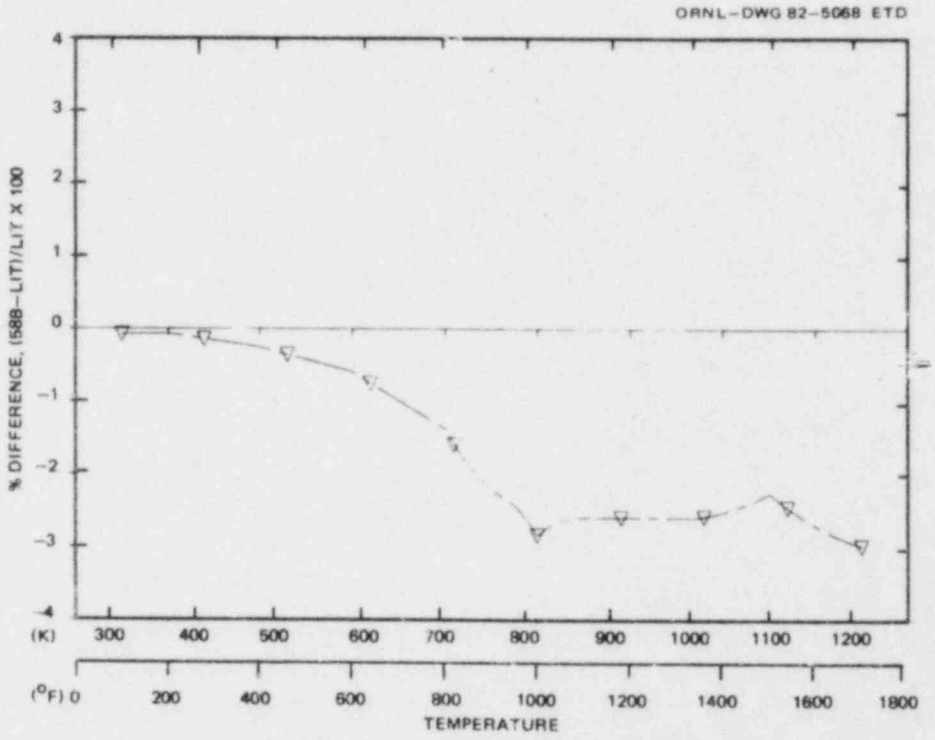

Fig. 7.7. Inconel 600 electrical resistivity comparison.

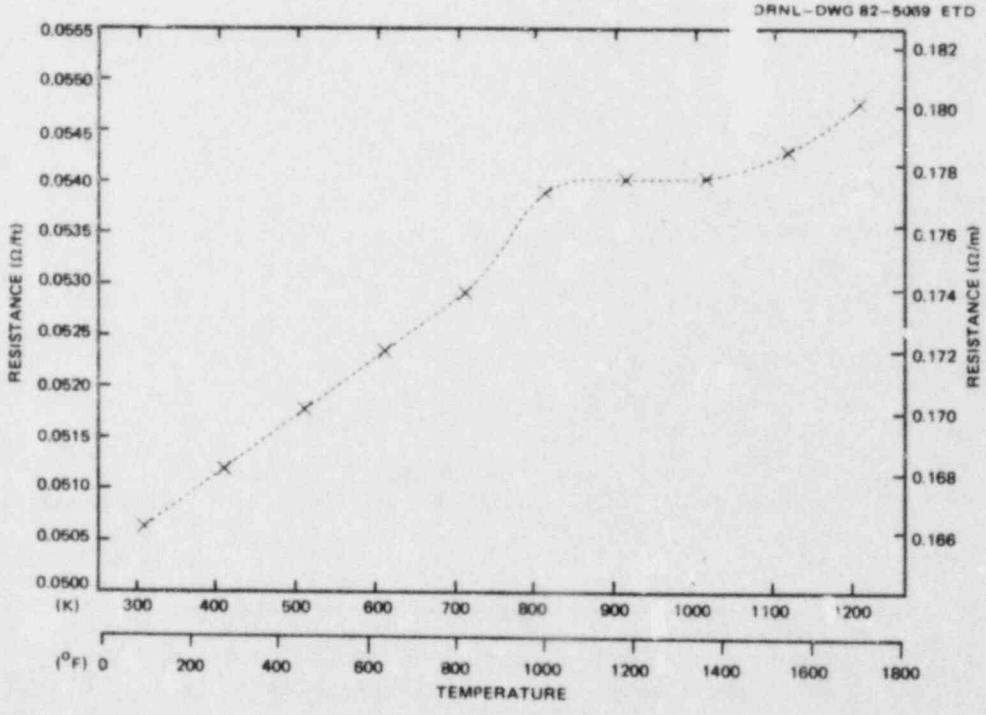

Fig. 7.8. FRS-058B heated length electrical resistance.

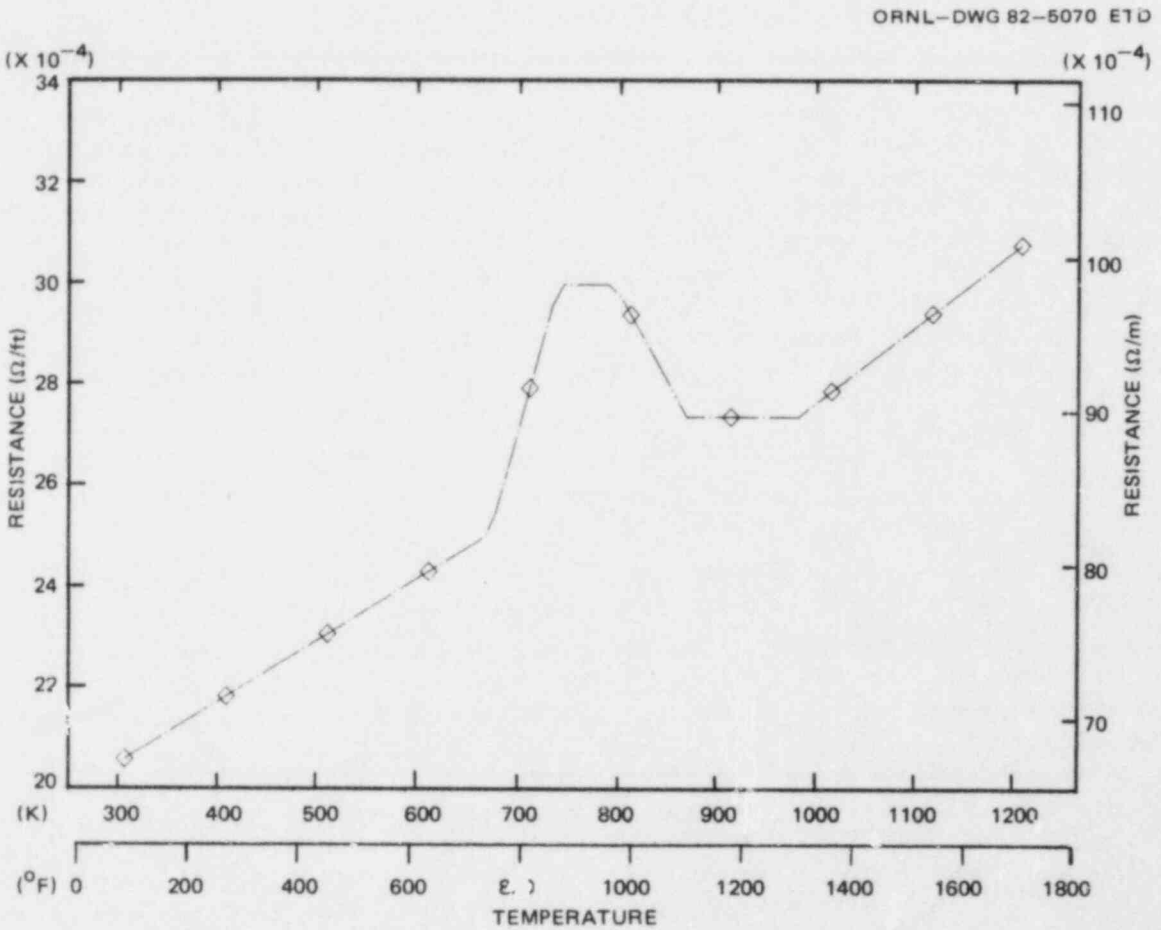

Fig. 7.9. [illegible]RS-0[illegible]B terminal end electrical resistance.

Using the in situ electrical resistance of the Inconel-600 (Fig. 7.8) and the terminal end electrical resistance (Fig. 7.9), the computed power input to the THTF core was ±1.0% of the observed power delivery to the core fluid.

8. FRS SURFACE EMISSIVITY

In many of the tests conducted in the THTF during 1979 and 1980, radiative heat transfer from the rod surface was a significant mode of heat removal from the FRS. Specifically in those tests in which the core was partially uncovered (i.e., the small-break LOCA tests and the steady-state film boiling tests), FRS surface temperatures reached 950 to 1150 K (1250 to 1610°F); at these temperatures radiation from the surface becomes an important mode of heat transfer. Heat transfer at the surface occurs by two mechanisms acting in parallel; that is, the total heat transferred at the surface is the sum of the heat transferred by convection and by radiation:

$$q_{total} = q_{convection} + q_{radiation} . \quad (8.1)$$

Because these tests (small-break LOCA and steady-state film boiling) are steady state, q_{total} is simply the power generated by the FRS that can be calculated given the current to the rod and the rod resistance (Sect. 7). If the objective of the test is to determine the convective component of the total heat transfer at the surface of the FRS, then the radiative component must be extracted from the total heat transferred. This determination of the radiant heat transfer requires that the rod surface emissivity be known. Estimates of the emissivity of stainless steel for different types of surfaces (i.e., polished or oxidized) can vary from 0.05 to 0.90. Also, the condition of the FRS cladding surface in the THTF does not necessarily fit in the literature categories and essentially is dependent on its environment and operating history (i.e., possible chemical corrosion, surface deposition, and surface discoloration due to high temperature). Because the facilities in the Infrared Inspection Section of the FRS TDL are available, it was decided to test one of the FRSs removed from the THTF during the bundle refurbishment in July–August 1980 to determine the surface emissivity.

S. D. Snyder used the circuit shown in Fig. 8.1 [FRS-026 (grid position 15)] for the FRS emissivity determination. The procedure used is as follows:

1. Take the FRS as received from the THTF (i.e., no surface preparation), and place the rod in the circuit as shown in Fig. 8.1.
2. Heat the FRS via resistance heating of the ACA to a desired temperature (as indicated by the FRS sheath and middle thermocouples), and determine the power to the rod and the rod temperature.
3. Repeat step two by 55 K increments over the range of 300 to 750 K, and then shut off the power and cool the rod with a fan.
4. Paint the FRS black and then repeat steps 1–3. (Two paints were used; each had a different temperature range over which it was applicable, and each had a known surface emissivity.)

These experiments could not be carried out in a vacuum, and as a result the total heat transferred at the surface (known) was the sum of the

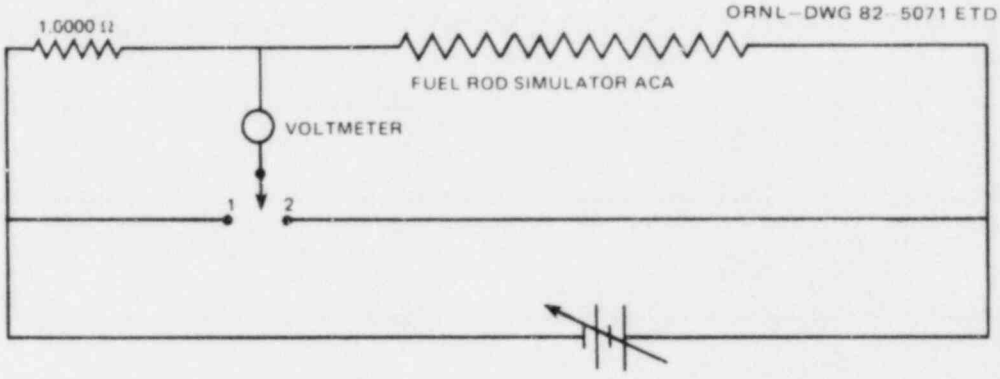

Fig. 8.1. Circuit used in FRS emissivity determination.

heat transferred by convection and radiation [Eq. (8.1)]. However, in the test apparatus, the convective heat transfer is via free (natural) convection to air that is adequately described by available correlations. The correlation used[46] is a Nusselt type of the form

$$\frac{hd}{K} = a\,[N_{Gr} \times N_{Pr}]^m , \tag{8.2}$$

where the parameters a and m are dependent on the product of the Grashof number (N_{Gr}) and Prandtl number (N_{Pr}). For the specified temperature range, the free convective film heat transfer coefficient [h in Eq. (8.2)] is plotted vs the rod temperature in Fig. 8.2. Thus, the convective heat transfer can be estimated by

$$q_{convection} = h\,A\,(T_{rod} - T_{sink}) , \tag{8.3}$$

where h is defined by Eq. (8.2) and Fig. 8.2, A is the surface area of the heated section of the FRS, and $T_{rod} - T_{sink}$ is the temperature difference between the rod and the surroundings. Then the radiant heat transfer is just the difference between the known power generation in the heated section and the convective heat transfer; that is,

$$q_{radiation} = q_{total} - q_{convection} .$$

The heat transfer at the rod surface (total, convective, and radiative) for the three experimental runs is given in Figs. 8.3–8.5. Run 2 was made with the rod painted with Krylon paint, which has an emissivity of 0.98 at temperatures >475 K; this paint turned to ash at ~700 K. Run 3 was made after painting the rod with Deshter paint, which has an emissivity of 0.92 at 670 K. A simplified formulation of radiant heat transfer is given by

$$q_{radiation} = \sigma A \varepsilon\,(T^4 - T_{sink}^4) . \tag{8.4}$$

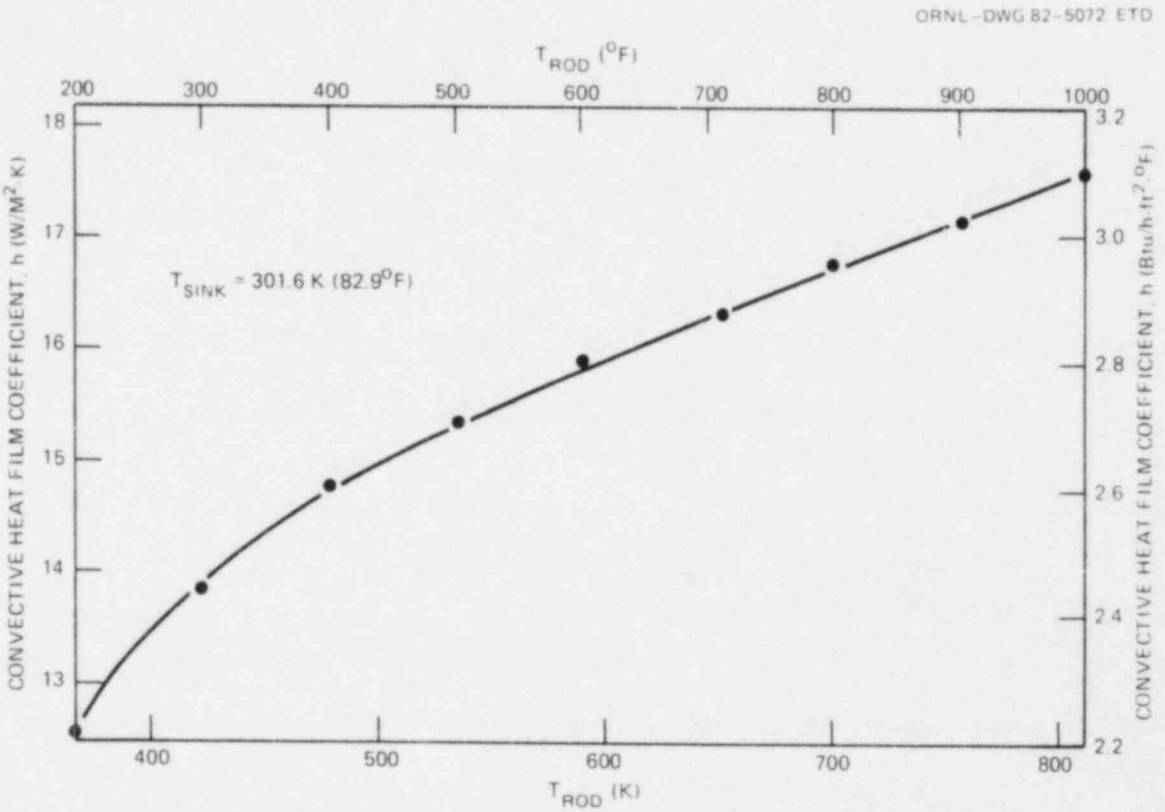

Fig. 8.2. Free convection film heat transfer coefficient as a function of rod temperature.

Given two surfaces (one with a known emissivity ε_1 and the second with an unknown emissivity ε_2) and letting

$$A_1 = A_2 ,$$

$$T_1 = T_2 ,$$

and

$$T_{sink_1} = T_{sink_2} .$$

Then,

$$\frac{q_{r_1}}{q_{r_2}} = \frac{\varepsilon_1}{\varepsilon_2} ,$$

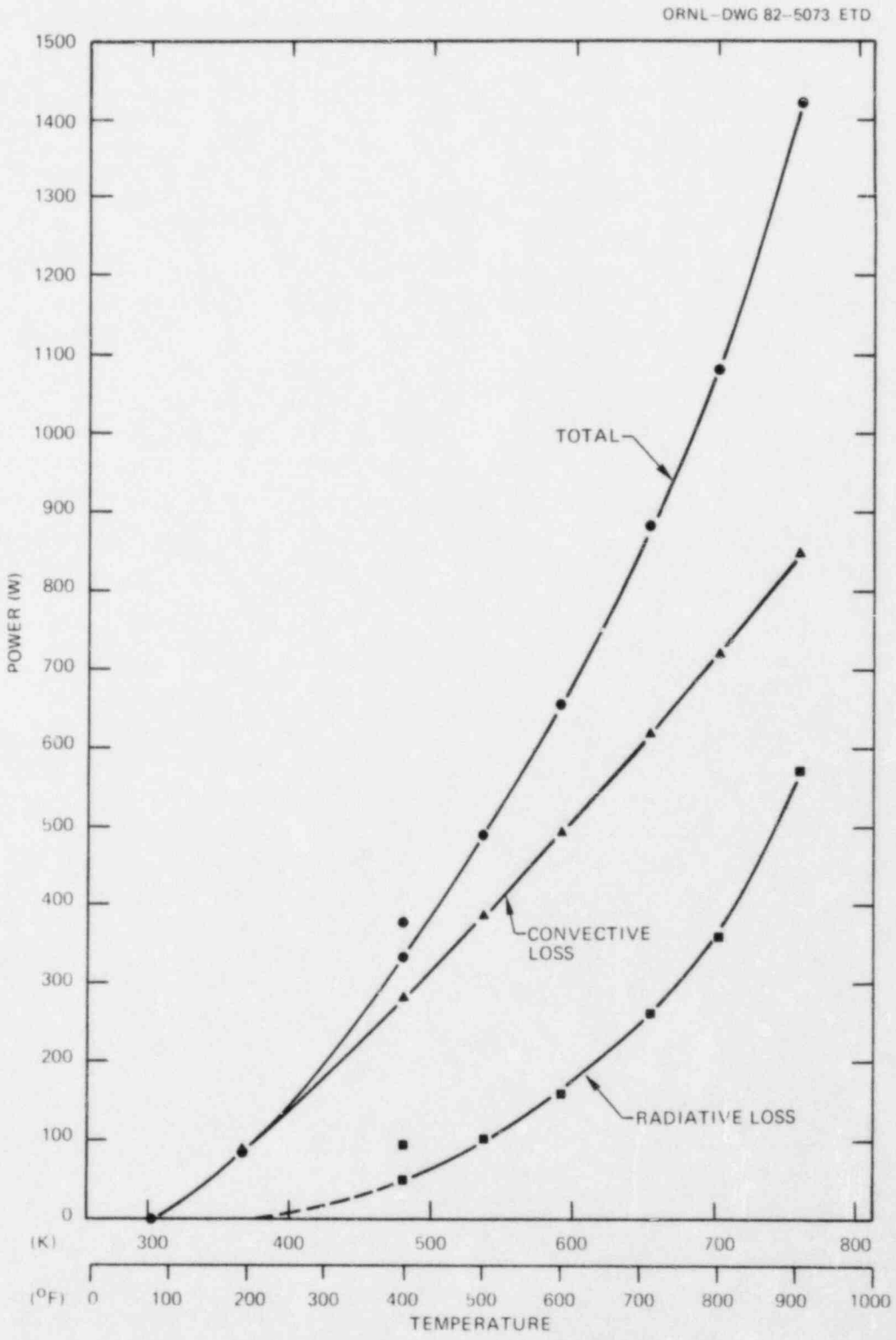

Fig. 8.3. Heat generation in the heated length of FRS-026 (unpainted).

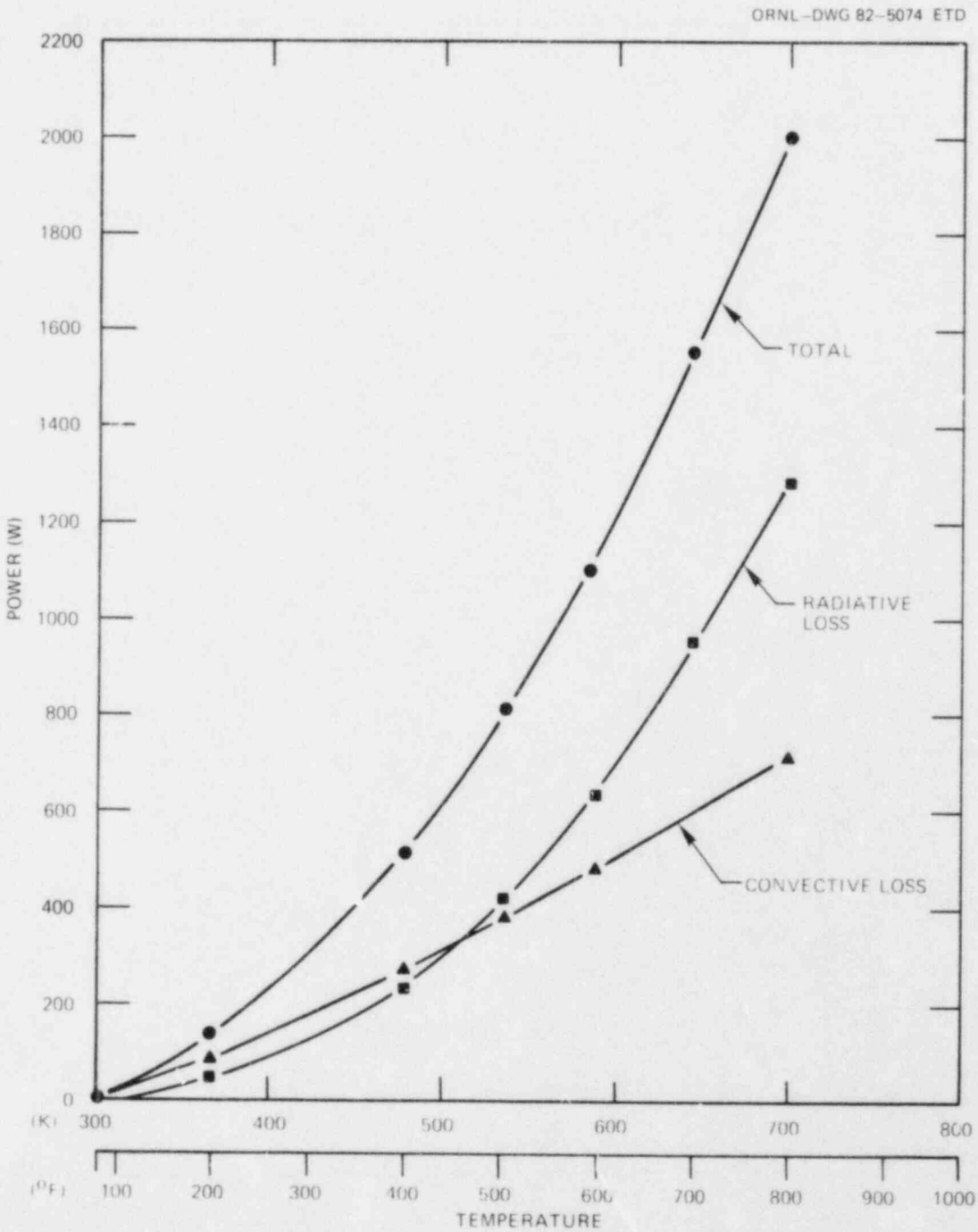

Fig. 8.4. Heat generation in the heated length of FRS-026 (painted with Krylon paint, ε ~ 0.98 at >475K).

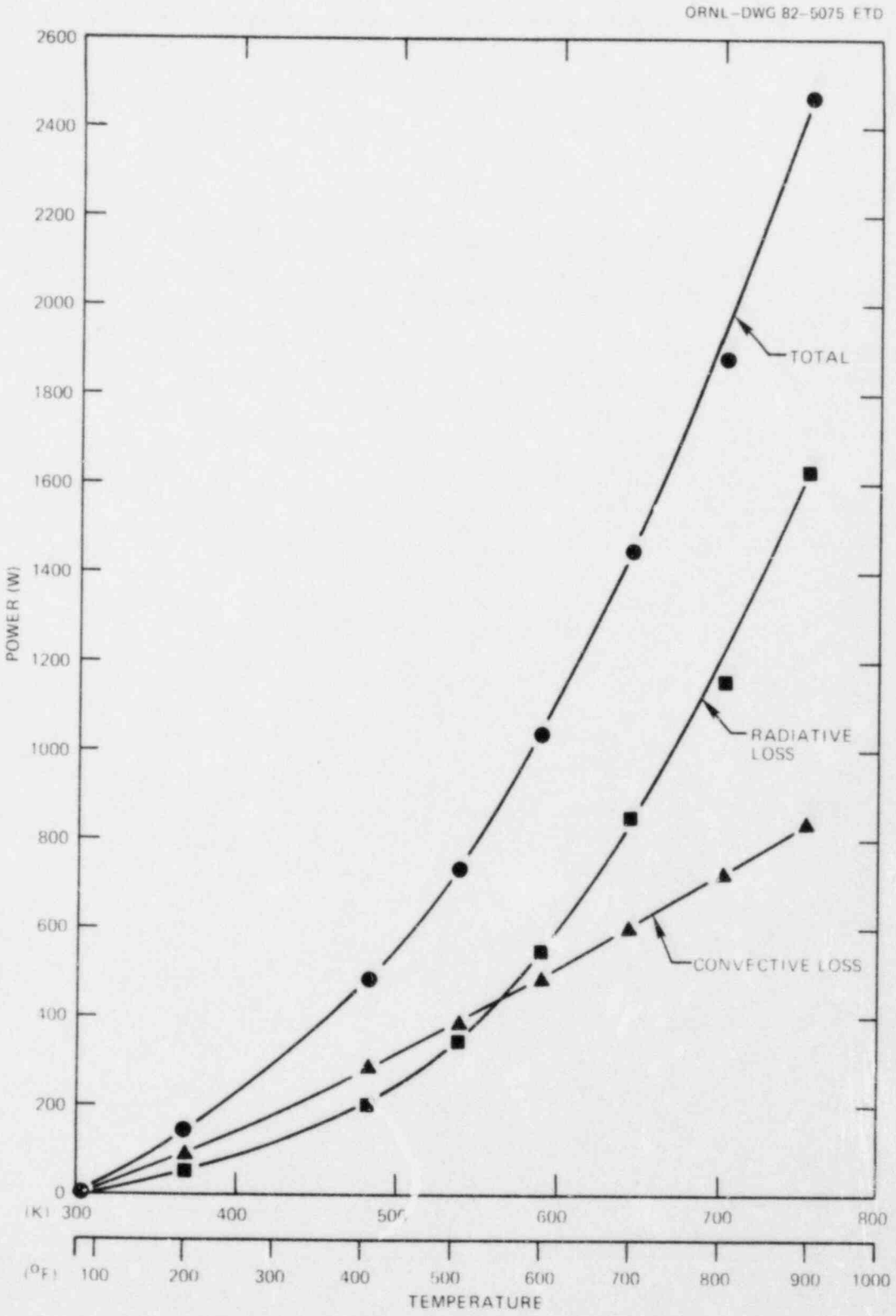

Fig. 8.5. Heat generation in the heated length of FRS-026 (painted with Deshler paint, ε ~ 0.92 at ~670K).

or

$$\varepsilon_2 = \varepsilon_1 \frac{q_{r_2}}{q_{r_1}} , \tag{8.5}$$

where the radiative heat transfer q_{r_1} and q_{r_2} are known and the emissivity ε_1 is known. Thus, the emissivity of the unpainted rod (i.e., the FRS as received from the THTF) can be estimated as a function of rod temperature from the plots in Figs. 8.3, 8.5, and the known[47] paint emissivities. The emissivity of the FRS-026 surface after removal from the THTF is shown in Fig. 8.6. The best linear least squares fit to the points in Fig. 8.6

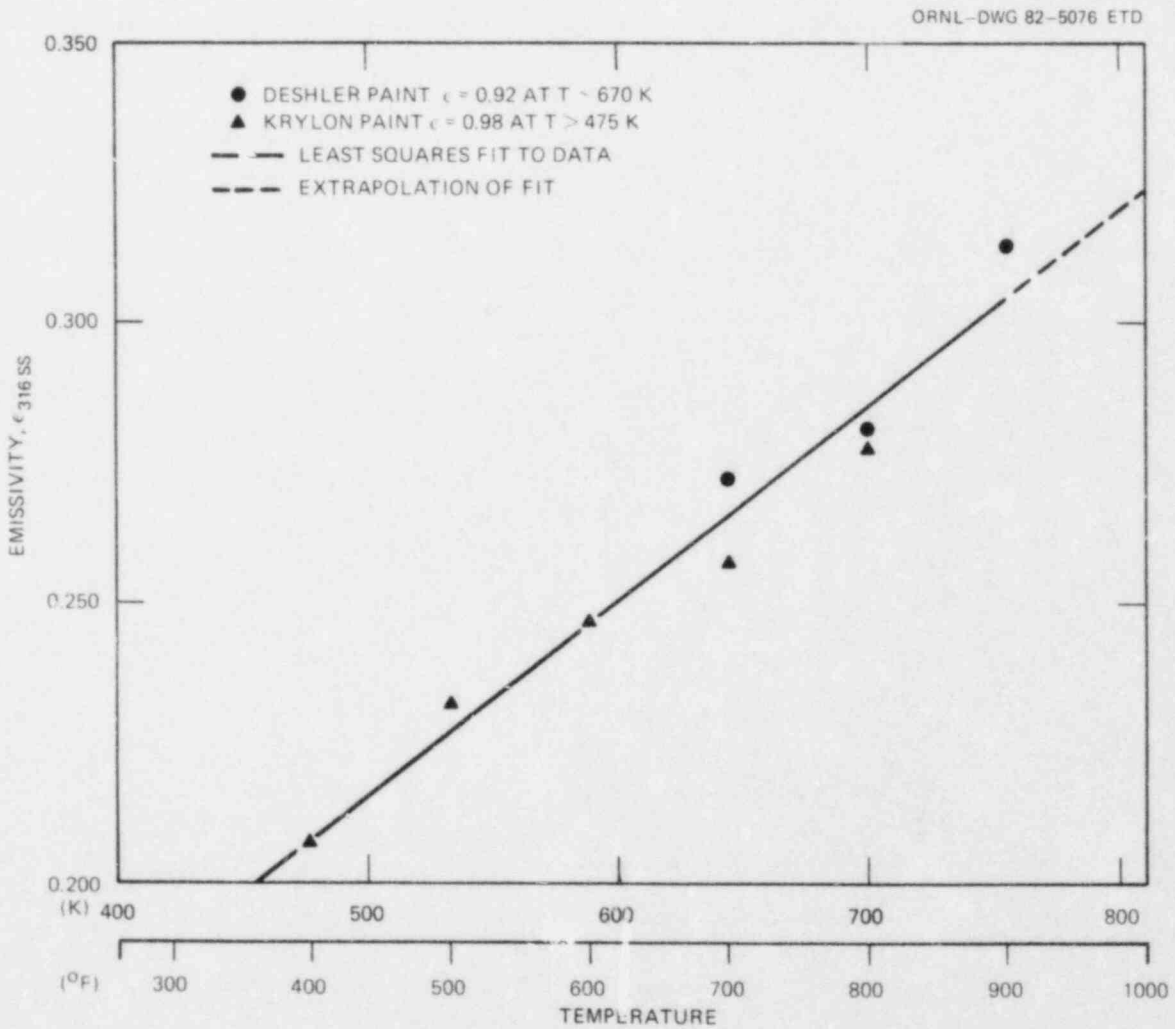

Fig. 8.6. Emissivity of FRS-026 surface after removal from the THTF.

takes the following form

$$\varepsilon\,(T) = 0.25617 + 0.000348\,(T - 616.67)\ , \qquad (8.6)$$

where T has units of K; or

$$\varepsilon\,(T) = 0.25617 + 0.000193\,(T - 650)\ , \qquad (8.7)$$

where T has units of °F. Using the available Infrared Inspection Section experimental apparatus, 750 K was approximately the maximum temperature to which the painted rods could be heated without oxidizing the paint (as noted, the Krylon paint oxidized at ~700 K). Therefore, for the range of temperatures of interest (i.e., 950–1150 K) an extrapolation of the experimental data must be made. Remember that it is an extrapolation beyond the range over which the data were gathered. For the temperature range of 950–1150 K, the estimated FRS surface emissivity in the THTF is 0.372–0.442.

9. CONCLUSIONS

A chronological history of the THTF Bundle 3 has been compiled. This compilation includes not only the original Bundle 3 but also two major refurbishments in 1980. The material documents the in-core instrument measurement sites and the actual operating history of the THTF (i.e., tests and experiments performed) with Bundle 3. Additionally, information is provided on the Bundle 3 FRSs (such as radial dimensions, heating element electrical resistivity, surface emissivity) that will be needed for thermal analysis of the FRS responses during THTF testing.

REFERENCES

1. *Project Description, ORNL-PWR Blowdown Heat Transfer Separate-Effects Program — Thermal Hydraulic Test Facility (THTF)*, ORNL/NUREG/TM-2 (February 1976).

2. L. J. Ott and R. A. Hedrick, *ORINC — A One-Dimensional Implicit Approach to the Inverse Heat Conduction Problem*, ORNL/NUREG-23 (November 1977).

3. B. R. Bass, *INCAP: A Finite Element Program for One-Dimensional Nonlinear Inverse Heat Conduction Analysis*, NUREG/CR-0832 (ORNL/NUREG/CSD/TM-8) (July 1979).

4. W. D. Turner, D. C. Ehod, and I. I. Siman-Tov, *HEATING5 — An IBM 360 Heat Conduction Program*, ORNL/CSD/TM-15 (March 1977).

5. L. J. Ott and K. W. Childs, *Surface Heat Flux Perturbations in BDHT Fuel Pin Simulators*, NUREG/CR-0610 (ORNL/NUREG-54) (April 1979).

6. J. D. White et al., *Quart. Prog. Rep. on Blowdown Heat Transfer Separate-Effects Program for April–June 1979*, NUREG/CR-0954 (ORNL/NUREG/TM-345) (October 1979).

7. D. G. Thomas et al., *Quart. Prog. Rep. on Blowdown Heat Transfer Separate-Effects Program for January–March 1978*, NUREG/CR-0133 (ORNL/NUREG/TM-205) (July 1978).

8. BDHT Memorandum No. 2278 from L. J. Ott to BDHT Staff, July 26, 1979; Subject: Location of FRS Thermocouples in THTF Bundle 3.

9. BDHT Memorandum No. 2327 from B. J. Veazie to W. G. Craddick; Subject: THTF Bundle 3 — Thermocouple Nomenclature.

10. D. G. Thomas et al., *Quart. Prog. Rep. on Blowdown Heat Transfer Separate-Effects Program for October–December 1977*, ORNL/NUREG/TM-175 (April 1978).

11. BDHT Memorandum No. 2349 from D. H. Cook to J. D. White; Subject: Location of Critical Points in Bundle 3.

12. J. D. White et al., *Quart. Prog. Rep. on Blowdown Heat Transfer Separate-Effects Program for July–September 1979*, NUREG/CR-1121 (ORNL/NUREG/TM-363) (December 1979).

13. W. G. Craddick et al., *Quart. Prog. Rep. on Blowdown Heat Transfer Separate-Effects Program for October–December 1979*, NUREG/CR-1306 (ORNL/NUREG/TM-381) (June 1980).

14. L. J. Ott and R. A. Hedrick, *ORTCAL — A Code for THTF Heater Rod Thermocouple Calibration*, NUREG/CR-0342 (ORNL/NUREG-51) (February 1979).

15. R. W. McCulloch et al., *Analysis and Repair of Water Contaminated Boron Nitride Insulation in BDHT-THTF Bundle 3 Fuel Rod Simulators*, NUREG/CR-2046 (ORNL/NUREG/TM-451) (June 1981).

16. BDHT Memorandum No. 2405 from L. J. Ott to BDHT Staff, May 2, 1980; Subject: Location of Test Section (FRS and Fluid) Thermocouples in the Refurbished THTF Bundle 3.

17. C. B. Mullins, *A Preliminary Assessment of Film Boiling Heat Transfer Correlations During Transient Upflow of High Pressure Water (Interim Report for THTF Test 3.03.6AR)*, ORNL/CF-81/266 (July 1980).

18. M. D. White, *Quick Look Report on Thermal Hydraulic Test Facility Test 3.04.7R Transient Film Boiling in Downflow, June 19, 1980*, CRNL/BDHT-2458 (July 1980).

19. R. C. Hagar, *Oak Ridge National Laboratory PWR Blowdown Heat Transfer Separate Effects Program Interim Report Test 3.05.5B*, ORNL/BDHT-2507 (October 1980).

20. BDHT Memorandum No. 2403 from T. M. Anklam and L. J. Ott to W. G. Craddick and J. D. White, May 2, 1980; Subject: Location of Thermocouples in FRSs (10) to be Fabricated by R. W. McCulloch.

21. BDHT Memorandum No. 2409 from C. R. Hyman to W. G. Craddick and J. D. White, May 9, 1980; Subject: Additional Considerations on Placement of Thermocouples within FRSs to be Fabricated by R. W. McCulloch.

22. BDHT Memorandum No. 2457 from T. M. Anklam, C. R. Hyman, and C. B. Mullins to R. W. McCulloch, July 16, 1980; Subject: Specifications for New 12 SMB FRSs.

23. BDHT Memorandum No. 2462 from T. M. Anklam, C. R. Hyman, and C. B. Mullins to R. W. McCulloch, July 21, 1980; Subject: Revised FRS Replacements.

24. BDHT Memorandum No. 2494 from L. J. Ott to BDHT Staff, September 5, 1980; Subject: Location of Test Section FRS Thermocouples in the Rerefurbished THTF Bundle No. 3.

25. BDHT Memorandum No. 2488 from L. J. Ott to W. G. Craddick, August 27, 1980; Subject: Shroud Wall Thermocouples.

26. W. G. Craddick et al., *Quart. Prog. Rep. on Blowdown Heat Transfer Separate-Effects Program for January-March 1980*, NUREG/CR-1483 (ORNL/NUREG/TM-394) (June 1980).

27. J. D. White et al., *Quart. Prog. Rep. on Blowdown Heat Transfer Separate-Effects Program for April-June 1980*, NUREG/CR-1628 (ORNL/NUREG/TM-402) (September 1980).

28. J. D. White et al., *Quart. Prog. Rep. on Blowdown Heat Transfer Separate-Effects Program for July-September 1980*, NUREG/CR-1837 (ORNL/NUREG/TM-425) (January 1981).

29. D. G. Morris et al., *A Preliminary Evaluation of Rod Bundle Post-CHF Heat Transfer to High Pressure Water in Transient Upflow (Interim Report for THTF Test 3.06.6B)*, ORNL/CF-81/265 (November 1980).

30. C. B. Mullins et al., *A Preliminary Evaluation of Post-CHF Steady State Rod Bundle Heat Transfer to High Pressure Water (Interim Report of THTF Test Series 3.07.9)*, ORNL/CF-81/268 (February 1981).

31. D. G. Morris and C. B. Mullins, *Quick Look Report on THTF Test 3.08.6C, Transient Film Boiling in Upflow, October 1, 1980*, ORNL/BDHT-2534 (January 1981).

32. T. M. Anklam, "Small Break LOCA Heat Transfer Testing at ORNL," presented to the NRC Heat Transfer Workshop, January 30, 1981.

33. B. R. Bass, J. B. Drake, and L. J. Ott, *ORMDIN: A Finite Element Program for Two-Dimensional Nonlinear Inverse Heat Conduction Analysis*, NUREG/CR-1709 (ORNL/NUREG/CSD/TM-17) (December 1980).

34. Letter No. MS-79-0235 from R. L. Ludwig to M. D. White, June 1979; Subject: Measurement of Sections from BDHT FRS 038.

35. BDHT Memorandum No. 2287 from L. J. Ott and J. A. Smolen to BDHT staff, August 8, 1979; Subject: Bundle 3 Fuel Rod Simulator Radial Dimensions.

36. BDHT Memorandum No. 2522 from L. J. Ott to BDHT Staff, December 9, 1980; Subject: Updated Bundle 3 Fuel Rod Simulator Radial Dimensions.

37. Letter No. 80J-1120-195 from R. L. Ludwig, Oak Ridge National Laboratory, to L. J. Ott, Oak Ridge National Laboratory, November 20, 1980; Subject: Measurement of Sections from BDHT FRS- 058B.

38. R. W. McCulloch et al., *Fabrication Technology Development of Fuel Rod Simulators for Blowdown Heat Transfer Tests* (to be published).

39. K. W. Childs, *Uncertainty in Calculated Surface Temperature and Surface Heat Flux of THTF Heater Rods*, NUREG/CR-1211 (ORNL/NUREG/CSD/TM-12) (December 1980).

40. B. J. Veazie, *Instrument Uncertainty Analysis for the THTF Loop*, a presentation given to THTF and Instrument and Control Personnel (January 1980).

41. S. D. Synder et al., *Infrared Inspection and Characterization of Fuel-Pin Simulators*, ORNL/NUREG/TM-55 (November 1976).

42. S. D. Snyder, "The Prevention and Cure of Diseased Fuel Rod Simulators – From Conception to Death – By Timely and Proper Inspection," paper presented at the International Symposium on Fuel Rod Simulators – Development and Application, Gatlinburg, Tennessee, October 22-24, 1980.

43. R. L. Anderson and T. G. Kollie, *Accuracy of Small Diameter Sheathed Thermocouples for the Core Flow Test Loop*, ORNL-5401 (April 1979).

44. Letter from R. W. McCulloch, Oak Ridge National Laboratory, to L. B. Thompson, Nuclear Regulatory Commission, January 25, 1980; Subject: Determination of a Recovery Anneal Process to Remove Coldwork from Type K Small Diameter Sheathed Thermocouples.

45. American Society for Metals, *Source Book on Industrial Alloy and Engineering Data*, Metals Park, Ohio, 1978.

46. J. H. Perry, *Chemical Engineers' Handbook*, Fourth Edition, McGraw-Hill, 1963.

47. S. D. Snyder, Oak Ridge National Laboratory, personal communication to L. J. Ott, Oak Ridge National Laboratory, 1980.

Appendix A

LOCATION AND NOMENCLATURE FOR FLUID THERMOCOUPLES IN THTF BUNDLE 3

The location (axial and subchannel) of all fluid thermocouples monitored in the original THTF Bundle 3 is presented in Fig. A.1. These core fluid thermocouples can be subdivided into four distinct groups. The naming convention and location of these subgroups are given in the following four sections.

A.1 Subchannel Thermocouples

The subchannel thermocouple rake is located ~2.3 cm above the upper end of the heated section (414.5 cm above the gauge line). The naming convention takes the following form

TE-12nn ,

where

nn = a number between 01-81 that equals the number of the subchannel in which it is located.

Figure A.2 indicates those subchannel thermocouples monitored by the CCDAS as of January 8, 1980.

A.2 Spacer-Grid Thermocouples

The spacer-grid fluid thermocouples are attached to core grids 2-7. The naming convention for these thermocouples has the following form

TE-29na ,

where

n = a number 1-6 designating the spacer-grid level as follows

Number	Between thermocouple levels	Actual Bundle 3 spacer-grid No.
1	A&B	2
2	B&C	3
3	C&D	4
4	D&E	5
5	E&F	6
6	F&G	7

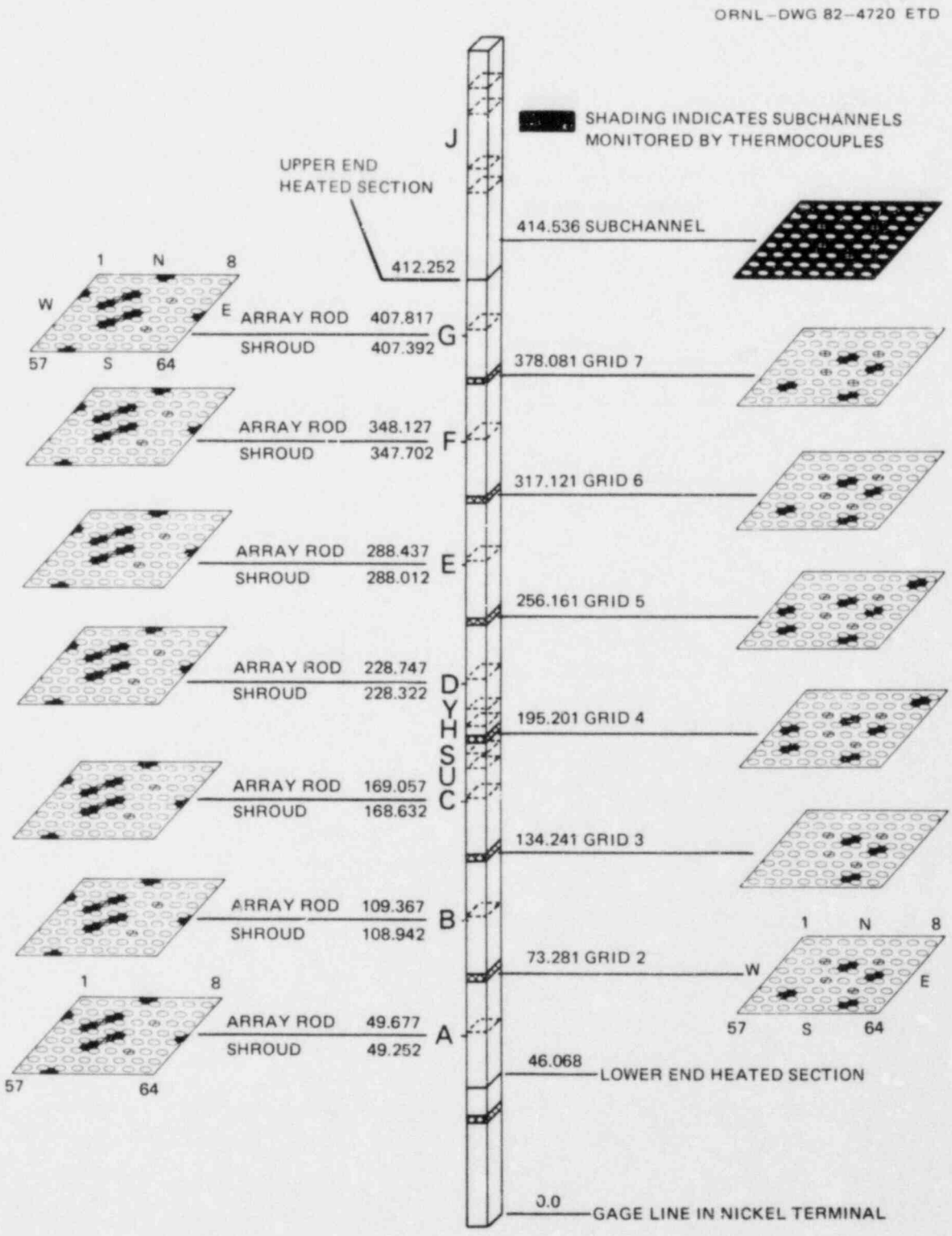

Fig. A.1. Location of fluid thermocouples in THTF Bundle 3. All dimensions are in centimeters and are referenced to the gage line in the nickel terminal.

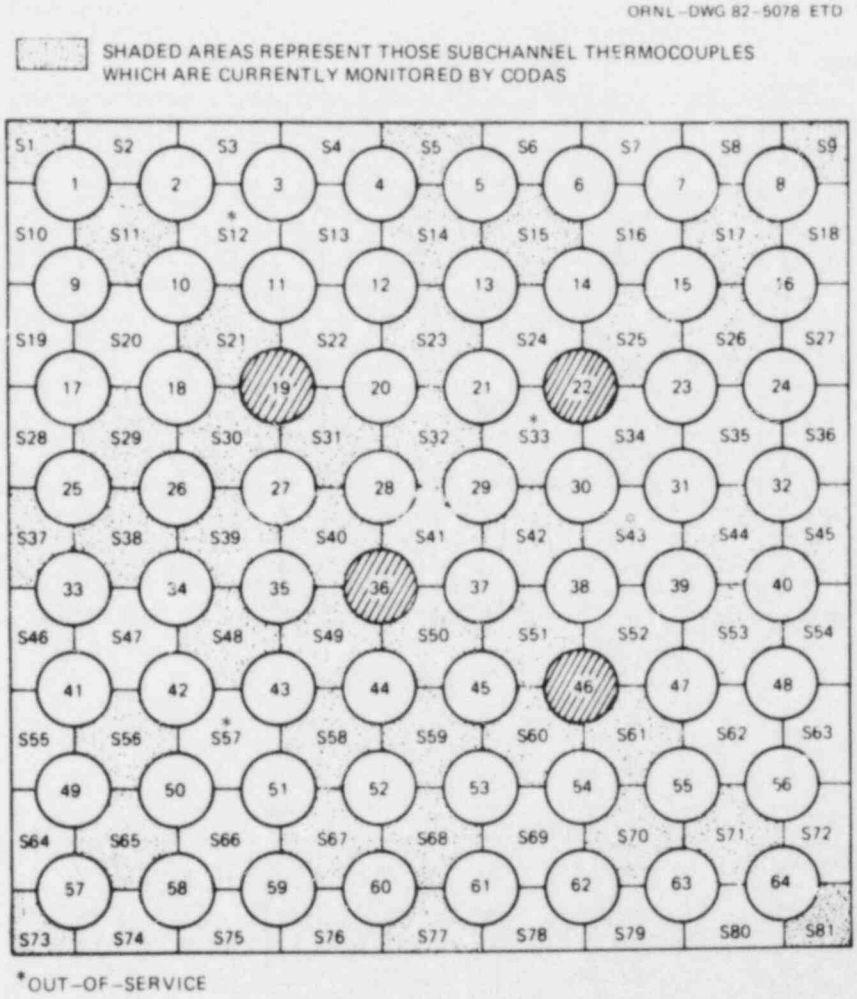

Fig. A.2. Subchannel thermocouples.

and

a = a letter "A–F" designating the subchannel into which the thermocouple is projecting, as follows

Letter	Subchannel
A	34
B	43
C	57
D	70
E	17
F	38

Those fluid subchannels monitored by spacer-grid thermocouples are indicated in Figs. A.3(a–f).

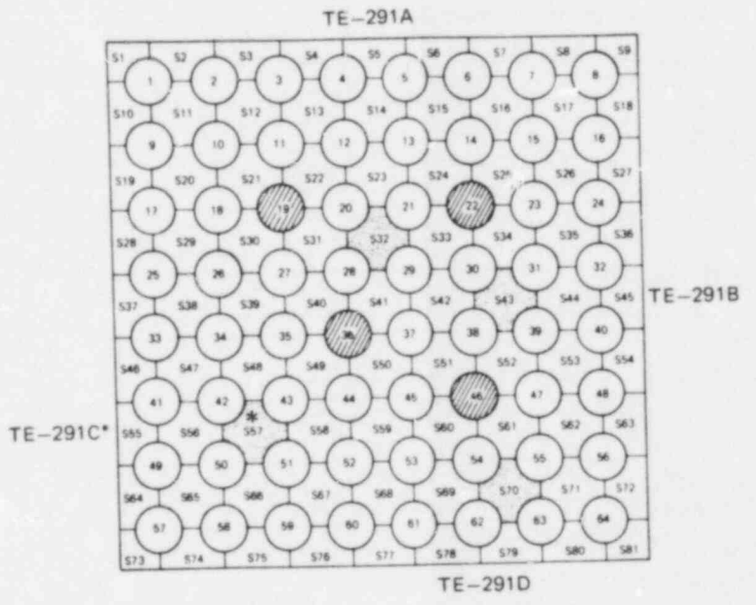

(a) SPACER GRID 2

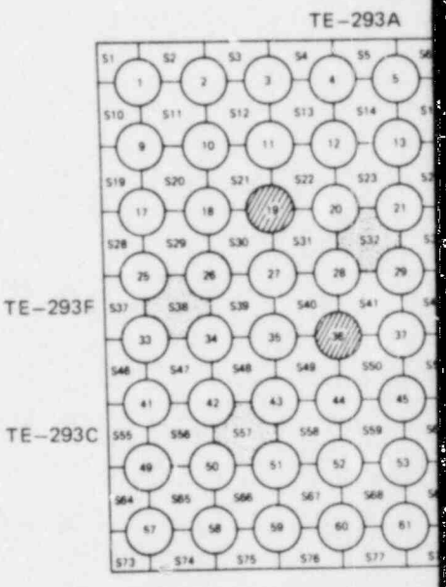

(c) SPACER GRID 4

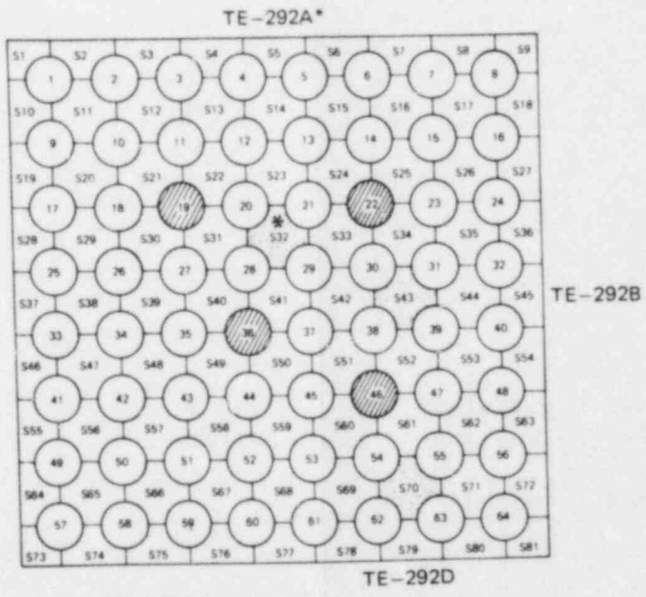

(b) SPACER GRID 3

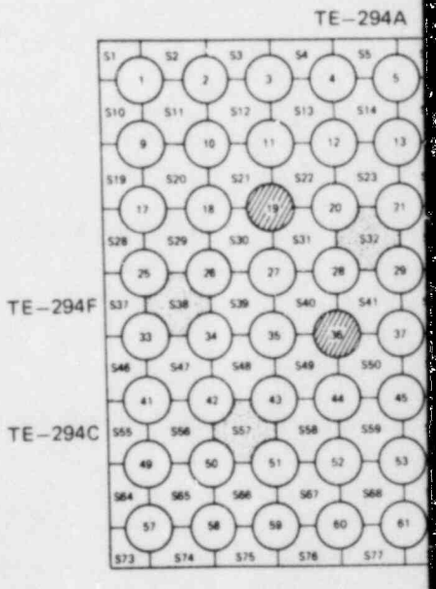

(d) SPACER GRID 5

● INACTIVE RODS

*OUT-OF-SERVICE (NOT MONITORED BY CODAS)

Fig. A.3. Spacer-gri

ORNL-DWG 82-5079 ETD

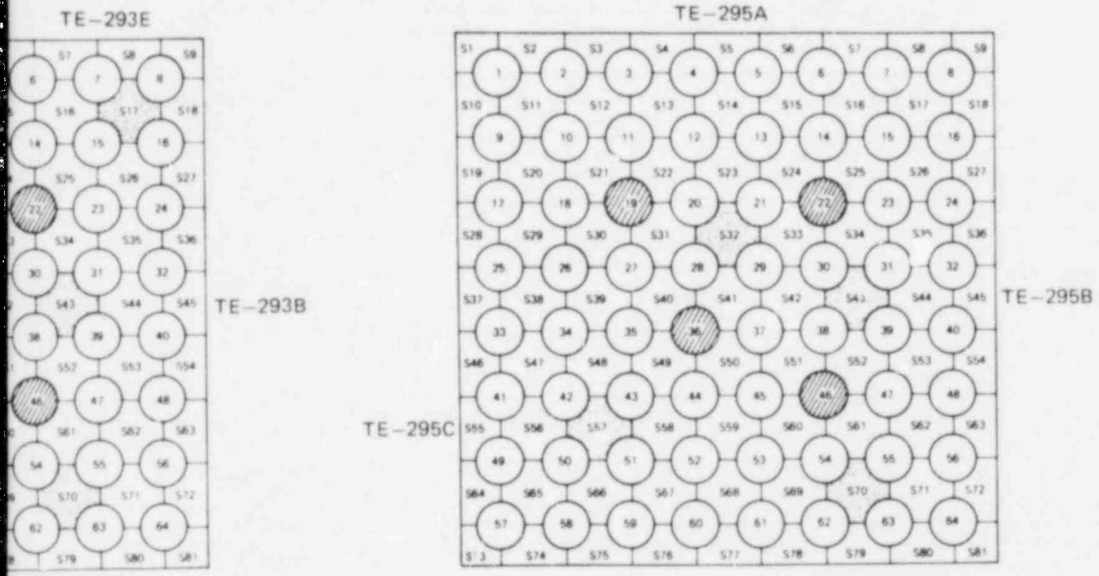

(e) SPACER GRID 6

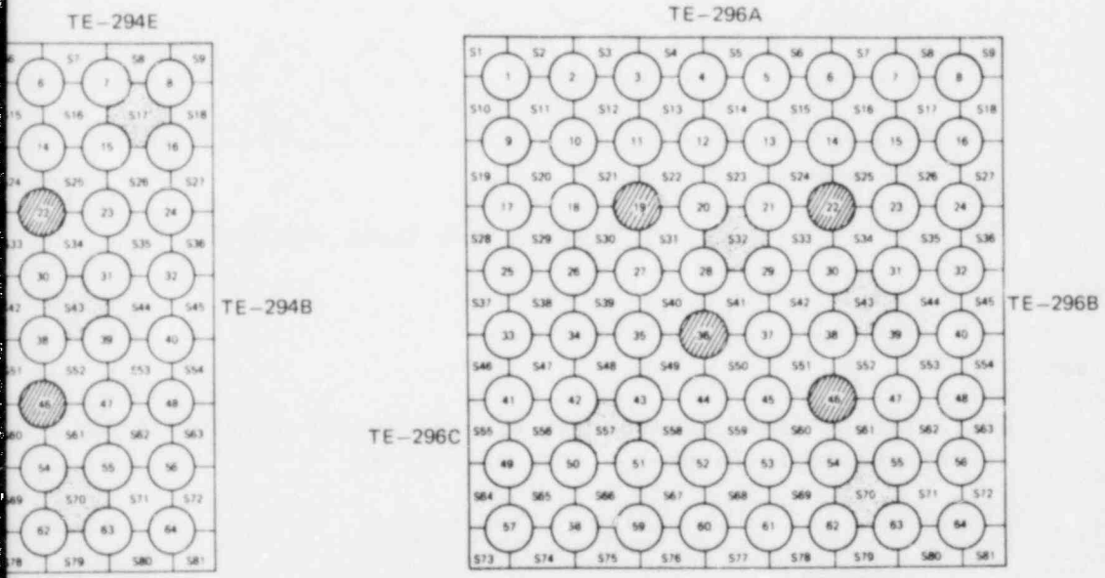

(f) SPACER GRID 7

d thermocouples.

A.3 Shroud-Box Thermocouples

Shroud-box thermocouples protrude through the shroud wall into the fluid in the wall subchannels. A typical installation is shown in Fig. A.4. The naming convention for these thermocouples has the following form

TE-18na ,

where

n = a number 1–7 designating the level of the thermocouple in the shroud box as follows:

Number	Thermocouple level
181	A
182	B
183	C
184	D
185	E
186	F
187	G

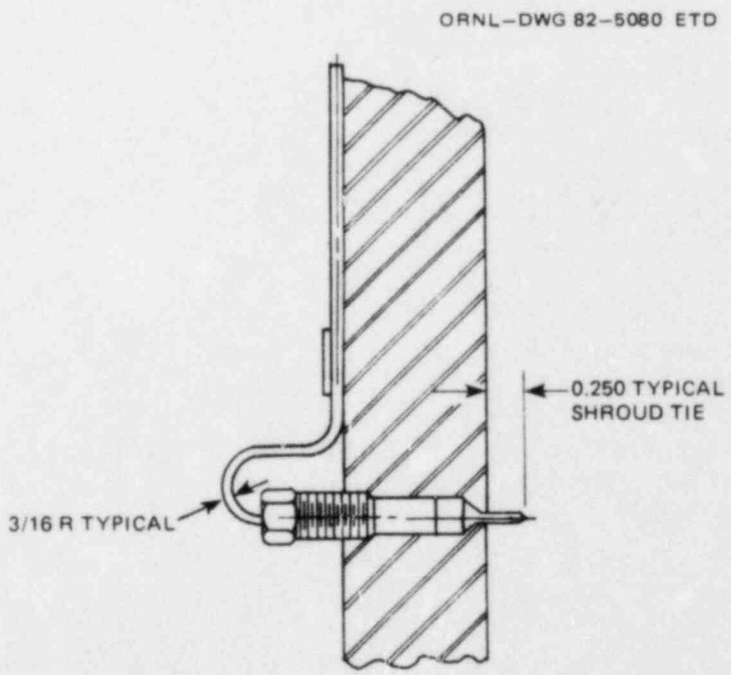

Fig. A.4. Typical installation of a shroud-box thermocouple. Dimensions are in inches (1 in. = 2.54 cm).

and

a = a letter designating the side of the box through which the thermocouple protrudes N, E, S, W (being the compass direction most closely matching the direction the side faces).

Those fluid subchannels monitored by shroud-box thermocouples are shown in Fig. A.5(a-g).

A.4 Thermocouple-Array Rod Thermocouples

The thermocouple-array rods occupied grid positions 19 and 36 in the original Bundle 3. Each array rod contains 14 thermocouples, and at each axial level in the core where there is a primary FRS thermocouple level two of these thermocouples protrude from the rod into the fluid (as illustrated in Fig. A.6). The naming convention for these thermocouples has the following form

TE-18na1 ,

where

n = the number 8 or 9 designating which grid position the thermocouple-array rod is located:

8 - grid position 19
9 - grid position 36

a = a letter "A" and "B" designating which of two subchannels associated with that rod into which the thermocouple protrudes.

Rod grid position	"A" subchannel	"B" subchannel
19	22	30
36	41	49

1 = the thermocouple level A-G (same as FRS thermocouple level designations).

Those fluid subchannels monitored by the thermocouple-array rod thermocouples are indicated in Fig. A.5(a-g).

ORNL-DWG 82-5081 ETD

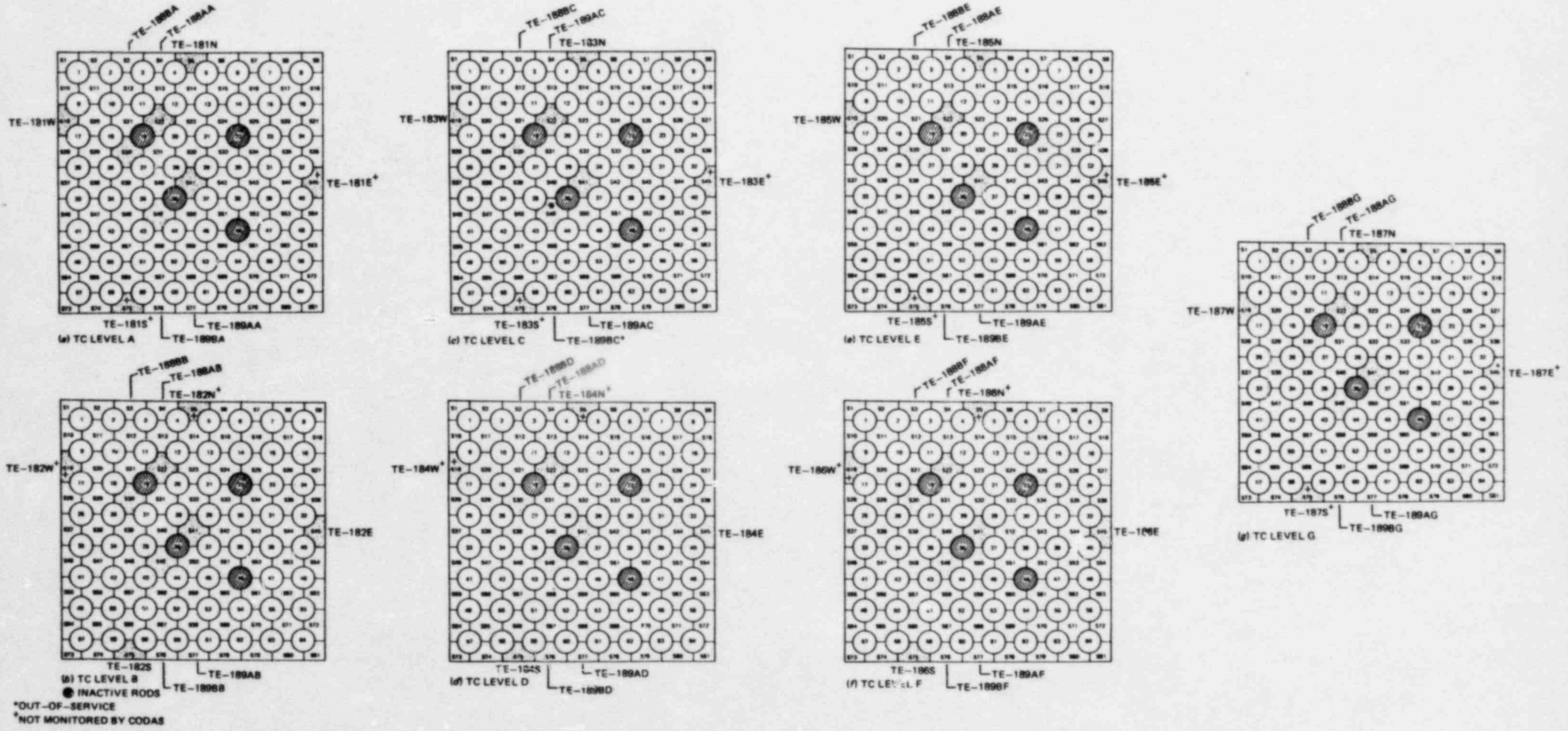

Fig. A.5. Shroud-box and thermocouple-array rod thermocouples.

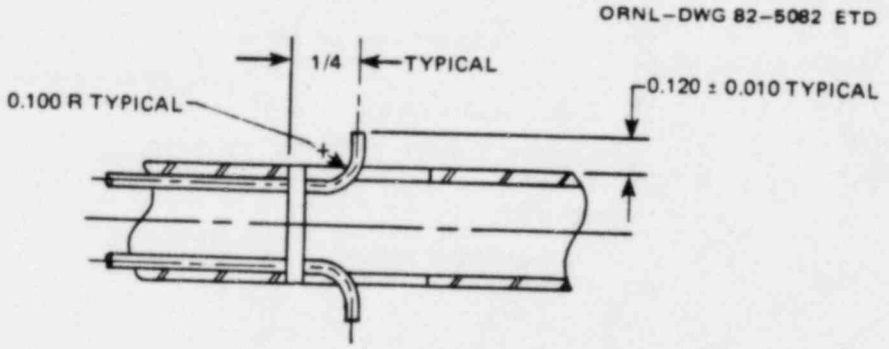

Fig. A.6. Cross section of thermocouple array rod illustrating protrusion of thermocouples from the rod. Dimensions are in inches (1 in. = 2.54 cm).

NUREG/CR-2609
ORNL/NUREG-75
Dist. Category AN

Internal Distribution

1. T. M. Anklam
2-3. W. G. Craddick
4. D. K. Felde
5. U. Gat
6. D. S. Griffith
7. H. W. Hoffman
8. A. L. Lotts
9. R. W. McCulloch
10. D. G. Morris
11. C. B. Mullins
12-16. L. J. Ott
17. J. P. Sanders
18. H. E. Trammell
19. D. B. Trauger
20. J. W. Wantland
21. G. L. Yoder
22. ORNL Patent Office
23. Central Research Library
24. Document Reference Section
25-26. Laboratory Records Department
27. Laboratory Records (RC)

External Distribution

28-29. Director, Division of Reactor Safety Research, Nuclear Regulatory Commission, Washington, DC 20555
30. Office of Assistant Manager for Energy Research and Development, Department of Energy, ORO, Oak Ridge, TN 37830
31-32. Technical Information Center, DOE, Oak Ridge, TN 37830
33-132. Given distribution as shown in category AN (NTIS-10)